

MEng Final Year Project Report:  
Biomechanical Loading of the Musculoskeletal System  
During Exercise

Sheng Kai Wong

Supervisor: Prof. Richie Gill  
Assessor: Dr. Samantha Hayward

May 12, 2025

Word Count: 12638

*I certify that I have read and understood the entry in the Student Handbook for the Department of Mechanical Engineering on Cheating and Plagiarism and that all material in this assignment is my own work, except where I have indicated with appropriate references.*



Department of Mechanical Engineering  
FACULTY OF ENGINEERING AND DESIGN

# Abstract

Osteoporosis, a disease characterised by a severely weakened skeleton as a result of reduced bone mineral density, is projected to rise in prevalence as the global population ages. Given the substantial mortality rates and societal costs associated with the disease, there is clear incentive to evaluate and strengthen current preventative healthcare recommendations. Among available interventions, exercise stands out as an accessible, cost-effective strategy with broad health benefits extending beyond osteoporosis prevention. While exercise is well recognised as a key contributor to musculoskeletal health, the specific biomechanical interactions responsible for this remains an open question. This study seeks to address this knowledge gap by investigating joint moment patterns at the hip, knee, and ankle during walking and running, using OpenSim simulations informed by motion capture and force plate data.

For this study, data from four participants were analysed, of which three yielded usable moment datasets for analysis. Simulation results indicated that while joint moments generally aligned with established literature, particularly at the hip during walking. However, systematic discrepancies in exact moment values were consistently observed, most notably at the knee and ankle joints, and during the high-acceleration stance phases of heel-strike and toe-off. Statistical variability analysis revealed that walking trials were approximately twice as consistent as running trials, and showed that simulation variability was greatest at the ankle, moderate at the knee, and lowest at the hip. Notably, scaling inaccuracies, particularly at the pelvis, emerged as a major source of moment variability, underscoring the importance of scaling during simulations.

These findings indicate that, while current musculoskeletal modelling pipelines can provide valuable insights, their feasibility remains constrained by vulnerability to scaling error which can significantly compromise joint-level outputs. However, the statistical analysis conducted in this study suggests that aggregating data across larger and more diverse participant groups may help mitigate this. Taken together, this work provides a case study of how scaling accuracy impacts simulation outcomes, offers preliminary evidence that aggregation may serve as a promising avenue to compensate for individual scaling error, and posits that statistical frameworks could play a valuable role in monitoring and improving simulation quality.

## Acknowledgments

First and foremost, my mother and father. Thank you for supporting me all my life. Through my academics, through my exploration, my worsts, my bests, my growing up, my everything. Mother, thank you for teaching me to make warm meals of comfort, how to love the world, and for answering every question I have ever had. Father, thank you for reading to me when I was too young to do so for myself, for teaching me to travel, and for being a perspective for years I had not yet seen. My parents, who have for the past five years kept me updated on home when I was halfway across the world. My parents, who have taught me to keep asking the question '*Why?*'. My parents, who have given me the space to make my own mistakes, the space to narrate my own becoming, and who I have caused so much stress in being their child. Thank you for everything. I love you.

My brother. You're alright I guess.

I also extend my thanks to my supervisor Professor Richie Gill and assessor Doctor Samantha Hayward, for guiding me through this final portion of my undergraduate studies, and in helping me shape my dissertation. I have enjoyed this project immensely, and my only regret was that I could not pursue it further.

Melanie, Yuka, Vita, Joel, Johyna - thank you for helping to proofread this caricatural piece of research, pointing out where I used one too many words, or a term too chauvinist. It was not easy to write this. It cannot have been much easier to read.

Finally, I would not be here if it were not for the teachers who oversaw my growing up. Mrs. Seymour and Mr. Lush, you played an irreplaceable role in shaping me into the person I am today. To have been your student in the tropics of Brunei is an experience that I will cherish forever dearly, and for that I thank you.

To the friends that I have had the joy of having met, my dogs Bruno and Hazel, and my monsterra houseplant Kaya for bringing me warmth. Thank you. Producing this modest stack of paper was a labor of love. Infuriating, terrifying, and a significant cause of liminal angst - but it has been one of the greatest privileges, and I would do it all again.

# Contents

<b>List of Figures</b>	vii
<b>List of Tables</b>	ix
<b>Acronyms</b>	1
<b>1 Artificial Intelligence Statement</b>	3
<b>2 Ethics Declaration</b>	3
<b>3 Introduction</b>	3
3.1 Research Context . . . . .	3
3.1.1 Osteoporosis . . . . .	3
3.1.2 Bone Mineral Density and Current Health Guidelines . . . . .	4
3.1.3 The Role of Exercise . . . . .	5
3.2 Overview of Biomechanical Analysis . . . . .	5
3.2.1 Bone Models . . . . .	6
3.2.2 Research Aims and Objectives . . . . .	6
<b>4 Literature Review: Current practices in Biomechanical Simulations</b>	7
4.1 The Biomechanical Simulation Workflow . . . . .	7
4.2 Raw Simulation Data . . . . .	8
4.2.1 Optics-based Motion Capture: Marker-based and Marker-less Methods . . . . .	8
4.2.2 Inertial Measurement Units . . . . .	9
4.2.3 Fluoroscopy . . . . .	9
4.2.4 Forces . . . . .	10
4.2.5 Electromyography . . . . .	10
4.3 Overview of Musculoskeletal Models . . . . .	11
4.3.1 Default Models in OpenSim . . . . .	11
4.4 Scaling and Inverse Kinematics . . . . .	11
4.4.1 Scaling . . . . .	11
4.4.2 Inverse Kinematics . . . . .	13
4.5 Estimating Muscle Force . . . . .	13
4.5.1 Static Optimisation and the Polynomial Criterion . . . . .	13
4.5.2 Computed Muscle Control . . . . .	14
4.5.3 The Biology of it all: The Muscle-Tendon Unit . . . . .	15
4.6 OpenSim-aided Workflows and Other Algorithms . . . . .	15
4.6.1 Developing Workflows . . . . .	15
4.6.2 Other Algorithms . . . . .	16
4.7 Literature Review Summary and Implications . . . . .	16
<b>5 Methodology</b>	17
5.1 Overview . . . . .	17
5.2 Raw data . . . . .	17
5.2.1 Source Description . . . . .	17
5.2.2 Participant Selection . . . . .	18
5.2.3 Selected Movement Trials and Pre-Processing . . . . .	18
5.3 Musculoskeletal Model Selection and Scaling . . . . .	19
5.3.1 Model Selection: The Rajagopal Model . . . . .	19

5.3.2 Scaling . . . . .	20
5.3.3 A Comment on Automated scaling and Scaling Error . . . . .	21
5.4 Inverse Kinematics . . . . .	22
5.5 Muscle Force Estimation . . . . .	22
5.5.1 Static Optimisation . . . . .	22
5.5.2 Computed Muscle Control . . . . .	23
<b>6 Results and Analysis I: Scaling and Inverse Kinematics</b>	<b>24</b>
6.1 Scaling . . . . .	24
6.2 Inverse Kinematics . . . . .	24
<b>7 Results and Analysis II: Biomechanical Moments Analysis</b>	<b>25</b>
7.1 Overview . . . . .	25
7.2 Omitted Data . . . . .	27
7.3 Walking Condition . . . . .	28
7.3.1 Aggregate Results . . . . .	28
7.3.2 Joint analysis: Acetabulofemoral Joint (Hip) . . . . .	29
7.3.3 Joint Analysis: Tibiofemoral Joint (Knee) . . . . .	29
7.3.4 Joint analysis: Talocrural Joint (Ankle) . . . . .	32
7.4 Running Condition . . . . .	33
7.4.1 Aggregate Results . . . . .	33
7.4.2 Joint analysis: Acetabulofemoral Joint (Hip) . . . . .	35
7.4.3 Joint Analysis: Tibiofemoral Joint (Knee) . . . . .	36
7.4.4 Joint analysis: Talocrural Joint (Ankle) . . . . .	36
7.5 Summary of Biomechanical Analysis . . . . .	37
<b>8 Results and Analysis III: Statistical Variability Analysis</b>	<b>38</b>
8.1 Statistical Approach and Rationale . . . . .	38
8.2 Variability Across Exercise Conditions . . . . .	39
8.3 Variability Across Joints . . . . .	40
8.4 Variability Across Participants . . . . .	45
8.5 Variability Analysis Summary and Limitations . . . . .	47
<b>9 Discussion</b>	<b>49</b>
9.1 Project Summary . . . . .	49
9.2 Interpretation . . . . .	49
9.3 Limitations . . . . .	50
9.3.1 Scope . . . . .	50
9.3.2 Methodological Factors . . . . .	50
9.4 Implications . . . . .	51
9.5 Future work and Recommendations . . . . .	51
<b>10 Conclusion</b>	<b>53</b>
<b>Appendices</b>	<b>69</b>
<b>Appendix A Marker Locations</b>	<b>69</b>
<b>Appendix B Markerset parent frames</b>	<b>69</b>
<b>Appendix C Scaling Tool</b>	<b>71</b>

C.1 Screenshot of Scaling Tool Setup . . . . .	71
C.2 Screenshot of Scaling Factor Setup . . . . .	71
<b>Appendix D Proposed Amendment to Automated Scaling Tool</b>	<b>73</b>
<b>Appendix E List of Trial files used</b>	<b>74</b>
<b>Appendix F Example of Applied Ground Reaction Force</b>	<b>74</b>
<b>Appendix G Initial setup of OpenSim Computed Muscle Control Tool</b>	<b>75</b>
G.1 CMC lookup table: main settings . . . . .	75
G.2 CMC lookup table: Integrator settings . . . . .	76
G.3 CMC task setup: changes from base Rajagopal model file [100] . . . . .	76
<b>Appendix H Uncleaned Aggregate Plot of Running Trials Across All Participants</b>	<b>76</b>
<b>Appendix I Denoising Filter Settings</b>	<b>78</b>
<b>Appendix J Uncleaned data plots (Unfiltered)</b>	<b>78</b>
J.0.1 Aggregate Plots for Walking and Running . . . . .	78
J.1 Ankle Joint . . . . .	78
J.2 Participant-wise Comparison of Moments, including Participant 10 . . . . .	78
<b>Appendix K Detailed Results Statistical Analysis</b>	<b>84</b>
K.1 Detailed reporting of moments . . . . .	85

# List of Figures

1	Diagram representing compromised bone tissue structure (right) compared to healthy tissue (left). Diagram courtesy of [3]. . . . .	4
2	Graph describing how bone mass changes throughout the typical human lifecycle. Graph courtesy of [27]. . . . .	4
3	Flow-chart showing the traditional work-flow to biomechanical simulations. Image courtesy of [58] and [59]. . . . .	7
4	An example of marker-based motion-capture. Image courtesy of [60]. . . . .	8
5	Example of an IMU motion-capture setup. Courtesy of [79]. . . . .	9
6	Example of an experimental motion-capture setup utilising fluoroscopy. Images courtesy of [84]. . . . .	10
7	The Rajagopal MSK model. Image courtesy of Rajagopal [100]. . . . .	12
8	Flow-chart representing Computed Muscle Control. Image courtesy of [121]. . . . .	14
9	A diagram the typical Hill-type muscle-tendon unit, showing the relationship of muscle-tendon length, muscle fiber length, tendon length, pennation angle. Where $l$ is the muscle-tendon length, $l_m$ is the muscle fiber length, $l^t$ is the tendon length, $\phi$ is the pennation angle. Image courtesy of [128]. . . . .	15
10	Marker locations for motion capture. Images courtesy of [56]. For a list of markers refer to Appendix B. . . . .	17
11	The annotated gait-cycle. Image courtesy of [163]. . . . .	19
12	The Rajagopal Model. Image courtesy of [100]. . . . .	20
13	generic Rajagopal model (left) and scaled P10 model (right) taken in the OpenSim workspace. . . . .	22
14	Visual representation of associating force plate data within the OpenSim workspace.	23
15	A comparison of unfiltered versus filtered moment data. <b>Note: These plots have been shrunk to visually communicate filtering effects. Filtered plots are shown in original size later in this analysis, whilst full-size unfiltered plots are available in Appendix J.</b> . . . . .	26
16	Combined figure caption describing both images. . . . .	27
17	Summary plots of lower-limb MSK joint moments, aggregated for all walking trials. <i>Moments normalised by participant body-weight and height (<math>BW \times Height</math>); time normalised as percentage (%) of stance phase.</i> <b>Joint DoFs:</b> Flex./Ext. = Flexion/Extension, Abd./Add. = Abduction/Adduction, Rot. Exter./Inter. = External/Internal Rotation, Plant. Flex./Ext. = Plantarflexion/Dorsiflexion. . . . .	30
18	Subplot comparison of hip joint moments across the stance phase for walking trials, broken down by participant and hip DOF. <i>Moments normalised by participant body weight and height (<math>BW \times Height</math>); time normalised as percentage (%) of stance phase.</i> <i>Moments normalised by participant body-weight and height (<math>BW \times Height</math>); time normalised as percentage (%) of stance phase.</i> <b>Joint DoFs:</b> Flex./Ext. = Flexion/Extension, Abd./Add. = Abduction/Adduction, Rot. Exter./Inter. = External/Internal Rotation. . . . .	31
19	Subplot comparison of knee flexion moments across the stance phase for walking trials, broken down by participant. <i>Moments normalised by participant body weight and height (<math>BW \times Height</math>); time normalised as percentage (%) of stance phase.</i> <i>Moments normalised by participant body-weight and height (<math>BW \times Height</math>); time normalised as percentage (%) of stance phase.</i> <b>Joint DoFs:</b> Flex./Ext. = Flexion/Extension. . . . .	32

20	Subplot comparison of ankle plantarflexion moments across the stance phase for walking trials, broken down by participant. <i>Moments normalised by participant body weight and height (<math>BW \times Height</math>); time normalised as percentage (%) of stance phase.</i> <i>Moments normalised by participant body-weight and height (<math>BW \times Height</math>); time normalised as percentage (%) of stance phase.</i> <b>Joint DoFs:</b> Plant. Flex./Ext. = Plantarflexion/Dorsiflexion. . . . .	33
21	Summary plots of lower-limb MSK joint moments, aggregated for all running trials for Participants 4 and 13. <i>Moments normalised by participant body-weight and height (<math>BW \times Height</math>); time normalised as percentage (%) of stance phase.</i> . . . . .	34
22	Subplot comparison of hip joint moments across the stance phase for running trials, broken down by participant and hip DOF. <i>Moments normalised by participant body weight and height (<math>BW \times Height</math>); time normalised as percentage (%) of stance phase.</i> <b>Joint DoFs:</b> Flex./Ext. = Flexion/Extension, Abd./Add. = Abduction/Adduction, Rot. Exter./Inter. = External/Internal Rotation. . . . .	35
23	Subplot comparison of knee flexion moments across the stance phase for running trials, broken down by participant. <i>Moments normalised by participant body weight and height (<math>BW \times Height</math>); time normalised as percentage (%) of stance phase.</i> . . . . .	36
24	Subplot comparison of ankle plantarflexion moments across the stance phase for running trials, broken down by participant. <i>Moments normalised by participant body weight and height (<math>BW \times Height</math>); time normalised as percentage (%) of stance phase.</i> . . . . .	37
25	Exercise-wise violin plot NSD and NMAD comparison across joint moment metrics (RMS, Peak+, Peak-) for walking, running, and aggregated trials. Rows indicate the statistical measure; columns separate aggregate, walking-only, and running-only conditions. . . . .	40
26	Joint-wise violin plot NSD comparison across joint moment metrics (RMS, Peak+, Peak-) for walking, running, and aggregated trials. Rows show joint of interest; columns separate aggregated, walking-only, and running-only conditions. . . . .	42
27	Joint-wise violin plot MAD comparison across joint moment metrics (RMS, Peak+, Peak-) for walking, running, and aggregated trials. Rows show joint of interest; columns separate aggregated, walking-only, and running-only conditions. . . . .	43
28	Participant-wise violin plot NSD comparison across lower-limb joint moment metrics: RMS, Peak positive (Peak+) and negative (Peak-) moments for walking, running, and aggregated trials. Rows show individual participants; columns separate aggregated, walking-only, and running-only conditions. <b>Note that no running NSD data was available for P10.</b> . . . . .	45
29	Participant-wise violin plot NMAD comparison across lower-limb joint moment metrics: RMS, Peak positive (Peak+) and negative (Peak-) moments for walking, running, and aggregated trials. Rows show individual participants; columns separate aggregated, walking-only, and running-only conditions. <b>Note that no running MAD data was available for P10.</b> . . . . .	46
30	Scatter plot showing asymmetry in peak hip extension moment at left and right joints for Participant 4 during walking trials. . . . .	48
31	Marker Locations for Motion-Capture, Courtesy of [56] . . . . .	69
32	Scale Tool Setup: Main settings . . . . .	71
33	Scale Tool Setup: For factors refer to Figure C.2 . . . . .	71
34	Example of how force-plate data was applied. Note that force and moments were applied to the calcanei . . . . .	74

35	CMC settings lookup table main page. Note that the tracking tasks here have been edited from the original Rajagopal CMC tasks to weigh lower limbs more, and upper limbs less. . . . .	75
36	CMC settings lookup table . . . . .	76
37	Uncleaned Aggregate Plot of Running Trials Across All Participants. Moments at various joints during stance period, normalised by $BW \times height$ . . . . .	77
38	Unfiltered moment plots for walking trials . . . . .	79
39	Unfiltered moment plots for running trials . . . . .	80
40	Unfiltered moment plots for walking trials . . . . .	80
41	Unfiltered moment plots for running trials . . . . .	81
42	Subplot comparison of hip joint moments across the stance phase for running trials, broken down by participant and hip DOF. <i>Moments normalised by participant body weight and height (<math>BW \times Height</math>); time normalised as percentage (%) of stance phase.</i> . . . . .	81
43	Subplot comparison of knee joint moments across the stance phase for running trials, broken down by participant. <i>Moments normalised by participant body weight and height (<math>BW \times Height</math>); time normalised as percentage (%) of stance phase.</i> . . . . .	82
44	Subplot comparison of ankle joint moments across the stance phase for running trials, broken down by participant. <i>Moments normalised by participant body weight and height (<math>BW \times Height</math>); time normalised as percentage (%) of stance phase.</i> . . . . .	82

## List of Tables

1	The three main scaling methods used in musculoskeletal modeling [41]. . . . .	12
2	Participant Data . . . . .	18
3	Dataset Trials used in this study (per participant) . . . . .	19
4	Cadaveric data used to inform the Rajagopal MSK model [100], [162]. . . . .	20
5	Measurement marker pairs used for MSK scaling using the OpenSim Scaling Tool .	21
6	Musculoskeletal (MSK) model scaling results. . . . .	24
7	Summary of excluded trials from muscle force analysis . . . . .	28
8	Summary of literature values used for joint moment analysis during walking stance phase. <i>Joint DoFs:</i> Flex./Ext. = Flexion/Extension, Abd./Add. = Abduction/Adduction, Rot. Ex./In. = External/Internal Rotation, Plant. Flex./Ext. = Plantarflexion/Dorsiflexion. . . . .	29
9	Summary of literature values used for joint moment analysis during running stance phase . . . . .	35
10	Summary of average RMS and peak positive and negative joint moments (Nm) for walking trials during stance phase, including SD. . . . .	38
11	Summary of average RMS and peak positive and negative joint moments (Nm) for running trials during stance phase, including SD. . . . .	38
12	Summary of data aggregation levels and statistical analysis approach . . . . .	39
13	Aggregated Statistical Summary of joint moment data (normalised SD and MAD), broken down for exercise condition comparison, rounded to two decimal places. See Appendix K for detailed results. . . . .	41
14	Statistical summary of joint moment data (NSD and NMAD), broken down for joint-wise comparison across hip, knee, and ankle joints. See Appendix K for detailed statistical breakdown. . . . .	44
15	Markerset parent frames . . . . .	70
16	Scaling Marker Weightings . . . . .	72
17	List of trial IDs used in producing this research from dataset [56]). . . . .	74

18	Computed Muscle Control task file amendments <i>Note: coordinate names ending in '_r' denote 'right', implying that task weighting changes were symmetric (i.e. same changes applied to '_l' coordinates)</i>	76
19	Filtering Parameters Used for Denoising Data for Moments Analysis. (Note: all moment data was normalised by participant body weight and height ( $BW \times H$ ) prior to filtering.)	78
20	Statistical Breakdown of Simulation Moment Data: Normalised Standard Deviation and Median Absolute Deviations across stance-cycle moment RMS, positive peak, and negative peak values. <i>Joint DoFs:</i> Flex./Ext. = Flexion/Extension, Abd./Add. = Abduction/Adduction, Rot. Ex./In. = External/Internal Rotation, Plant. Flex./Ext. = Plantarflexion/Dorsiflexion.	84
21	Summary of Results: Peak and RMS Moments at the Hip, Knee, and Ankle Joints During Stance. <i>Joint DoFs:</i> Flex./Ext. = Flexion/Extension, Abd./Add. = Abduction/Adduction, Rot. Ex./In. = External/Internal Rotation, Plant. Flex./Ext. = Plantarflexion/Dorsiflexion.	85

## Acronyms

**AST** Automatic Scaling Tool. 21, 73

**BMD** Bone Mineral Density. 3–6

**BMI** Body Mass Index. 18

**BW** Body Weight. vii–ix, 30–37, 77, 81, 82

**CMC** Computed Muscle Control. 14, 22, 23, 27, 49

**CT** Computed Tomography. 12

**DOF** Degrees of Freedom. vii–ix, 11, 13, 20, 25, 27, 31–33, 35, 37, 81

**DXA** Dual-Energy X-ray Absorptiometry. 3

**EMG** Electromyography. 10, 13, 15

**EOM** Equation of Motion. 13

**FEM** Finite Element Model. 6, 15

**GRF** Ground Reaction Force. 23

**ID** Inverse Dynamic. 7

**IK** Inverse Kinematics. 7, 13, 22

**IMU** Inertial Measurement Unit. vii, 9, 15

**JRF** Joint Reaction Force. 18

**MAD** Median Absolute Deviation. viii, ix, 38, 39, 41, 43, 46, 78

**Mo-Cap** Motion Capture. 6, 8–10, 15, 17, 18, 20, 32, 49, 53

**MRI** Magnetic Resonance Imaging. 11, 12

**MSK** Musculoskeletal. vii–ix, 3, 5–13, 15, 16, 18–24, 27, 28, 30, 32, 34, 36, 49–51, 73

**MVD** Minimum Viable Dose. 5

**NHS** National Health Service. 3

**NMAD** Median-Normalised Median Absolute Deviation. viii, ix, 38–41, 44–46, 49, 51

**NSD** Mean-Normalised Standard Deviation. viii, ix, 38–42, 44–46, 49, 51

**PBM** Peak Bone Mass. 4, 5

**RMS** Root-Mean-Square. x, 21, 24, 37, 39, 40, 84

**RRA** Residual Reduction Algorithm. 11

**SD** Standard Deviation. ix, 3, 32, 33, 38, 39, 41, 44

**SO** Static-Optimisation. 14

**STA** Soft Tissue Artifact. 8, 10, 18, 23

**UK** United Kingdom. 3

# 1 Artificial Intelligence Statement

Artificial Intelligence was used in the proof-reading of this report. No Artificial Intelligence was used during the research phase and writing portions of this document, nor in generating data. The student acknowledges that this work is their own, and that ChatGPT-4 was used to assist in proofreading [1].

## 2 Ethics Declaration

This research was approved by the ethics board prior to commencing under the application reference number **9156-10780**. For further enquiries contact [skw43@bath.ac.uk](mailto:skw43@bath.ac.uk).

## 3 Introduction

### 3.1 Research Context

#### 3.1.1 Osteoporosis

Osteoporosis is a Musculoskeletal (MSK) disease characterised by an individual having a severely weakened skeletal system as a result of compromised bone-tissue microstructure (Figure 1) [2]. Diagnosis is typically done via Dual-Energy X-ray Absorptiometry (DXA) scan that measures an individual's Bone Mineral Density (BMD). If an individual's BMD is between 1 - 2.5 Standard Deviation (SD)s less than a healthy individual in their twenties, they are diagnosed with osteopenia, and if this difference exceeds that >2.5 SDs, they are diagnosed with osteoporosis.[2]

Osteoporosis is a progressive disease, and osteoporotic fracture is associated with unfavourable mortality rates [2], [4], [5]. Hip fractures are the most severe, traditionally associated with a "1-in-3" (30%) mortality rate in the first year post-injury [6]. Vertebrae fractures are similarly severe, although less documented, with reported one-year mortality rates between 7-11% [7], [8]. Whilst there is evidence that mortality-rates are improving [6], [9], [10], patients who do survive an initial fracture are subsequently at-risk to recurrent injury thereafter [11]. This is associated with significantly reduced health-related quality standard of living [12]–[14], and is noted to be largely detrimental even with current treatments.

Fracture risk rises exponentially with an individual's age [15], [16], with estimates suggesting that nearly half of all women and one in five men over 50 will sustain an osteoporotic fracture in their lifetime [17]–[19]. This presents a growing concern as the global population ages [20], with the proportion of individuals over 60 projected to effectively triple from between the years 2015 to 2100 (12% to 34%). Correspondingly, osteoporotic fracture incidence rates are also expected to rise, with annual hip fractures alone projected to increase from 1.66 million annually in 1990 to 6.26 million by 2050 [21], [22].

In the United Kingdom (UK), osteoporotic care cost the National Health Service (NHS) an estimated £4.7 billion in 2019 [23], [24], a figure projected to rise, as fragility fractures are expected to increase by 27% over the next decade [23]. Given the growing incidence of fractures, associated health burden, and economic impact of this disease, there is an incentive to reassess and where possible, improve clinical guidelines surrounding the disease.

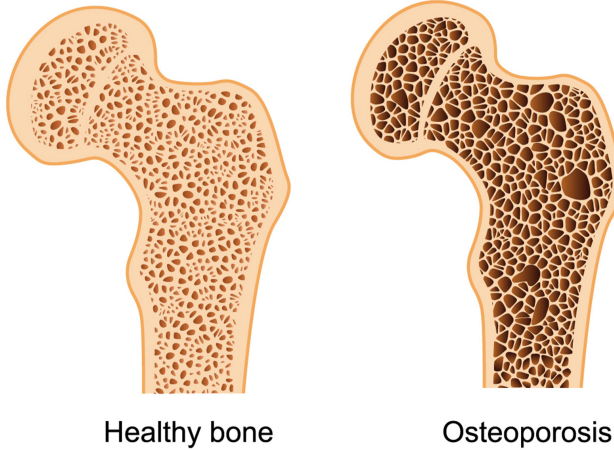


Figure 1: Diagram representing compromised bone tissue structure (right) compared to healthy tissue (left). Diagram courtesy of [3].

### 3.1.2 Bone Mineral Density and Current Health Guidelines

The single largest risk factor for osteoporotic fracture is low BMD. Consequently, preventative osteoporotic care primarily focuses on maximising BMD retention throughout an individual's lifetime [2]. BMD is mediated by the biological bone re-modelling cycle, whereby old and damaged bone tissue is continually removed replaced over time [25]. As an individual ages, this process' behaviour changes throughout their life, affecting their BMD (Shown in Figure 2).

In youth, BMD increases at a fairly constant rate, with this rate spiking significantly during adolescence. As this rate of increase levels-off post-puberty, BMD continues to increase modestly before Peak Bone Mass (PBM) is achieved between ages 30-40 years. Thereafter, the body's ability to replace old tissue begins to decline, leading to the gradual decrease of BMD values with age [2], [26].

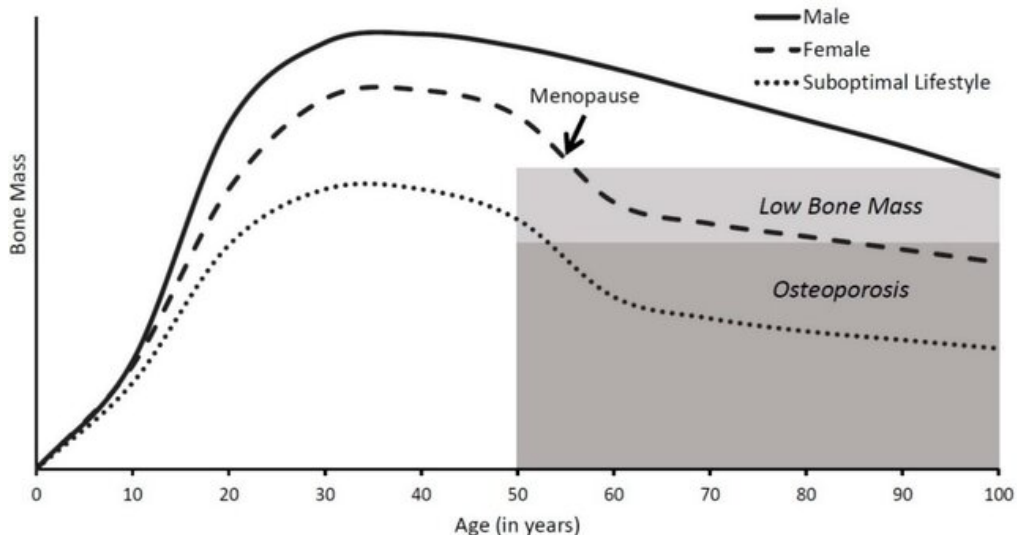


Figure 2: Graph describing how bone mass changes throughout the typical human lifecycle. Graph courtesy of [27].

It is widely accepted that once PBM is achieved, BMD loss cannot, outside of exceptional cases, be reversed [2]. This puts the elderly at a higher risk of osteoporotic fracture compared to their younger counterparts [15], [16], and for individuals experiencing menopause, this risk is further exacerbated due to endocrine factors [28].

Given this, age-related BMD management focuses on minimising BMD loss through various means [2]. These can be broadly categorised into; nutrition, hormonal supplementation (particularly regarding individuals experiencing menopause), reducing detrimental habits such as smoking, and exercise [16], [23], [29].

### 3.1.3 The Role of Exercise

Given its low economic cost and extensively documented health benefits outside of MSK health [30], exercise has been of particular interest in osteoporotic care.

The positive correlation between regular exercise and MSK health, and subsequently lower osteoporotic fracture rates, has been widely noted [30] and is one of the most recurrent recommendations to maintaining one's health globally [31]. In the case of osteoporosis, various cross-sectional and meta-analytical research has been done to investigate its role in treatment [30], [32]–[34], reporting that higher activity levels are highly correlated with better BMD retention over time. However, whilst the beneficial MSK health impacts of exercise are well-documented qualitatively, there is still an ambiguity regarding the quantitative nature of this relationship.

Addressing this ambiguity has been an area of medical interest for several reasons. In the first case, literature indicates that exercise has unfavourable attrition rates with individuals who do not already engage with it, with at best, just two thirds of participants maintaining an exercise regime throughout clinical studies [35], [36]. This has led to an incentive to produce the ‘magic pill’ or ‘Minimum Viable Dose (MVD)’ exercise regime, based on the notion that a low-investment regimes would have higher retention rates amongst sedentary individuals [35], [37]. In the second case, there is an incentive to determine how the exercise ‘intensity’ affects MSK health [38], [39]. High-intensity training is associated with shorter training sessions and time-investment, while low-intensity is associated with easier movements, making them suitable for people otherwise unable to engage with more strenuous activities [31]. The relationship between intensity and MSK health is an ongoing area of research, but thus far, literature has not reached consensus [38], [39]. Consequently, there is an ongoing need to address this gap within research.

## 3.2 Overview of Biomechanical Analysis

In order to quantify the effects of exercise on MSK health, there is a need for realistic, validated, and wide-ranging biomechanical loading data associated with various exercise movements, and to then characterise how this data interplays with the MSK system itself [40], [41]. *In vivo* measurements, whilst desirable, are challenging to collect in large amounts due to ethical concerns and technological limitations. Direct MSK joint measurements do exist in databases such as Orthoload [42] and direct measurement in prosthetic devices [43], but pose limitations in availability and in the biased sample of participants involved (e.g. individuals who are disproportionately elderly, amputees, etc.).

In order to bypass this, various simulative solutions have been developed to produce a viable, non-invasive methodology for conducting biomechanical analysis and examining the MSK system. In

the context of BMD management, this broadly falls into two categories: the ongoing development of accurate, biologically informed bone-remodelling algorithms, and the development of various biomechanical simulation frameworks.

### 3.2.1 Bone Models

Bone can be characterised as a hierachal, composite material with mechano-adaptive properties. That is, bone tissue can adapt its mechanical properties and biological structures over time in response to any repetitive mechanical stimulus (or lack thereof) that it is exposed to[26]. This process has been extensively studied [26], [44], and is typically defined using the relationship known as Wolff's law [25], [45].

Over the years, various bone-remodelling numerical algorithms and Finite Element Model (FEM)s have been produced to emulate this biological process in varying degrees of physiological detail, and in various parts of the skeleton [46], [47]. The most recent literature documents improvements in the numerical modelling of the cohesion zone (cortical bone) and phase-field (trabecular bone) tissues, as well as their integration into existing FEMs [48]. However, it is also noted consistently throughout literature that for increasingly complex bone models to be medically useful, there is a need for increasingly realistic and resolute biomechanical loading data to subject these models to [48], [49].

### 3.2.2 Research Aims and Objectives

Therein lies the crux of this research, which is to contribute to the growing database of MSK loading conditions that serve as inputs for numerical bone models. To achieve this, this study utilised OpenSim, an open-source biomechanical modelling software [50], with the aim of generating realistic and validated biomechanical loading data, specifically in the lower limb (hip, knee and ankle joints). OpenSim was selected over alternatives such as the AnyBody Modeling System [51] and Motek's Human Body Model [52] due to its widespread use in academic literature and open-source accessibility [40], making it well-suited for the project scope.

Notably, both MSK joint forces and moments are crucial in characterising biomechanical loading and its relevance to bone health [53], [54]. However, estimating joint forces typically requires additional simulation steps, calibration, and validation as it requires additional physiological detail compared to moments analysis [40], [55]. This was beyond the feasible scope of this project, and as a result, the analysis in this study focused on joint moments and producing muscle loading conditions, providing a foundation to potentially extend towards joint force estimation in future work.

This project analysed the joint moment loading conditions experienced by the lower-limb during the stance phase of walking and running. Experimental data, including Motion Capture (Mo-Cap) and force-plate measurements, were obtained from a previous study exploring marker-less, machine-learning-assisted motion capture techniques [56]. For this research, data from four of the fifteen available participants were processed, with three participants producing viable data for analysis. For each participant, three gait cycles for both walking and running were analysed, with two stance phases available per gait cycle.

## 4 Literature Review: Current practices in Biomechanical Simulations

Biomechanical modeling software plays a critical role in understanding human movement and internal MSK loading, with applications spanning rehabilitation, sports science, and personalized medicine [40], [41], [57]. One such software is OpenSim, which has emerged as a widely used platform for multi-body MSK simulations, offering tools for scaling MSK models, performing inverse kinematics, and estimating muscle forces [50]. This literature review explores key simulation methodologies used within OpenSim, including raw data acquisition from human subjects, MSK model construction, algorithmic approaches for kinematics and force estimation, and the typical biomechanical simulation workflow. Special emphasis is placed on the numerical techniques underpinning the simulation process, but recent developments in model-personalisation and process methodologies are also explored.

### 4.1 The Biomechanical Simulation Workflow

Whilst there are minor differences in numerical modelling between software packages, most biomechanical simulations typically follow a similar workflow, described in Fig 3. First, a generic MSK model is scaled to match the physiology of the subject being studied. The model is then placed into an Inverse Kinematics (IK) algorithm, where joint angle and displacement data is produced to match the movement of a real subject. If musculoskeletal loading data is desired, this kinematic data is then fed into an Inverse Dynamic (ID) algorithm with any relevant force data applied, producing a set of biomechanical loading conditions for a given movement. Notably, the optimisation algorithms involved in IK and ID can range between platforms, but typically involve optimising for a given objective function [41]. Depending on the type of simulation being run, outputs can vary, but typically include data relating to joint loads and moments, marker kinematics, and delayed neurological action.

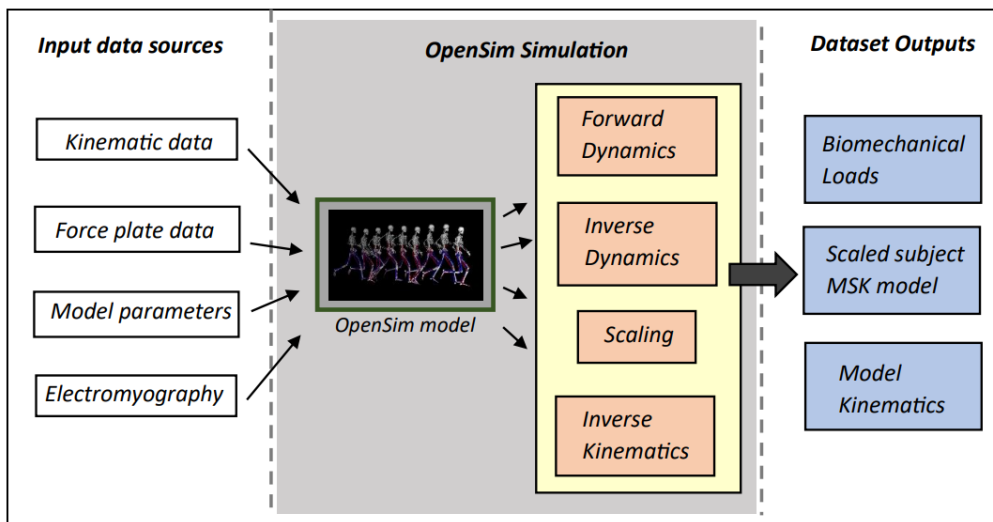


Figure 3: Flow-chart showing the traditional work-flow to biomechanical simulations. Image courtesy of [58] and [59].

## 4.2 Raw Simulation Data

Within biomechanics, subject motion data forms a core foundational input to any MSK simulation [41]. Currently, motion data comes in three notable forms: traditional optics-based Mo-Cap, inertial measurement units (IMUs), and fluoroscopy. Of these, optical methods remain the primary method of motion data collection, with a 2024 literature review noting that out of 113 studies, 86.21% employed optical systems [40].

### 4.2.1 Optics-based Motion Capture: Marker-based and Marker-less Methods

Traditional optical motion capture systems are marker-based, involving placing a series of labelled markers on known anatomical landmarks of a subject (Example in Figure 4) which are then tracked by an array of calibrated cameras [41], [60]. Markers can be classified as 'active' if they directly emit light or electrical pulses, or 'passive' if they are reflective or visually contrasted against a background using colour. Marker-based tracking is one of the most long-standing approaches Mo-Cap, and remains the most widely-used method today [40], [41].

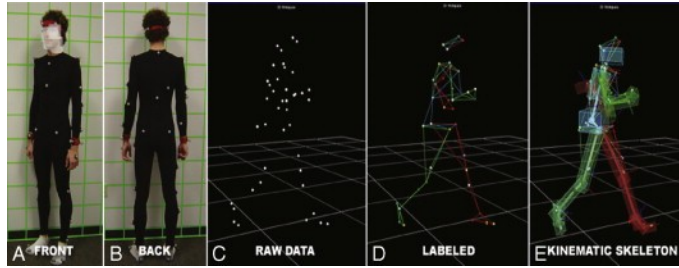


Figure 4: An example of marker-based motion-capture. Image courtesy of [60].

However, despite their widespread use, marker-based tracking presents several limitations. The associated camera equipment is expensive, and data collection requires considerable setup time and operator expertise [40]. Additionally, marker-based tracking is prone to Soft Tissue Artifact (STA) error, where marker motion deviates from true MSK movement due to the compliance of skin and other intermediary tissue [61], [62]. This is especially pronounced at the skin-marker interface [61], and has prompted the development of constrained kinematic models and filtering algorithms to minimise associated errors [63].

In response to these limitations, one solution has been the development of marker-less tracking, often with the use of depth-perception cameras pioneered by the introduction of the Kinect [64]–[66]. This enables for basic kinematic tracking using fewer hardware components and setup costs compared to marker-based methods, but often at the cost of reduced accuracy due to limitations in camera count and resolution. There have also been significant developments in recent years involving the use of machine-learning, incorporating computer vision to automatically estimate joint positions and segment orientations from video data, enabling for motion reconstruction without needing markers [67]–[69].

The reliability of marker-less tracking is still under evaluation, particularly in regards to accuracy, computational cost, and consistency across trials. This is noted in recent literature, where despite highlighting the rapid progression in these techniques [70], [71], there is still a significant trade-off between convenience and biomechanical precision [72]. Consequently, as marker-less systems continue to improve and may become more prevalent in future workflows, marker-based Mo-Cap remains the gold-standard approach in biomechanical research. Its relative accessibility, compatibility,

ity with existing musculoskeletal modelling tools, and the ability to achieve high spatial resolution continue to make it the preferred choice in most current applications.

#### 4.2.2 Inertial Measurement Units

Inertial Measurement Unit (IMU) - based Mo-Cap captures segment kinematics by attaching inertial sensors to the body (Figure 5) and inferring estimated motion from their measured accelerations and velocities. While traditionally seen as significantly less accurate than optical systems, technological advancements have increased their reliability in recent years [73], [74]. Hafer et al. [75] reported that although IMU- and marker-derived inverse kinematics differed in the lower limbs, these discrepancies could be reduced through algorithmic correction. Building on this, Pacher et al. [76] also showed that multibody optimisation pipelines could be adapted for IMU data in patient populations, supporting its use in scenarios where optical systems are less feasible.

Nonetheless, IMU accuracy remains limited, particularly in the transverse and frontal planes. Couvertier et al. [77] confirmed that IMUs still underperform compared to optoelectronic systems, and as such, IMUs are often used as supplementary data sources rather than driving inputs. However, Ahmed et al. [78] recently proposed a fully IMU-driven pipeline using implant-based inputs, marking a promising step toward standalone IMU workflows.

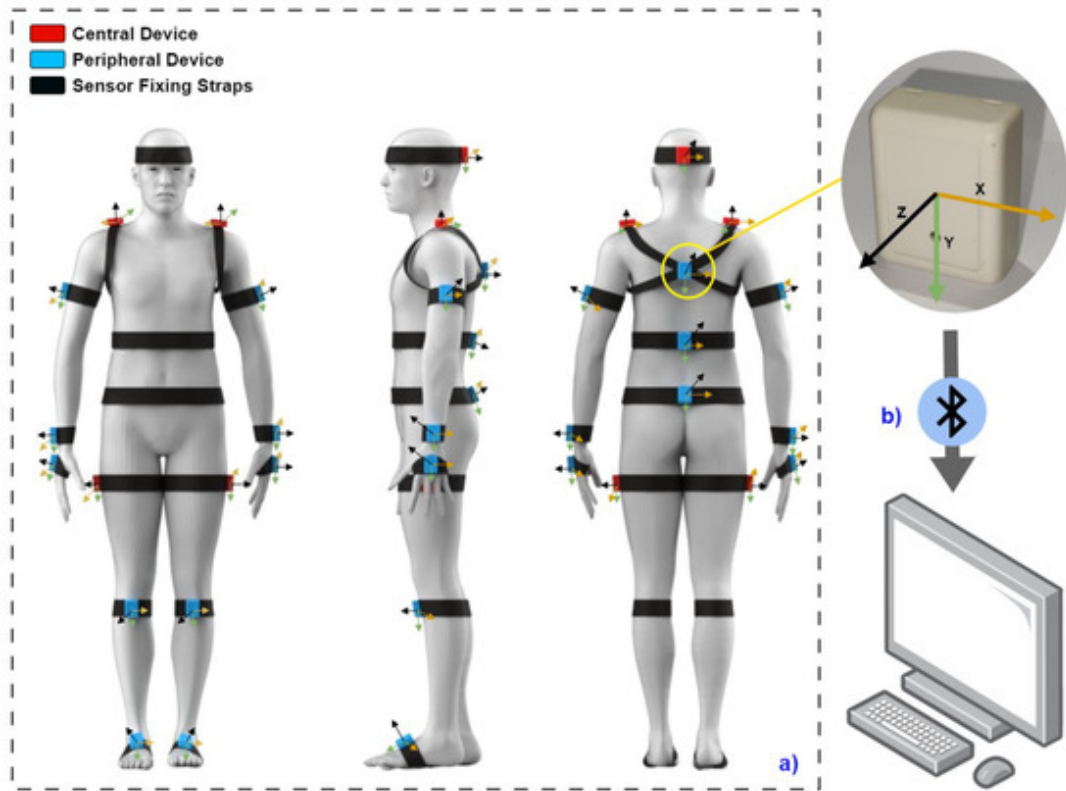


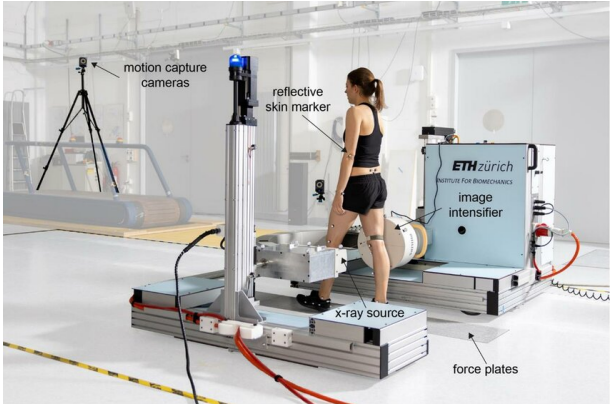
Figure 5: Example of an IMU motion-capture setup. Courtesy of [79].

#### 4.2.3 Fluoroscopy

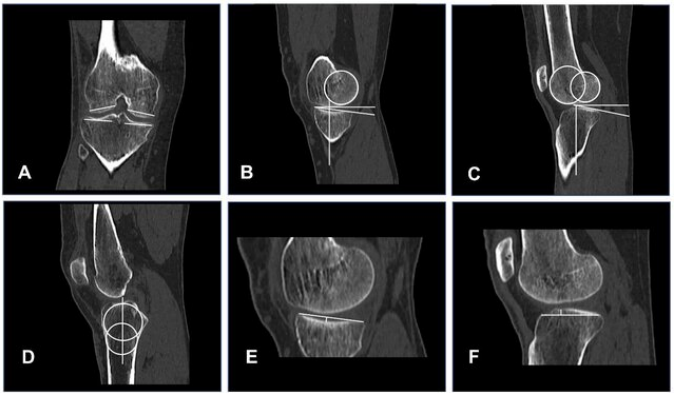
Fluoroscopy (Figure 6) is a medical imaging technique that employs continuous, high-speed X-ray scans, typically around 100 Hz, to capture dynamic motion of the body segment of interest [80]. By registering these 2D scans with a 3D MSK model, fluoroscopy enables precise tracking of internal skeletal motion while maintaining safe levels of radiation exposure [81], [82]. This approach offers

significantly improved accuracy over traditional Mo-Cap techniques, particularly in reducing STA error.

However, fluoroscopy has a fairly limited field of view (with recent advancements noting an area of  $0.5 \times 0.5$  m [83]), and is associated with high levels of technical complexity and setup costs [40]. For this reason, fluoroscopy as a Mo-Cap tool remains uncommon, and is typically used only in specific clinical cases where the area of interest consists of a small number of joints [80].



(a) Fluoroscopy motion-capture setup



(b) Example of a fluoroscopy scan

Figure 6: Example of an experimental motion-capture setup utilising fluoroscopy. Images courtesy of [84].

#### 4.2.4 Forces

Force and moment data is typically recorded via embedded force plates or instrumented treadmills [40]. Force plates are simple to use, and offer good flexibility in how they can be orientated in a given setting. However, given that they typically cover a small area, multiple force plates are often needed for a given study, and their discrete placement often causes unrealistic gait alteration and introduces dynamic inconsistencies [40]. This necessitates the use of corrective algorithms in post-processing to de-noise errors within experiments and ensure compatibility within simulation [40], [85]. Instrumented treadmills form an extension of this, integrating forceplates within the treadmill belt for use in gait study [81], [86]. However, given their specific use-case to gait analysis, they remain somewhat uncommon [40].

#### 4.2.5 Electromyography

The final major source of experimental biomechanics data is associated with neuromuscular activity, where electrical signals from the nervous system are recorded using Electromyography (EMG). This serves as a valuable input to MSK models as a means of increasing physiological accuracy, as well as providing a form of validation of muscle-activation outputs [87].

EMG is inherently limited by its sensitivity to noise from environment and artefacts, as well as errors in measuring several muscles/muscle groups at once [88]. As a result, EMG is very rarely used to drive MSK simulations directly, and instead used as supplementary data to inform simulations [89], guide physiological constraints [90]–[92], or as a form of model validation [41]. EMG has been crucial in the advancement of personalised MSK models, and has been particularly valuable in examining the biomechanical impacts of neurological diseases such as cerebral palsy [93] and Parkinsons [94], in addition to chronic conditions such as lower-back pain [95].

## 4.3 Overview of Musculoskeletal Models

Over the years, numerous human MSK OpenSim models have been developed, including models for specific segments like the ankle [96], knee [97], and lumbar-pelvic joint [98]. Comprehensive lower-body models have also been made [99], in addition to torso-leg configurations tailored for gait analysis [50], and full-body musculoskeletal models [100].

The ability for such a diverse range of MSK models to be developed is in part due to OpenSim's object-based MSK software structure, allowing for bodies and actuators to be added and removed with ease [50]. Over the years, this has allowed for a diverse range of applications, such as simulating physiological surgery [50], modeling prosthetic limbs in amputees [101], [102], and the hind-limb biomechanics of an emu (bird) [103].

MSK models are typically informed by data collected from real-life subjects, often using a combination of Magnetic Resonance Imaging (MRI) scans and cadaveric data [41]. To be simulated, MSK models must incorporate various assumptions to reasonably function, such as cylindrical and ellipsoidal wrapping surfaces [87], single Degrees of Freedom (DOF) joints, and slipless contact interfaces [41]. Consequently, given their idealised nature, MSK models have strengths and limitations depending on the study context, and it is not uncommon for specialised MSK models to be developed for the analysis of specific movement tasks [104]–[106]. As such, whilst every model has limitations influenced by the specifications of its design [41], selecting the appropriate model can enable for biomechanical results to be derived with encouraging accuracy [40], [50].

Given the limited resources of this project, MSK selection was limited to the default full-body models readily available within OpenSim. These included the Full Body Running Model (FBRM) developed by Hamner [107], the Rajagopal model designed for gait-analysis [100], the Lai et al. model [108], and the Full Body FBM16 model introduced by Caruthers [109].

### 4.3.1 Default Models in OpenSim

In 2017, Roelker et al. [110] conducted a comparative analysis of lower-limb joint loading in four models including the FBRM, and FBM16, revealing a positive correlation between model complexity and sensitivity, with simpler models being less sensitive to high-noise data. It was found that FBM16, being the most complex, had the most discrepancy between measured and simulated values.

The Rajagopal model (Pictured in Figure 7), while not featured in the Roelker study, shares structural lineage with both FBRM and FBM16. Specifically, it was geometrically simplified for computational efficiency by replacing elliptoidal-wrapping with cylindrical-wrapping (Figure 7.c) [100]. Comparative studies focused on specific joints in this model have yielded mixed results, with Curreli et al. [111] reporting the Rajagopal model to be the most accurate for predicting tibiofemoral joint reaction forces at the knee, and Mathai and Gupta [112] reporting the LLLM model to be most accurate for hip dynamics analysis.

## 4.4 Scaling and Inverse Kinematics

### 4.4.1 Scaling

Traditionally, MSK scaling methods can be categorised into three groups (Table 1 [41]). Type-I scaling involves the direct measurement of the subject's proportions, typically with the use of a tape-measurer, before geometrically scaling the MSK properties to match them. Type-II scaling is algorithm based, looking to minimise the residual errors between markers on the MSK model and the real subject (Eq. 1 shows the Residual Reduction Algorithm (RRA) equation, used by

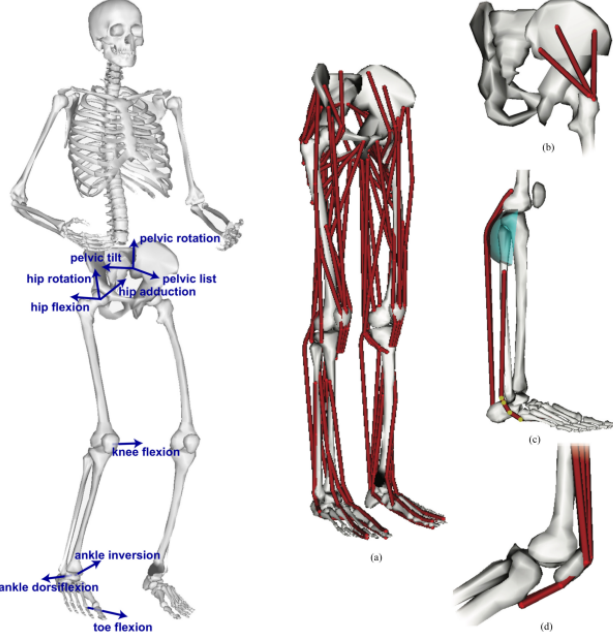


Figure 7: The Rajagopal MSK model. Image courtesy of Rajagopal [100].

the OpenSim scaling tool, where  $x$  denotes displacements,  $\theta$  denotes joint angles, and  $w_i$  and  $w_j$  represent weight factors for markers and joints respectively [50]). Finally, Type-III scaling involves the use of medical imaging, typically via Computed Tomography (CT) or MRI scans.

Type	Description	Tools
I	Direct anthropometric measurement	Tape measure
II	Algorithmic matching of markers	OpenSim Scaling Tool
III	Imaging-based (CT/MRI)	Finite Element Integration

Table 1: The three main scaling methods used in musculoskeletal modeling [41].

Type-I scaling, whilst cheap and easy to implement, tends to lead to the most significant scaling error of the three [40], [41]. Type-II scaling improves on this [40], but is in turn dependent on accurate and well-documented marker placement on the body (typically placed on bony landmarks), often making it resource-intensive. Type-II scaling within the modelling workspace is also often labour-intensive, involving an iterative process of manually adjusting markers within the OpenSim workspace to better match the real subject, although there have been efforts to automate this process [113]. Of the three categories, Type-III scaling produces the most physiologically accurate models, but is extremely labour-intensive, expensive, and technically demanding [41]. Throughout literature, Type-II methods are the most common, with a 113 study review [40] reporting that about half (52.69%) used Type-II, 26.72% used Type-I, and 8.62% used Type-III.

With the various limitations associated with current scaling methods [114], there has been an interest in automating the scaling process, particularly in the case of Type-II and Type-III scaling [115]. However, this remains an ongoing area of research, and currently remains uncommon [40], [115].

$$\text{Squared Error} = \sum_{i=1}^{\text{markers}} w_i \left( x_i^{\text{subject}} - x_i^{\text{model}} \right)^2 + \sum_{j=1}^{\text{joint angles}} \omega_j \left( \theta_j^{\text{subject}} - \theta_j^{\text{model}} \right)^2 \quad (1)$$

#### 4.4.2 Inverse Kinematics

Like Type-II scaling, Inverse Kinematics IK is a redundant problem, and is typically solved by minimising some weighted sum of residual displacement and angle errors (as denoted in Eq. 1) between the MSK model and the real-life subject. By repeating this process at a set of time frames for a given motion, the musculoskeletal model can be made to replicate the subject's movements [50], [116].

### 4.5 Estimating Muscle Force

In biomechanical modelling, the key numerical challenge in estimating individual muscle forces is that the multi-body MSK system is a severely over-constrained problem [41]. That is, there are significantly more unknown values (muscle-generated forces and torques) than degrees of freedom (Equation of Motion (EOM)s). Consequently, individual muscle forces cannot (currently) be solved analytically without some form of numeric simplification. (For reference, the London Lower Limb Model (LLLM) [99], representing the hip and two lower limbs, models 38 muscles to account for 16 DOFs.)

To compensate for this, various numerical approaches have been developed to solve for MSK loads, with notable algorithms being static optimisation, advanced static optimisation, forward dynamics, computed-muscle control [50], and EMG-driven solutions [41], [117], [118]. However, depending on the type of simulation being run, these approaches have various strengths and limitations associated with them.

Typically, deriving a numerical solution for the dynamic MSK system involves modelling it as a rigid, multi-body system and assuming that muscle is recruited in the most optimal manner for a given action [41], [65]. This formulation is then solved as an inverse dynamics problem, in which a cost function is defined (typically to be minimised) whilst maintaining dynamic equilibrium throughout the system. This is represented in Eq. 2, where  $H$  represents the cost function to be minimised [41].

$$\min H(\mathbf{f}^{(m)}) C\mathbf{f} = M\dot{\mathbf{v}} + \mathbf{b} - \mathbf{g}^{(\text{app})}, \quad \text{subject to} \quad 0 \leq \mathbf{f}^{(m)} \leq \mathbf{s}^{(M)} \quad (2)$$

Various optimisation criterions have been presented over the years to define  $H$ , such as the min-max criterion [65], the soft-actuation criterion [65] and the polynomial criterion [65]. However, there is ongoing debate as to whether optimal-muscle recruitment is a fair assumption to make in biomechanical modelling, and if so, which criterion is most accurate [41], [65]. For example, there is evidence that optimising for minimum joint loads may be more accurate in modelling osteo-arthritis patients [55], whereas minimising for co-activation may be favourable for representing the elderly [119].

#### 4.5.1 Static Optimisation and the Polynomial Criterion

Of the various criterions proposed for  $H$ , the most extensively used throughout literature is the polynomial criterion with a second- or third-order exponent (denoted as  $p$  in Eq. 3) [41].

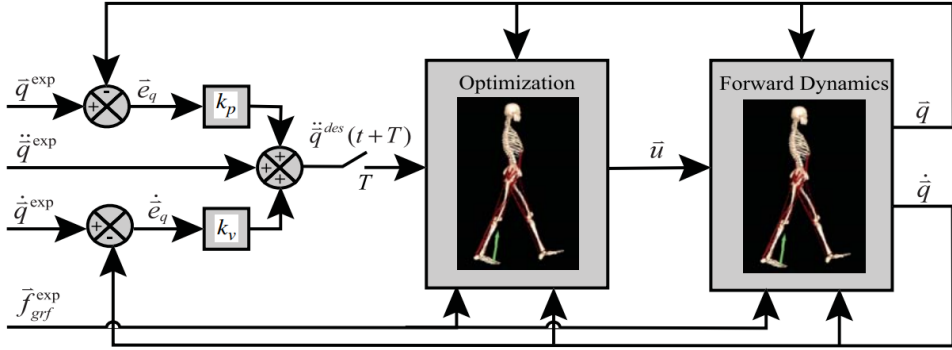


Figure 8: Flow-chart representing Computed Muscle Control. Image courtesy of [121].

$$H(\mathbf{f}^{(M)}) = \sum_{i=1}^{n^{(M)}} \left( \frac{f_i^{(M)}}{s_i^{(M)}} \right)^p \quad (3)$$

Whilst widely used, the polynomial criterion is limited in that it depends heavily on accurate physiological characteristics [87], [120], typically measured from cadavers, and it has also been critiqued for having limited kinematic accuracy due to its simplified representation of passive muscle forces [55], [120]. However, whether these limitations have significant effect compared to other sources of error remains an open question [41].

#### 4.5.2 Computed Muscle Control

Static-Optimisation (SO), in its root form (Eq.3), allows for muscle activations and forces to be solved for a system at a given time. That is, muscle forces are derived using force-length and force-velocity assumptions using data captured from inverse kinematics, and dynamic properties of the system are ignored [55]. By ignoring previous and future time-steps in a simulation, SO can be a computationally efficient process compared to other integrative methods.

However, in ignoring dynamic properties such as activation dynamics and tendon compliance (how far tendons stretch for a given force), SO is limited in its ability to model high-acceleration or transient-state behaviour. Within OpenSim [50], this limitation can be partially addressed using the built-in Computed Muscle Control (CMC) tool developed by Thelen and Anderson [121].

Computed Muscle Control (CMC) differs from traditional static optimisation in that it solves a dynamics problem using a proportional–integral–derivative (PID) control law, considering both past and future timesteps (represented in Figure 8). This allows for it to account for more complex neuromuscular phenomena compared to traditional SO, such as activation delays, passive muscle forces, and motion tracking error [121], [122].

As a result, CMC tends to return more physiologically accurate steady-state muscle force predictions than SO [120], but at the cost of significantly greater computational cost and increased sensitivity to noise. This sensitivity can be mitigated through filtering and de-noising techniques, but remains a known challenge [55], [121]. These differences between CMC and SO highlight the need of appropriate method selection based on the biomechanical application, where SO may be sufficient for large-batch simulation processing or low-acceleration cases, but CMC may be more suitable for high-acceleration movements if there is specific need for high accuracy.

#### 4.5.3 The Biology of it all: The Muscle-Tendon Unit

The foundational mechanics of muscle–tendon behavior within biomechanical modelling is largely based on research published by Hill in 1938 [122], [123], which was derived primarily from cadaveric experiments. While various refinements have been proposed to the model since then, the core principles of the Hill-type muscle model have remained largely unchanged [124]. The standard Hill Muscle-tendon model (Represented in Figure 9) is defined by four primary parameters: optimal fiber length, maximum isometric force (typically estimated from muscle cross-sectional area), pennation angle, and tendon slack length [41]. Furthermore, to represent dynamic muscle behavior such as activation dynamics and neurological delays, most simulation frameworks build on the work of Zajac in 1989 [122], with research into neuro-muscular properties such as co-activation and muscle synergies being an ongoing area of development [55], [125], [126].

In OpenSim, it is worth noting that optimal fiber length and muscle slack length are scaled linearly during the MSK scaling process, whereas maximum isometric forces are not. This is because due to the reliance on physiological measurement, and represents a known limitation of the Hill-Type model [127]. However, by addressing this parameter during the scaling process, highly-accurate results can still be produced [41], [127].

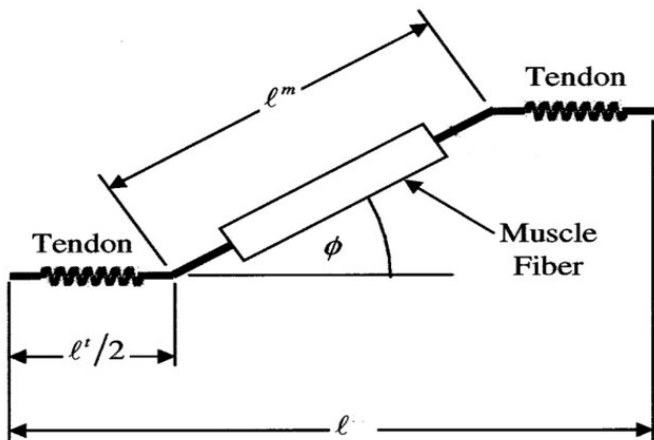


Figure 9: A diagram the typical Hill-type muscle-tendon unit, showing the relationship of muscle-tendon length, muscle fiber length, tendon length, pennation angle. Where  $l$  is the muscle-tendon length,  $l_m$  is the muscle fiber length,  $l^t$  is the tendon length,  $\phi$  is the pennation angle. Image courtesy of [128].

### 4.6 OpenSim-aided Workflows and Other Algorithms

#### 4.6.1 Developing Workflows

As OpenSim continues to develop, so has the variety of OpenSim-aided workflows. On the front-end, OpenSim’s OpenSense [129] and Moco [130] offer toolsets for real-time musculoskeletal (MSK) simulation using inertial measurement unit IMU data [131], [132], and hybrid workflows incorporating live EMG and motion capture (Mo-Cap) data are also being actively explored [40], [133].

On the back-end, the integration of FEM bone models with biomechanical simulations is also becoming increasingly common. Examples of FEM-OpenSim workflows can be found knee [134], tibia [135], [136], as well as other joints such as the hip [137]–[139] and ankle [140], [141]. However, FEM-aided simulations provided valuable tools for MSK analysis, but are computationally and technically

complex, requiring subject-specific anatomical data from CT or MRI scans and often target highly localised areas [40]. Regardless, advances in imaging and processing capabilities continue to make such methods more accessible, and will likely play a role in advancing future research.

#### 4.6.2 Other Algorithms

Whilst beyond the scope of this project, it is also important to note the range and rapid pace of algorithmic development within the OpenSim workspace. These include tools for estimating metabolic cost [50], [142], performing trajectory optimisation [143], and defining various conceptual optimisation criteria for biomechanical modelling [144], [145]. Notably, machine learning is becoming an increasingly influential area within algorithms, with applications spanning motion tracking [56], [68], scaling, inverse kinematics, and EMG integration [146]–[148]. With its capacity for rapid personalisation and automation, machine learning presents a promising tool in the development of all methodological stages in the Opensim workflow.

### 4.7 Literature Review Summary and Implications

This literature review examined the various methodologies and tools used in biomechanical simulations, particularly focusing on the numerical approaches used within OpenSim. From the acquisition of raw data to MSK model construction and estimation of muscle forces, the available methodologies within each component of the simulation pipeline play a role in affecting the overall quality of experiments.

In motion capture, optical methods remain the dominant standard, although IMUs and markerless approaches are gaining traction. Similarly, while generic MSK models have proven effective, there is an interest in moving towards personalised, EMG-informed simulations for improved accuracy, and automating such processes. Current research reflects a growing interest in validating and enhancing simulation outputs through hybrid data sources and algorithmic refinements, and machine-learning has particularly been a notable contributor in aiding this. As musculoskeletal modeling continues to evolve, future developments are expected to further continue improving on technical efficiency whilst progressively adding improvement to physiological detail.

## 5 Methodology

### 5.1 Overview

This section covers the methodology section of this study, detailing the process by which raw Mo-Cap data used to run OpenSim simulations to generate joint moment outputs for the lower limb. Specifically, joint moments at the hip, knee, and ankle were of interest during the stance phase of two gait movements; walking and running.

### 5.2 Raw data

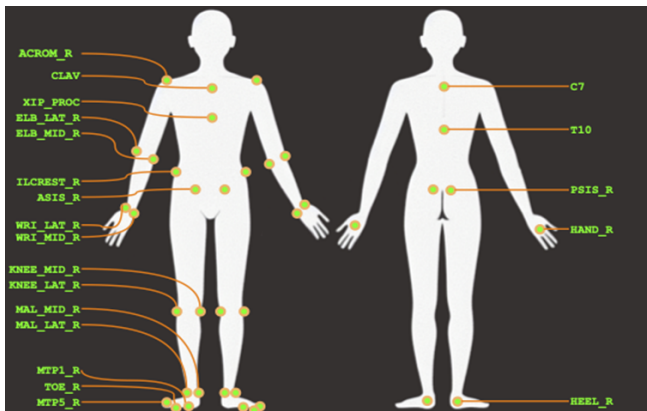
#### 5.2.1 Source Description

Raw Mo-Cap and force-plate data for this study was sourced from a biomechanics database associated with a previous project conducted by [56], centered on developing a marker-less Mo-Cap system. This dataset included both marker-based and marker-less Mo-Cap data for a variety of movement trials such as walking, running, and jumping, for fifteen healthy participants (7 males and 8 females).

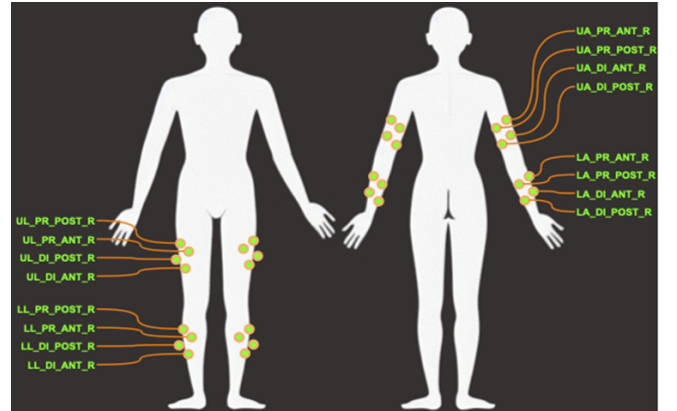
Mo-Cap data from this database came in three main forms:

- HD colour video from a 9-camera machine vision system
- Marker tracks from a 200 Hz optical Mo-Cap system synchronised with the video system
- Analogue force-plate data from floor-embedded force-plates, recorded at 1000 Hz

Participants were recorded performing multiple repetitions of each movement while wearing a full set of 70 markers, illustrated in Figure 10, to enable marker-based motion tracking. This was later repeated without markers to support marker-less tracking validation. For each trial, Mo-Cap and force-plate data was stored in the standard C3D file format in concordance with [149], [150]. For full documentation of this data base, refer to the original source [56].



(a) Marker locations for joint clusters



(b) Marker locations for arm and leg clusters

Figure 10: Marker locations for motion capture. Images courtesy of [56].  
For a list of markers refer to Appendix B.

### 5.2.2 Participant Selection

Of the fifteen available participants, four were selected for use in this study. This comprised of two males and two females (information shown in Table 2), with gender balance prioritised to avoid missing intricacies associated with sex. Whilst evidence of neuro-activation delay differences across gender remain minimal [151], sexual dimorphism, particularly in the pelvis/hip, is notable [152]. This has been reported to significantly influence gait and joint kinematics, with females on average showing a greater anterior pelvic tilt when walking (approximately 4° in the sagittal plane compared to near-neutral in males [153]). The result of this tilt has been studied to affect pelvis Joint Reaction Force (JRF) differences across gender [153]–[155], underscoring the need to consider gender-specific anthropometrics during MSK modelling.

Using participant weights and statures (Table 2), Body Mass Index (BMI)s were calculated as medically defined in [156], with two participants classified as overweight and two normal. Although significantly high BMI values have been shown to affect JRFs and muscle activation patterns [157], [158], it has been noted that this does not directly compromise simulation validity compared to healthy-weight individuals [159]. However, this does not negate the potential effects of STA error, highlighting the importance of accurate scaling [61].

Finally, whilst age-related changes in neuromuscular coordination and gait have been reported throughout literature [119], [160], [161], these effects are generally considered to only become significant in individuals over 50 years of age. Given that all selected participants were aged between 24 and 38 years, age-related variability was deemed negligible for the purposes of this study as the MSK model used was based on physiological data from individuals of similar ages [100], [162]. More information on this MSK model can be found in Section 5.3.1.

Table 2: Participant Data

Participant ID	Age (Years)	Sex	Weight (kg)	Stature (m)	BMI
P03	28	M	91.7	1.89	25.7 (OW)
P06	24	M	77.4	1.68	27.4 (OW)
P10	38	F	57.8	1.66	21.0 (N)
P13	30	F	72.8	1.76	23.5 (N)

*BMI category: (N) = Normal, (OW) = Overweight*

### 5.2.3 Selected Movement Trials and Pre-Processing

In total, this study analysed data from 28 trials in the [56] dataset (Refer to Table 3 for list), corresponding to one static trial, three walking trials, and three running trials for each participant (For the list of corresponding filenames used, refer to Appendix E). Walking and running trials included kinematic and force plate data for one complete gait cycle (see Figure 11), as well as kinematic data spanning between two to six gait cycles. Due to the novelty of the marker-less Mo-Cap techniques used in this database, marker-less trials from this dataset were not considered for this study, and instead marker-based trials were chosen to allow for comparison across published literature.

Walking and running movements were selected for analysis due to the extensive body of OpenSim literature on gait analysis, allowing for results comparison [40]. Trials for the 'hop' and 'counter-movement jump squat' movements were also considered, but scope-limitations, had to be excluded.

Table 3: Dataset Trials used in this study (per participant)

Trial Type	Number of Trials
Static	1
Walking	3
Running	3

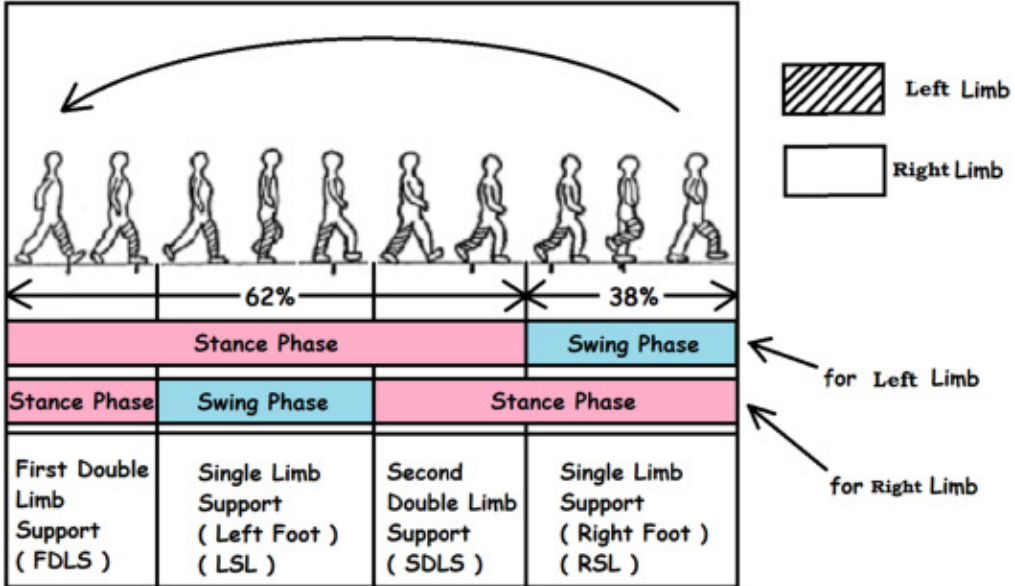


Figure 11: The annotated gait-cycle. Image courtesy of [163].

To prepare data for simulation, C3D files corresponding to each trial were processed using the "*c3dExport.m*" MATLAB script included within the OpenSim API [50]. This used the raw C3D data to generate marker (.trc) and force .mot files as required for use in OpenSim.

### 5.3 Musculoskeletal Model Selection and Scaling

#### 5.3.1 Model Selection: The Rajagopal Model

For this study, the Rajagopal model (Pictured in Figure 12) was chosen for its relative computational efficiency and widespread use in lower-limb gait analysis [100]. Originally developed for full-body gait analysis, the model was designed to address the long computation times commonly associated with previous models whilst maintaining simulation accuracy.

To achieve this balance between MSK complexity and efficiency, the model incorporates several simplifications. The knee is modelled with a single degree of freedom (extension/flexion), and the head and torso are treated as a single rigid segment [100]. Upper limb anatomy is also greatly simplified, making it suitable for tracking gross upper-body motion, but not for detailed upper-limb analysis [100]. Computational costs were further reduced by modelling 17 of the 40 lower-limb muscles in each leg with rigid tendons [164], and using cylindrical wrapping surfaces rather than the ellipsoidal geometries associated with earlier models (Refer to Figure 12.c to view cylindrical wrapping) [100], [40], [41].

Overall, the model comprises of 80 Hill-type muscle-tendon units actuating the lower limbs and 17 ideal torque actuators driving the upper body. Its musculotendon parameters were derived from

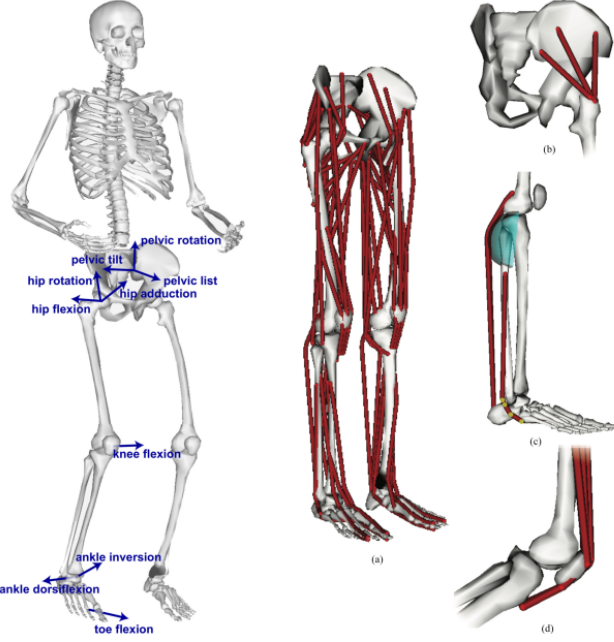


Figure 12: The Rajagopal Model. Image courtesy of [100].

a combination of MRI and cadaveric data collected from 24 young adults, shown to Table 4 for participant data [162], offering a more representative anatomical basis than most earlier models, which often relied on anthropometric data from single or predominantly male subjects [40], [100].

Table 4: Cadaveric data used to inform the Rajagopal MSK model [100], [162].

Characteristic	Mean $\pm$ SD	Range	Units
Age	$25.5 \pm 11.1$	12–51	years
Height	$171 \pm 10$	145–188	cm
Body mass	$71.8 \pm 14.6$	47.5–107.0	kg
BMI	$24.3 \pm 4.0$	18.9–35.1	$\text{kg}/\text{m}^2$
Sex distribution	8 females, 16 males	—	—

### 5.3.2 Scaling

Prior to scaling, an *.xml* file was created to define the marker set based on the list of markers documented in [56] and the body-map provided in Figure 10. Each marker was assigned to the parent body frame corresponding to the closest anatomical bone represented in the Rajagopal model, with foot markers defined relative to the calcanei, thigh markers to the femur frame, etc. (For a complete list of markers and their corresponding parent frames, see Appendix B). Finally, wrist flexion and wrist deviation were locked at  $0^\circ$  for the remainder of this study, as were the subtalar and metatarsal-phalangeal joints, replicating the methodology outlined in [100]. This was done to avoid noise in these DOFs, as they were unlikely to be captured with enough video accuracy by the Mo-Cap methods outlined in [56], [100].

Scaled models were then produced for each subject (with an example model in Figure 13) using the OpenSim scale tool [50], using each subject’s body-weight and static trial marker file to initiate scaling. Markers on the thigh, shank and lower extremities were weighted heaviest for scaling with an arbitrary relative weighting of 5.0, while markers on the torso and upper limbs were weighted

3.0 and 1.0 respectively. This was done to prioritise lower-limb accuracy as this was the area of interest in this study, with further documentation on weights and scaling provided in Appendix C.

Table 5: Measurement marker pairs used for MSK scaling using the OpenSim Scaling Tool

Marker Pair		
Measurement	Marker 1	Marker 2
Pelvis	ILCREST_R	ILCREST_L
Tibia	KNEE_LAT_R	MAL_LAT_R
	KNEE_LAT_L	MAL_LAT_L
	MAL_MED_R	KNEE_MED_R
	MAL_MED_L	KNEE_MED_L
Femur	KNEE_LAT_R	ILCREST_R
	KNEE_MED_R	ILCREST_R
	KNEE_MED_L	ILCREST_L
	KNEE_LAT_L	ILCREST_L

To ensure anthropometric scaling, scaling factors for the pelvis, femur and tibia were initiated using relative distances for certain markers (Refer to Table 5 and Appendix C.2). This was to ensure that individual anthropometric proportions were captured, noting that the default proportions of the Rajagopal model were for a 73 kg, 1.76 m tall male [100], and proportionate scaling may not be appropriate, particularly for the female subjects [152].

In an iterative process, markers on the unscaled model were adjusted manually and then compared to the markers in each participant’s static trial. This was done until the overall Root-Mean-Square (RMS) scaling error was below 0.04 m and the maximum marker error for all lower limb markers were less than 0.05 m. These values were chosen based on the recommendations provided in the tool’s official documentation [165], [55].

### 5.3.3 A Comment on Automated scaling and Scaling Error

It should be noted that in an effort to reduce scaling error, various automatic scaling methods were explored. However, it was found that most of the available options were developed in Python or C++, requiring technical expertise beyond the scope of this study, which was conducted using MATLAB. Given this limitation, the only suitable tool identified was the OpenSim Automatic Scaling Tool (AST) toolbox developed by Di Pietro et al. [113].

However, while the AST toolbox aligned with the technical requirements of this study, it did not yield reliable results in practice. Specifically, when initial marker placements differed significantly from target locations, the optimisation algorithm exhibited exponential divergence, failing to converge. In response, the section of code responsible for this behaviour was identified, and a proposed amendment to introduce a damping component to the algorithm is documented in Appendix D. Unfortunately, due to time constraints, this modification could not be fully tested or validated and as such, automated scaling was ultimately abandoned in favour of the traditional, manual approach described earlier.

Another scaling method that was trialled was using the pre-processing Python-based scripts provided in the original dataset [56]. However, these scripts were originally designed for Linux environments and relied on shell commands and file path conventions incompatible with Windows systems

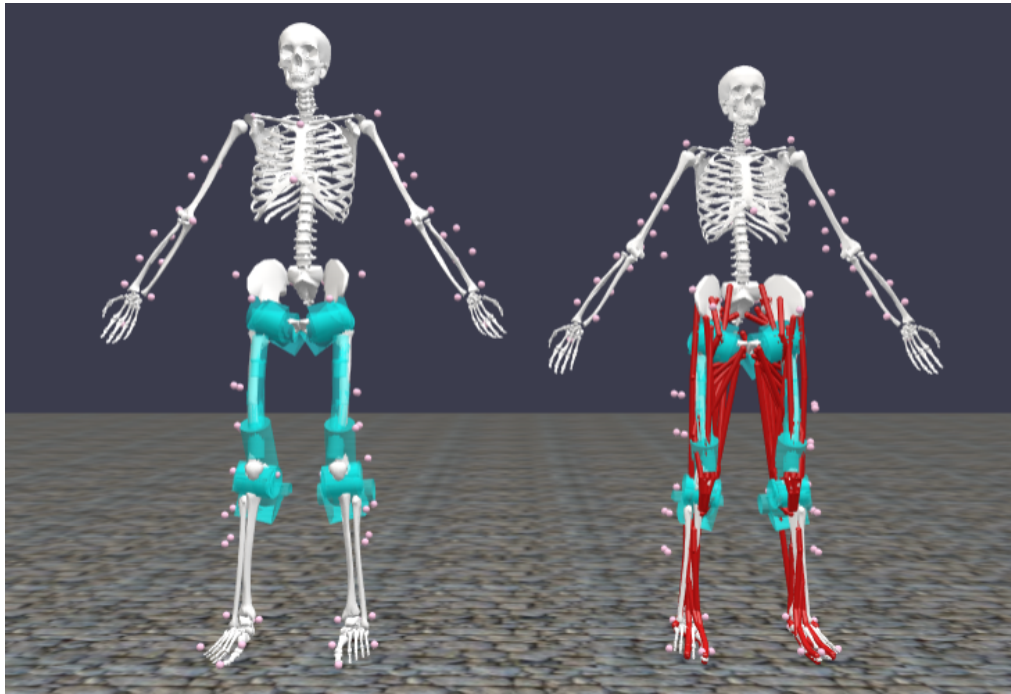


Figure 13: generic Rajagopal model (left) and scaled P10 model (right) taken in the OpenSim workspace.

that this study used. Adapting them for use in this project proved unfeasible within the given time-frame, and they were likewise set aside.

## 5.4 Inverse Kinematics

After scaling, inverse kinematics (IK) was performed using the OpenSim IK tool [50] for each movement trial and each subject, producing a total of corresponding 24 MSK motion files (note that static trials were excluded from this step). As with scaling, lower limb markers were assigned higher weightings than those on the torso and upper limbs to prioritise them during the IK optimisation process. This marker weighting scheme, identical to that used during scaling, is detailed in Appendix C.2.

## 5.5 Muscle Force Estimation

Muscle force estimation was then carried out using two methods within the OpenSim workspace: the static optimisation tool and the CMC tool. For further detail, refer back to Section 4.5.

### 5.5.1 Static Optimisation

Static optimisation was done using a second-order polynomial objective function (Shown in Eq.4, where  $p$  is the order). Motion files generated by the IK tool previously were used to guide the simulation, filtered at 6 Hz to limit noise [55], [166]. Static optimisation was done at every step for a time window of approximately 0.5 s before the first heel strike on a force plate to 0.5 s after the final toe-off (e.g. if first force plate heel-strike occurred at approximately 2.1 s and final toe-off at 2.6 s, then the static optimisation time window was set to 1.6 - 3.1 s. )

$$H(\mathbf{f}^{(M)}) = \sum_{i=1}^{n^{(M)}} \left( \frac{f_i^{(M)}}{s_i^{(M)}} \right)^p \quad (4)$$

The model was then appended with the ideal reserve actuators provided with the default Rajagopal model documentation [100], and external force and moment loads from the force plates were applied to the calcanei of their respective limbs as noted in Appendix F. It should be noted that this approach represents a simplification, omitting (STA) under the calcanei and any footwear worn by the subject, and assumes a single-point contact at the calcanei throughout stance. Figure 14 shows an example of a scaled 5.3.1 associated with Ground Reaction Force (GRF) data.

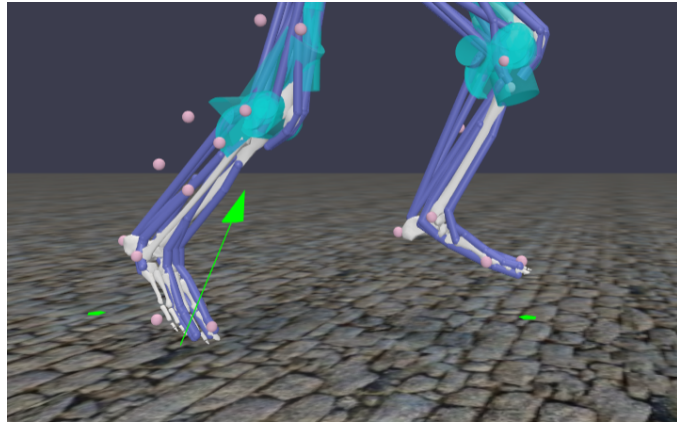


Figure 14: Visual representation of associating force plate data within the OpenSim workspace.

### 5.5.2 Computed Muscle Control

Finally, MSK forces were estimated using the OpenSim CMC tool in order to account for the dynamic factors not considered during static optimisation [50], [121]. In an analogous manner to static optimisation setup, motion files from inverse kinematics were used as the desired motion file and filtered at 6 Hz. Time windows were set to  $\pm 0.4$  s of first heel-strike and final-toe off (note the shorter time interval than that used in static optimisation), and the CMC look-ahead window (i.e. the numeric integration interval) was set to 0.01 s. Integration settings were left as the default OpenSim values and can be found in Appendix G.2.

Default CMC reserve actuators [100] were then appended to the model, and external loads were applied to the model's calcanei as before in static optimisation. Finally, CMC was set up using a modified version of the default Rajagopal tracking tasks, in which weights were adjusted to prioritise accurate lower limb motion over other degrees of freedom. A full list of these changes is provided in Appendix G.3.

## 6 Results and Analysis I: Scaling and Inverse Kinematics

### 6.1 Scaling

Scaling was performed iteratively using the OpenSim Scale Tool to align the generic Rajagopal MSK model to participant anthropometry based on static trial marker data. Table 6 summarises the results, including RMS marker errors and the largest individual marker mismatch for each model. While all RMS errors remained within acceptable thresholds ( $< 0.04$  m), several trials exhibited localised outliers, particularly in the lower arm and elbow regions, likely due to soft tissue artefact or suboptimal marker placement. However, as the focus of this study was on lower-limb biomechanics and further manual adjustment did not yield improvements, these discrepancies were considered acceptable.

Table 6: Musculoskeletal (MSK) model scaling results.

Participant ID	Weight (kg)	RMS Error (m)	Maximum Marker Error	
			Marker	Value (m)
P04	91.7	0.0250	KNEE_MED_L	0.0398
P06	77.4	0.0364	ELB_MED_L	0.0820
P10	57.8	0.0388	LA_PR_POST_R	0.0737
P13	72.8	0.0381	ELB_LAT_R	0.0777

### 6.2 Inverse Kinematics

Inverse kinematics (IK) was then performed using OpenSim IK Tool to compute joint angles and marker positions that best matched the experimental marker trajectories from dynamic trials. IK relies on the same underlying least squares optimisation approach as scaling [50], minimising marker position errors frame by frame for a given MSK model. Due to this similarity, the quality of the IK results is largely dependent on the accuracy of the prior scaling step and no further tuning or marker weighting adjustments were applied beyond those already set during scaling.

Quantitative error reporting from IK is typically redundant given the similarity to scaling outputs. Nonetheless, marker RMS and maximum marker errors during IK remained within acceptable bounds ( $< 0.04$  m and  $< 0.05$  m respectively), and visual inspection of joint motion trajectories confirmed that reconstructed kinematics were smooth and biomechanically plausible. Consequently, IK results were not analysed further.

## 7 Results and Analysis II: Biomechanical Moments Analysis

### 7.1 Overview

The following section reports the results of biomechanical moment analysis for both walking and running conditions, focusing on the hip, knee, and ankle joints across participants. Specifically, moments analysis was done during the stance (foot-on-ground) phase of the gait cycle, when lower-limb joints experience significantly more loading than in swing during walking gait [167], [168]. For each exercise condition, moment loading patterns were first examined in aggregate across all trials and participants. This was followed by a closer analysis of hip joint moments (DOFs labeled in Figure 16a), as well as separate examinations of knee and ankle moments to assess how simulation quality varied across the musculoskeletal DOFs.

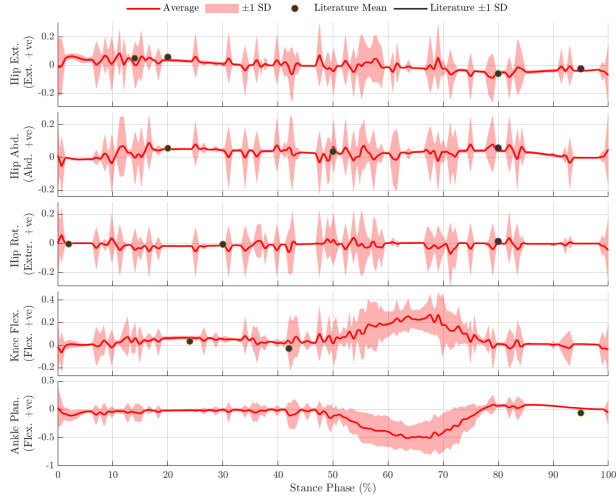
During analysis, all biomechanical moments were normalised to participant body weight and height and time-normalised over the stance phase to enable consistent comparisons across participants and trials. During data processing, ‘Stance’ was defined as ‘the continuous period over which when force-plates measured vertical forces exceeding 10 N’ (As common in studies of this type [85], [169]–[171]). Each simulation included two stance phases (one heel-strike and toe-off per limb), and each participant completed three trials per exercise condition, yielding up to six stance phases per participant, per exercise. This provided a sufficient sample size to support more robust statistical analysis, detailed later in Section 8. Selected outputs were also compared against published literature as a form of qualitative error assessment.

Data was processed using a combination of gradient-based and median-tolerance filtering. First, excessively noisy points were identified using a gradient threshold, with affected points removed and interpolated over to maintain continuity. Thereafter, remaining outliers were excluded by calculating median moment values over the stance phase and removing points exceeding a predefined tolerance relative to the median. Full details of the filtering parameters are provided in Appendix I, and examples of plots before and after cleaning are provided in Figure 15.

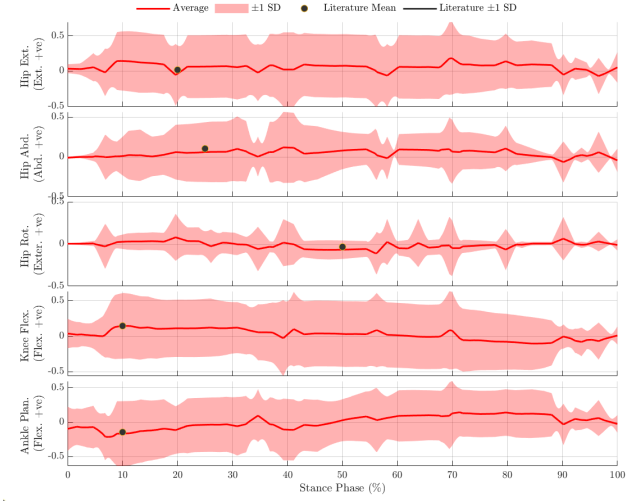
Overall, walking simulations consistently produced higher-quality and more stable results than running. Walking trials showed smoother moment profiles with relatively low inter-trial variability across participants and required less aggressive denoising. In contrast, running simulations were significantly more variable across all participants and joint degrees of freedom, with increased noise, less consistent moment patterns, and pronounced variability in peak magnitudes and timing, particularly at the knee and ankle joints. Frequent oscillations of large amplitude were also observed in the running data, often in the orders of magnitude.

Due to these challenges, several running trials were excluded from statistical analysis, as outlined in Section 7.2, with Participant 10’s running data was removed entirely from aggregate analysis, and instead provided in Appendix J. As a result, walking trials may represent a more viable dataset for interpreting overall joint loading patterns, while running results are presented cautiously to highlight general trends within this study.

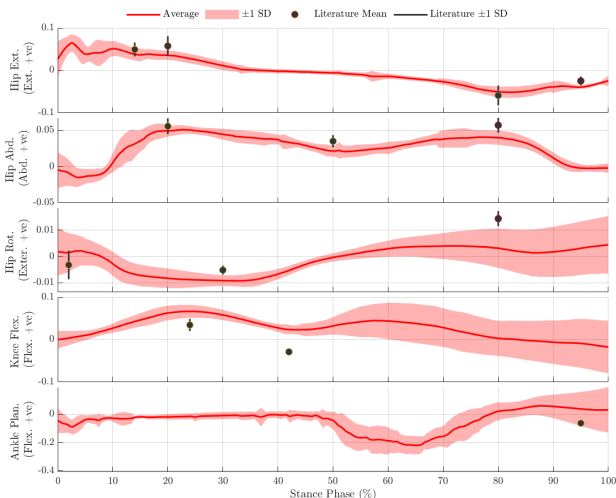
The subsections that follow are organised by exercise condition, beginning with aggregate results and proceeding to joint-specific and participant-level analyses.



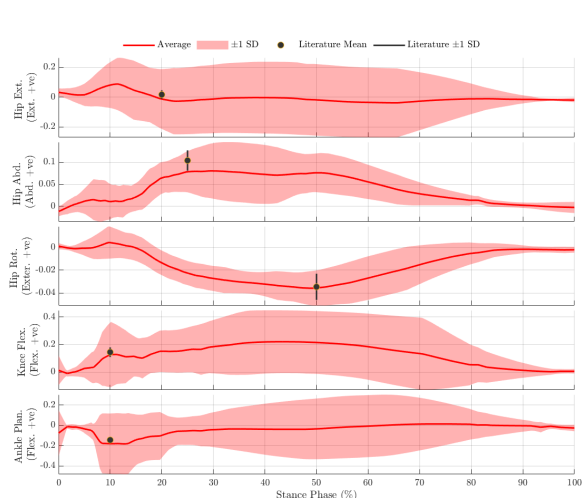
(a) Unfiltered aggregate moment plots for walking exercise condition.



(b) Unfiltered aggregate moment plots for running exercise condition.

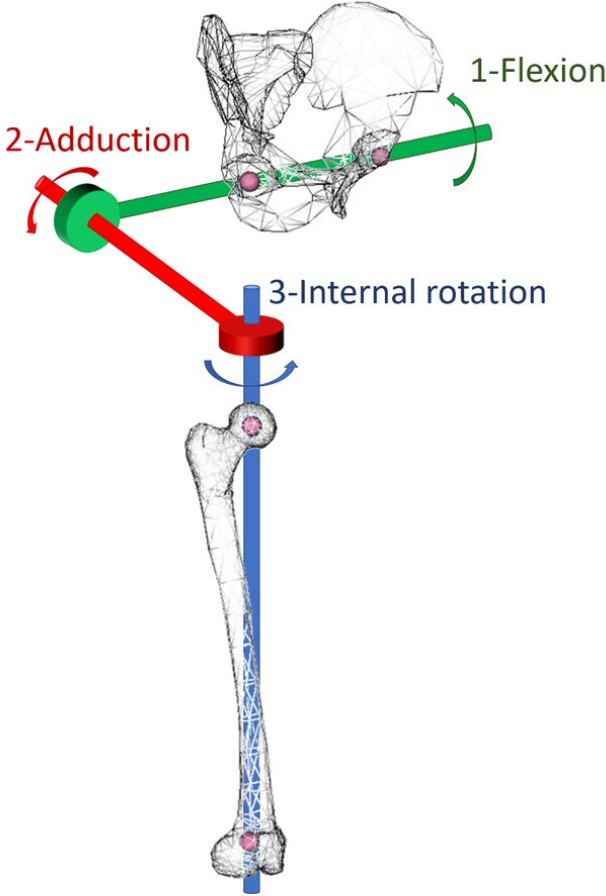


(c) Filtered aggregate moment plots for walking exercise condition.

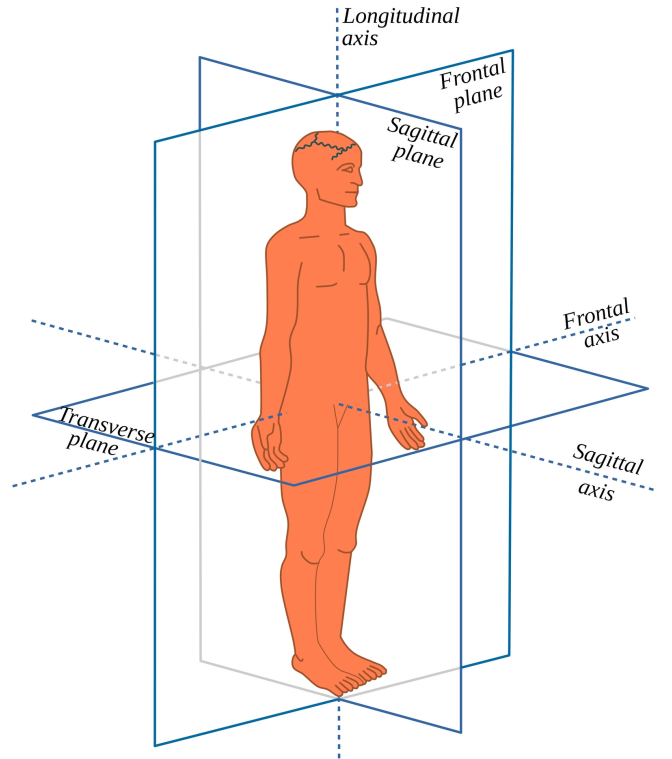


(d) Filtered aggregate moment plots for running exercise condition.

Figure 15: A comparison of unfiltered versus filtered moment data. Note: These plots have been shrunk to visually communicate filtering effects. Filtered plots are shown in original size later in this analysis, whilst full-size unfiltered plots are available in Appendix J.



(a) Image showing sign convention for hip DOFs.  
Diagram courtesy of [172].



(b) Image showing biomechanical planes of reference. Image courtesy of [173].

Figure 16: Combined figure caption describing both images.

## 7.2 Omitted Data

Due to limitations in data quality and processing issues, a number of trials were excluded from muscle force analysis, detailed in Table 7. Of these, the most notable exclusions were due to the failure of the CMC tool, which consistently failed to produce a complete biomechanical solution across all dynamic trials. Multiple troubleshooting strategies were attempted based on official OpenSim documentation to overcome this, including: loosening algorithm task tracking weights, adjusting MSK actuator strengths, and constraining model DOFs [55], [174]. However, despite this, CMC still failed to converge on a numerical solution across the dataset, and of the 24 dynamic trials processed, only one (Participant 10, Running trial 01) yielded a complete output. Given the poor convergence behaviour and heavy manual tuning required to produce it, this trial was ultimately excluded from analysis due to methodological concerns. Consequently, subsequent biomechanical analysis was done exclusively using results of static optimisation.

Of the remaining dataset, Participant 06 was also excluded from analysis after post-processing revealed corrupted force-plate data. Specifically, force plate ground positions were not correctly calibrated during data collection, which rendered inverse dynamics and subsequent biomechanical solutions invalid. Given the time constraints, it was not feasible to run an equivalent set of simulations for another participant from the same dataset, and the subject was therefore omitted entirely from the results.

Finally, muscle force estimates for Participant 10 in the running condition were excessively noisy and insensitive to smoothing techniques, likely due to MSK scaling inaccuracies being amplified by the high-acceleration movement. As a result, while their walking data was retained for aggregate inter-participant analysis, the running data was excluded and only considered separately.

Table 7: Summary of excluded trials from muscle force analysis

Tool	Participant	Trials	Reason for Exclusion
CMC	All	Running and Walking trials	Failed to converge despite troubleshooting attempts; successful trial excluded due to poor methodological reliability
-	P06	Running and Walking trials	Corrupted force plate data
-	P10	Running trials	Output excessively noisy

## 7.3 Walking Condition

### 7.3.1 Aggregate Results

Figure 17 summarises the lower-limb joint moment trends during the stance phase of walking, aggregated across all participants and trials. Published literature values are overlaid in black for comparison, with full references listed in Table 8.

Overall, the walking simulations showed relatively good consistency across all participants and trials and generally followed patterns reported in the literature. Notably, knee flexion and hip abduction moments exhibited the characteristic "double-hump" stance-profile widely described throughout literature [175]–[177], with two distinct peaks occurring during mid-stance. Similarly, hip flexion and rotation moments followed the tilde " $\sim$ " moment profile reportedly observed during stance, with peak flexion occurring in early stance [54], [175], [178], [179], suggesting that the aggregate walking simulations are broadly comparable to prior findings.

However, while the simulation results showed agreement with the literature in terms of overall pattern and shape, absolute moment values often differed. As seen in Figure 17, simulated maximum and minimum peak moments frequently fell outside the range of the reported values in the literature, indicating systematic magnitude discrepancies despite having comparable stance profiles.

Results also showed noticeable variability at certain points of the stance-phase, reflected by the widening standard deviation bands in Figure 17. This is variance peaks during heel-strike in early stance, such as in hip extension during 0–10% phase, and toe-off in late stance, such as in knee flexion during 80–100% phase. This observation is consistent with general simulation behaviour, as these phases involve the most rapid joint accelerations during the stance phase. This transient state can lead to oscillatory behaviour, which in turn produces the observed rapidly increasing simulation variance.

In addition to time-dependent variability, simulation variability tended to increase with the joint's distance from the pelvis. While hip and knee moments showed the most comparability with literature values, ankle moments deviated markedly, particularly during late stance, with discrepancies spanning several orders of magnitude (see ankle flexion plot in Figure 17). This variability pattern is consistent with prior research, noting that limb extremities are more susceptible to simulation noise. This is due to their higher accelerations relative to proximal segments [117], [180], with previous research noting that across gait MSK modelling, the ankle joint tends to show the greatest

discrepancies between simulations, even when hip and knee outcomes are relatively consistent [117], [118].

Table 8: Summary of literature values used for joint moment analysis during walking stance phase. *Joint DoFs:* Flex./Ext. = Flexion/Extension, Abd./Add. = Abduction/Adduction, Rot. Ex./In. = External/Internal Rotation, Plant. Flex./Ext. = Plantarflexion/Dorsiflexion.

Joint	Movement	Early	Mid	Late	Units	Source
Hip	Flex.	59.7 ± 19.7	-71.3 ± 28.2	30.1 ± 12.6	Nm	[175]
	Abd.	67.5 ± 13.2	42.0 ± 10.1	5.0 ± 12.3	Nm	[175], [179]
	Rot. Ext.	3.9 ± 6.6			Nm	[179], [181]
			0.09 ± 0.03	0.25 ± 0.05	Nm/kg	[182]
Knee	Ext. (Walk)	3.25 ± 1.8	1.48 ± 1.8	–	% BW×H	[183]
Ankle	Plant. Flex.	–	–	79.3 ± 21.8	Nm	[184]

### 7.3.2 Joint analysis: Acetabulofemoral Joint (Hip)

Figure 18 presents the moment–stance plots for the hip joint across all participants. Overall, there was minimal inter-participant variability across all moment profiles, with hip flexion and abduction moments showing the highest consistency across participants.

Whilst hip moment predictions largely followed expected profile patterns (most notably the ‘double-hump’ abduction profile [175], [177] and “~” extension profile [175], [178]), they frequently deviated from specific literature values. This was most prominent in hip adduction, which consistently predicted moment profiles that appeared to be translated upwards relative to literature. That is, peak adduction moments were consistently smaller in magnitude than reported throughout the stance period, and peak adduction moments larger.

Examining participants individually, some discrepancies in simulation behaviour can be observed. In particular, moment plots for Participants 4 and 13 show notable variability and noise across the stance phase, with the most pronounced fluctuations occurring during the early and late stance phases in the hip adduction and rotation moments of Participant 13. In addition to the expected variability associated with heel-strike and toe-off, some moment profiles also displayed elevated variability during mid-stance, such as the hip extension moment in Participant 4 between 50–60% of stance, and the hip abduction moment in Participant 13 between 40–75%.

Of the three participants, Participant 10 demonstrated the smoothest moment profiles, with minimal variability across the stance phase. However, despite this relative stability, the absolute peak moments for Participant 10 still deviated from literature values, overshooting or undershooting by a considerable margin.

### 7.3.3 Joint Analysis: Tibiofemoral Joint (Knee)

Similar to the simulation results observed for hip adduction, knee flexion moment profiles (shown in Figure 19) were consistently shifted upward in magnitude compared to literature reports throughout the stance phase, even though the overall “double-hump” moment pattern [175] was preserved. Interestingly, peak knee moments in the simulations occurred during the second half of the stance phase (visible as the higher and noisier second peaks in the plots) which contrasts with typical

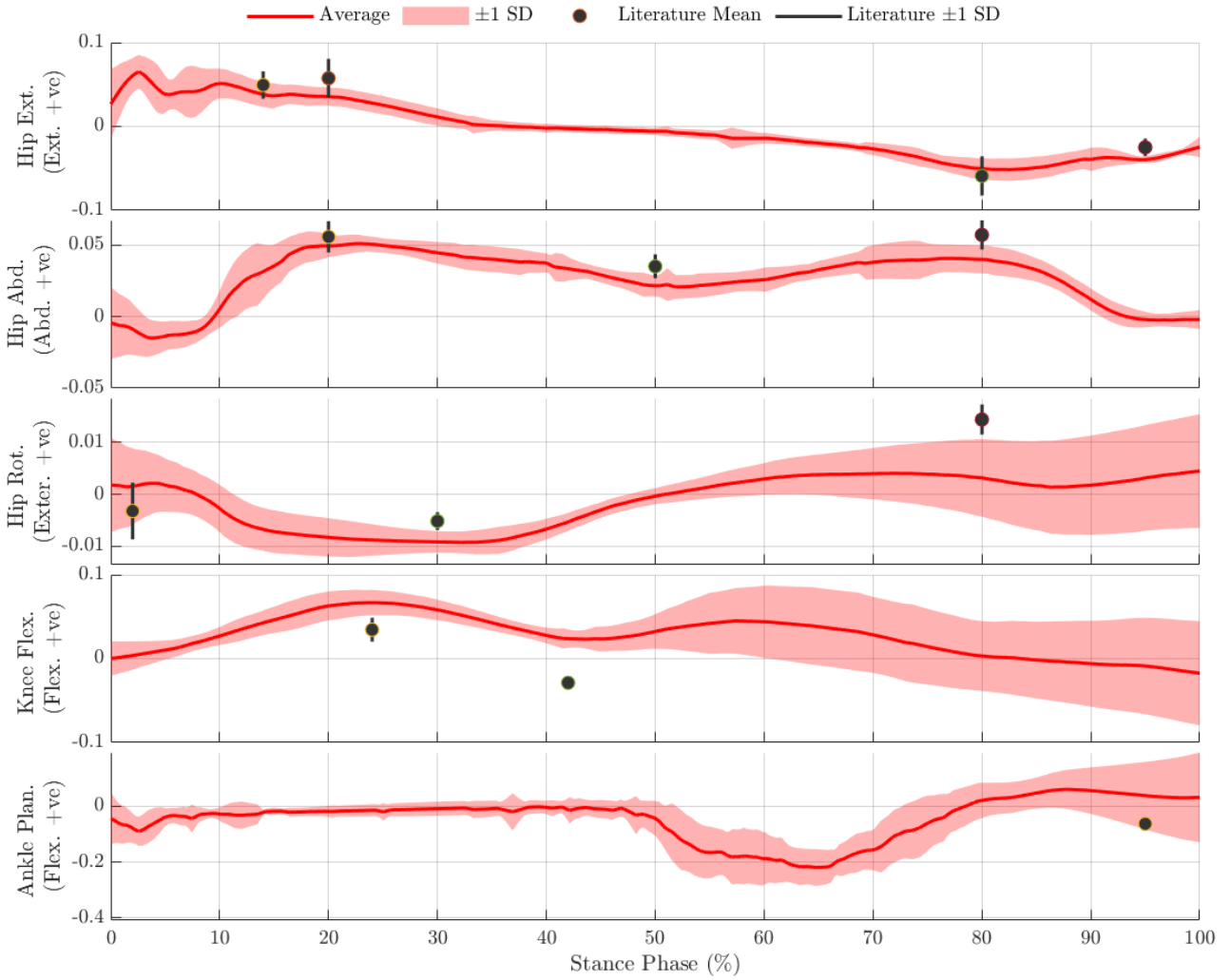


Figure 17: Summary plots of lower-limb MSK joint moments, aggregated for all walking trials. *Moments normalised by participant body-weight and height (Body Weight (BW)  $\times$  Height); time normalised as percentage (%) of stance phase.* **Joint DoFs:** Flex./Ext. = Flexion/Extension, Abd./Add. = Abduction/Adduction, Rot. Exter./Inter. = External/Internal Rotation, Plant. Flex./Ext. = Plantarflexion/Dorsiflexion.

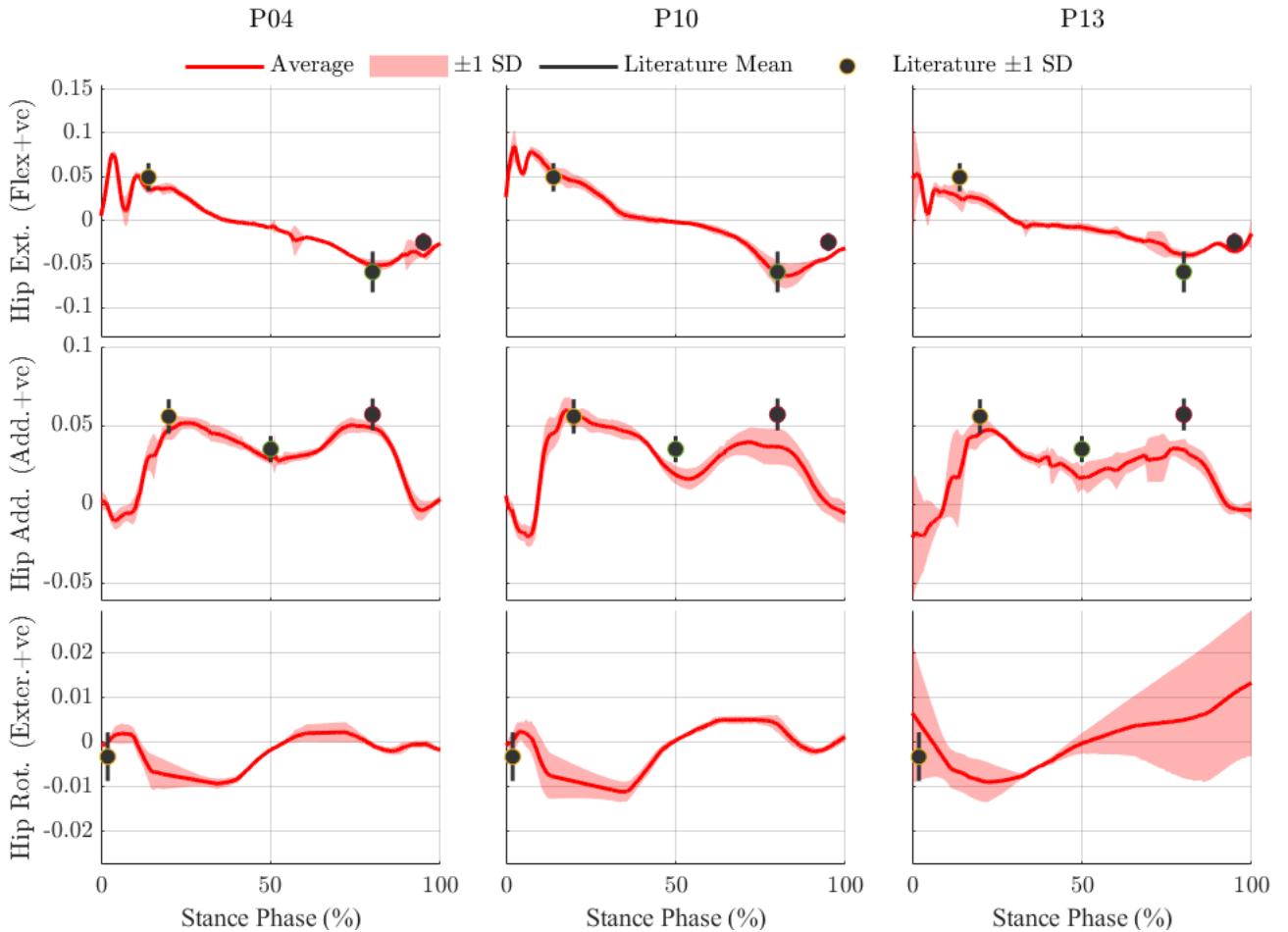


Figure 18: Subplot comparison of hip joint moments across the stance phase for walking trials, broken down by participant and hip DOF. *Moments normalised by participant body weight and height ( $BW \times Height$ ); time normalised as percentage (%) of stance phase.* Moments normalised by participant body-weight and height ( $BW \times Height$ ); time normalised as percentage (%) of stance phase. **Joint DoFs:** Flex./Ext. = Flexion/Extension, Abd./Add. = Abduction/Adduction, Rot. Exter./Inter. = External/Internal Rotation.

healthy walking gait, where peak moments are usually observed at the first of the two peaks (view literature data points on plots) [167], [185].

This combination of elevated knee flexion moments and shifted hip abduction profiles is particularly notable, as it is characteristic to crouch gait patterns described in the literature [186], [187]. This suggests that despite none of the participants in this study exhibiting clinical crouch gait during Mo-Cap [56], simulation outputs implied otherwise, possibly indicating a form of methodological error.

Alternatively, the elevated knee flexion moments may reflect limitations of the MSK model itself, as the Rajagopal model used in this study represents the knee as a single DOF hinge joint [100]. As a result, moments occurring in other DOFs, such as knee abduction and rotation, may be transferred into the sagittal plane, contributing to the observed upward shift in knee flexion moments.

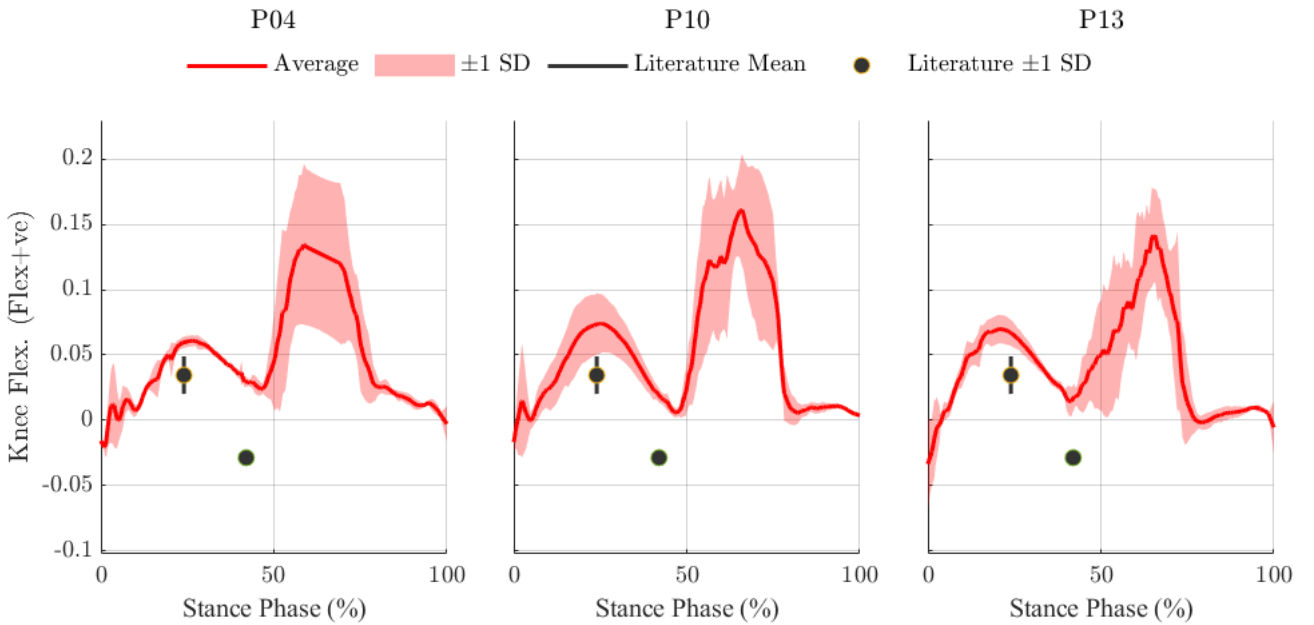


Figure 19: Subplot comparison of knee flexion moments across the stance phase for walking trials, broken down by participant. *Moments normalised by participant body weight and height ( $BW \times Height$ ); time normalised as percentage (%) of stance phase. Moments normalised by participant body-weight and height ( $BW \times Height$ ); time normalised as percentage (%) of stance phase.*

**Joint DoFs:** Flex./Ext. = Flexion/Extension.

### 7.3.4 Joint analysis: Talocrural Joint (Ankle)

Finally, moment profiles for the ankle joint, shown in Figure 20, exhibited the largest deviations from literature values, with variance often differing by an order of magnitude (notably, literature-based SD bands are barely visible in Figure 20).

This deviation is not unexpected, given that the ankle was modeled as a single DOF, with the subtalar and metatarso-phalangeal joints locked during simulation. Considering the aforementioned challenges of simulating lower-limb extremities under high acceleration [117], [180], these discrepancies largely reflect the limitations of the MSK modeling assumptions adopted in this study [40]. Notably, despite these magnitude differences, peak ankle plantarflexion still occurred during the second half of stance (50–75%), which aligns with typical walking gait patterns [168]. This further

suggests that the deviations from literature values may stem more from model simplifications and scaling error than from a fundamental error in methodology.

It is also important to note that while the narrow SD bands in Figure 20 may give the impression that simulations for Participants 10 and 13 were relatively stable during heel-strike and toe-off, this interpretation is misleading. In these cases, oscillations and noise were sufficiently severe that affected data points were removed during filtering, creating an apparent but artificial reduction in variability (To view an uncleaned plot, refer to Appendix J.1).

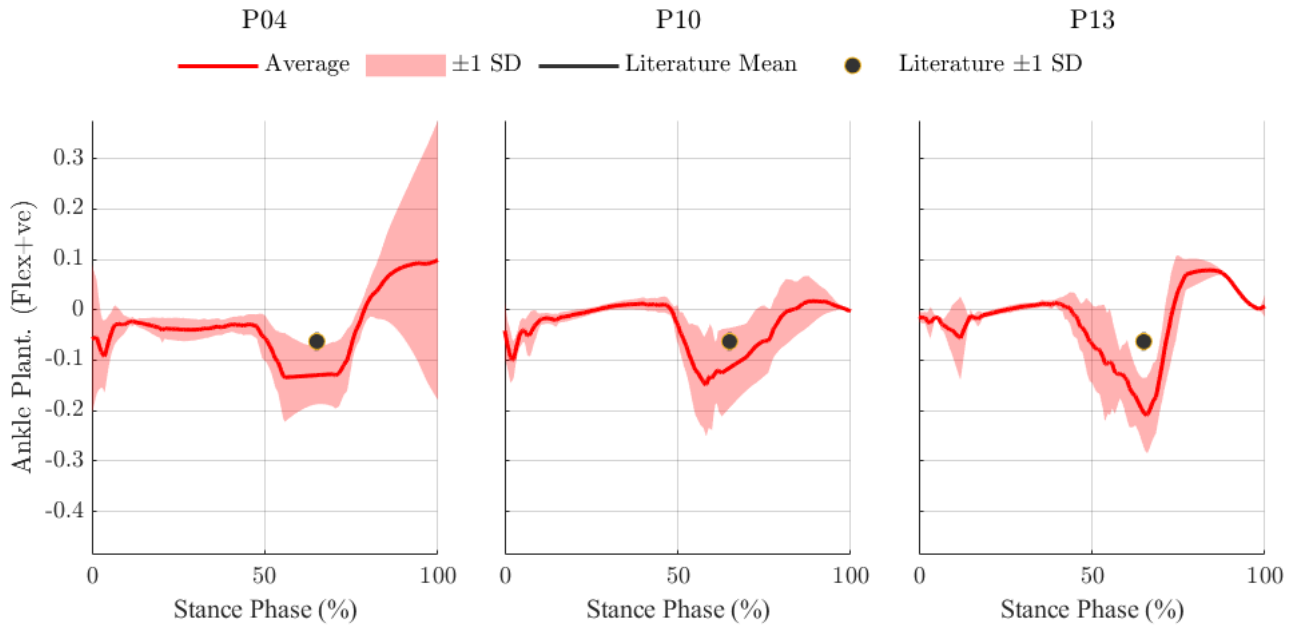


Figure 20: Subplot comparison of ankle plantarflexion moments across the stance phase for walking trials, broken down by participant. *Moments normalised by participant body weight and height ( $BW \times Height$ ); time normalised as percentage (%) of stance phase. Moments normalised by participant body-weight and height ( $BW \times Height$ ); time normalised as percentage (%) of stance phase. Joint DoFs: Plant. Flex./Ext. = Plantarflexion/Dorsiflexion.*

## 7.4 Running Condition

### 7.4.1 Aggregate Results

Figure 21 shows the moment plots across all lower-limb joint DOFs, aggregated across participants 4 and 13 (note that participant 10 was excluded from aggregate analysis), with the literature values used for comparison tabulated in 9. Compared to walking trials, running simulations exhibited substantially greater variability and noise, as reflected by the noticeably wider SD bands in the aggregate plots throughout stance. While this increased variability can be partly attributed to the inherently higher accelerations and biomechanical demands of running, it may also be influenced by the exclusion of Participant 10, which reduced the sample size from eighteen to twelve stance phases.

In terms of general variability patterns, running trials showed a notable deviation from walking. While walking trials displayed the greatest variability at heel strike and toe-off, running trials exhibited their highest variability during mid-stance. This likely reflects the larger accelerations and dynamic demands imposed on the model during this phase compared to walking, which can amplify noise and oscillatory behaviour.

Despite these differences, physiological trends were broadly consistent across exercises. Hip moments remained relatively comparable to literature values and showed lower variability overall, while knee and ankle moments exhibited progressively greater deviations. Notably, an exception was observed in the hip extension moments, which displayed substantially more variability compared to hip abduction and rotation. This suggests that running trials were particularly noisy in the sagittal plane, where the largest magnitude accelerations typically occur.

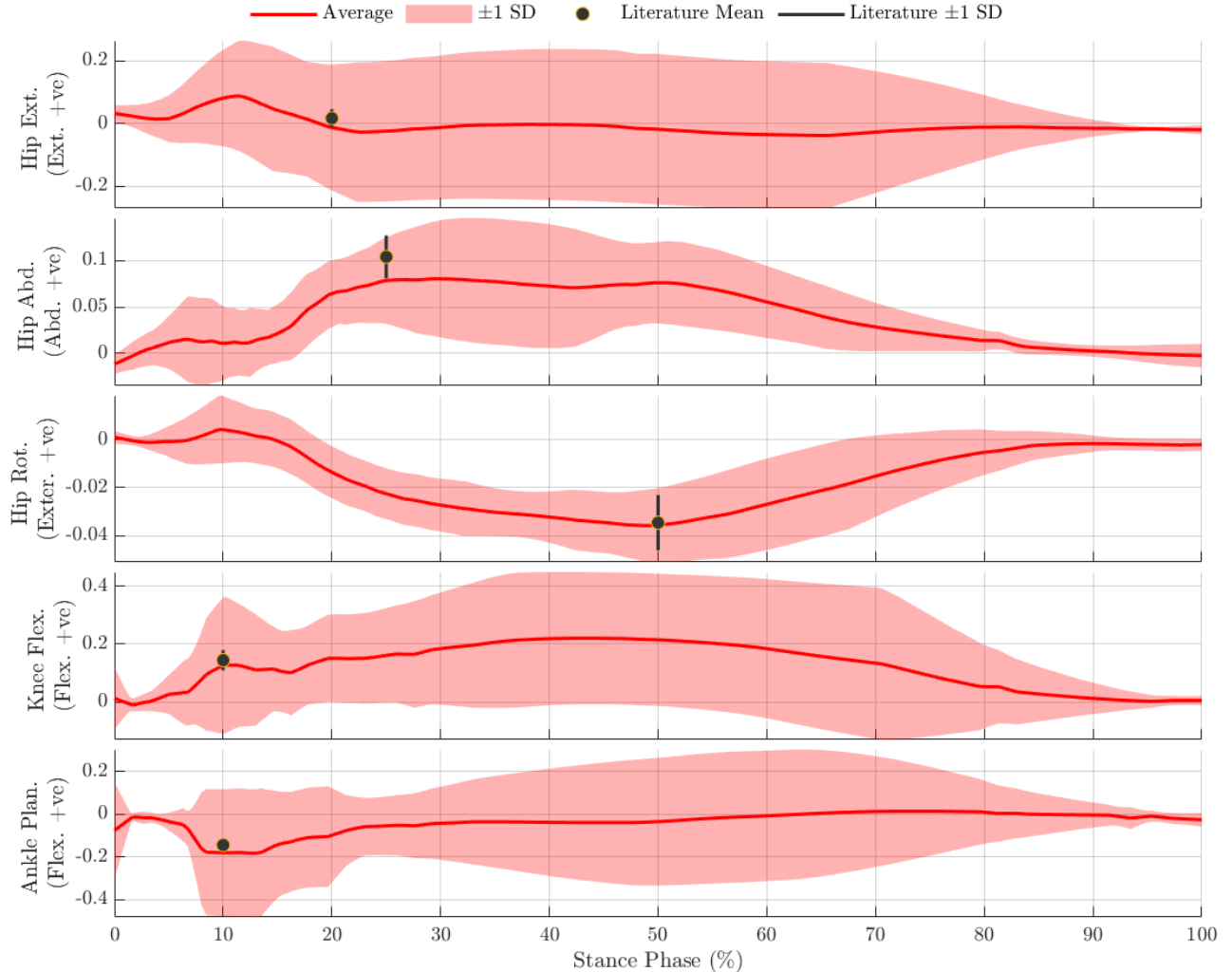


Figure 21: Summary plots of lower-limb MSK joint moments, aggregated for all running trials for Participants 4 and 13. *Moments normalised by participant body-weight and height ( $BW \times Height$ ); time normalised as percentage (%) of stance phase.*

Table 9: Summary of literature values used for joint moment analysis during running stance phase

Joint	Movement	Early	Mid	Late	Units	Source
Hip	Flex.	$0.3 \pm 0.5$	—	—	Nm/kg	[182]
	Abd.	—	$1.8 \pm 0.4$	—	Nm/kg	[182]
	Rot. Ext.	—	$-0.6 \pm 0.2$	—	Nm/kg	[182]
Knee	Ext. (Walk)	—	$2.5 \pm 0.6$	—	Nm/kg	[182]
Ankle	Plant. Flex.	$-2.5 \pm 0.4$	—	—	Nm/kg	[188]

#### 7.4.2 Joint analysis: Acetabulofemoral Joint (Hip)

Examining hip moments individually by participant (Pictured in Figure 22, hip abduction and rotation profiles were highly consistent, whereas the sagittal plane hip flexion showed greater variability. Overall, hip abduction and flexion moment profiles aligned reasonably well with literature, with average values falling within reported ranges. Peak hip abduction occurred during early to mid-stance, while peak internal rotation was observed at mid-stance—both patterns consistent with the expected running gait cycle [182].

Across participants, Participant 4 exhibited substantially more variability compared to Participant 13. While this may reflect underlying simulation noise, it could also be related to asymmetric loading patterns, as explored later in Section 8.4, corresponding to the left and right limbs.

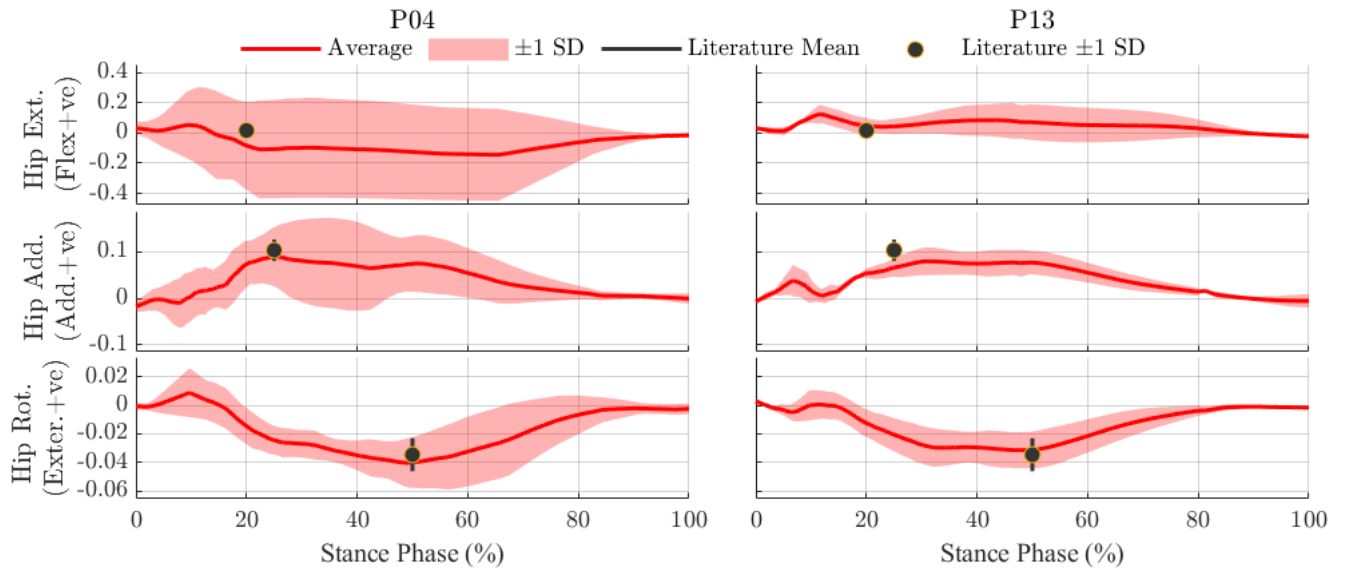


Figure 22: Subplot comparison of hip joint moments across the stance phase for running trials, broken down by participant and hip DOF. *Moments normalised by participant body weight and height ( $BW \times Height$ ); time normalised as percentage (%) of stance phase. Joint DoFs: Flex./Ext. = Flexion/Extension, Abd./Add. = Abduction/Adduction, Rot. Exter./Inter. = External/Internal Rotation.*

### 7.4.3 Joint Analysis: Tibiofemoral Joint (Knee)

Figure 23 presents the knee joint moment profiles during running, separated by participant. Overall, the simulated knee flexion moment profiles diverged noticeably from those reported in the literature [182], [189]. While Participant 4 exhibited a peak knee flexion moment during mid(40–50%)-stance that was broadly consistent with reported normative patterns, Participant 13 displayed peak flexion moment significantly earlier (10–20% stance), highlighting an inconsistency in the simulated data.

Additionally, pronounced variability was observed throughout the entire stance phase for Participant 4, with significant fluctuations despite filtering. Participant 13, by contrast, showed the highest variability in just after heel strike in early stance. These inconsistencies and high variability levels limit the reliability of these results, and suggest that both simulation noise and potential methodological factors (such as MSK idealisations or scaling inaccuracies) may have influenced simulation quality.

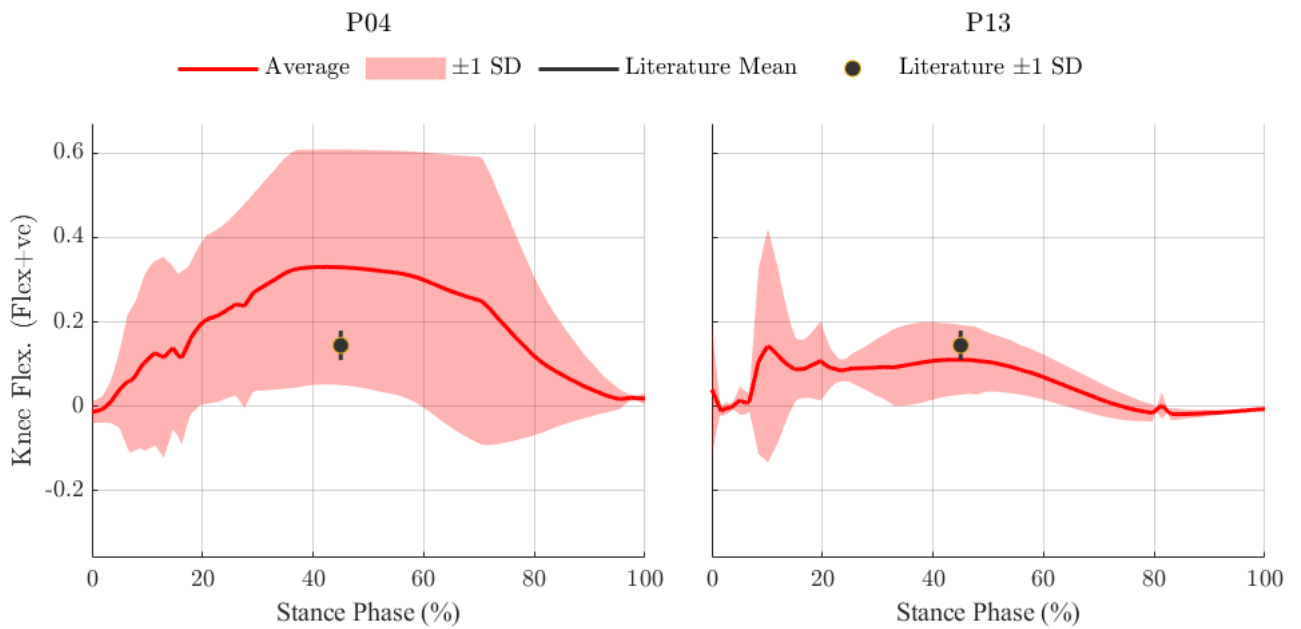


Figure 23: Subplot comparison of knee flexion moments across the stance phase for running trials, broken down by participant. *Moments normalised by participant body weight and height ( $BW \times Height$ ); time normalised as percentage (%) of stance phase.*

### 7.4.4 Joint analysis: Talocrural Joint (Ankle)

Similar to the trends observed in the walking trials, ankle moments (Shown in Figure 24) exhibited the highest variability among all measured lower-limb degrees of freedom. For Participant 4, the simulated moment profile deviated noticeably from reported literature patterns, with peak plantarflexion moment occurring during mid-stance (40–60%), rather than the early stance phase typically reported [188]. Participant 13, while showing peak moments during heel strike (0–10% stance) as expected, still demonstrated substantial variability across the stance phase.

Notably, ankle moment profiles for running trials displayed even greater variability than that observed during walking. This reflects not only limitations in simulation methodology outlined earlier, but also the inherent challenges of accurately capturing the high-acceleration behaviours. That is, the elevated accelerations associated with running likely amplified the noise already associated with distal joint kinematics.

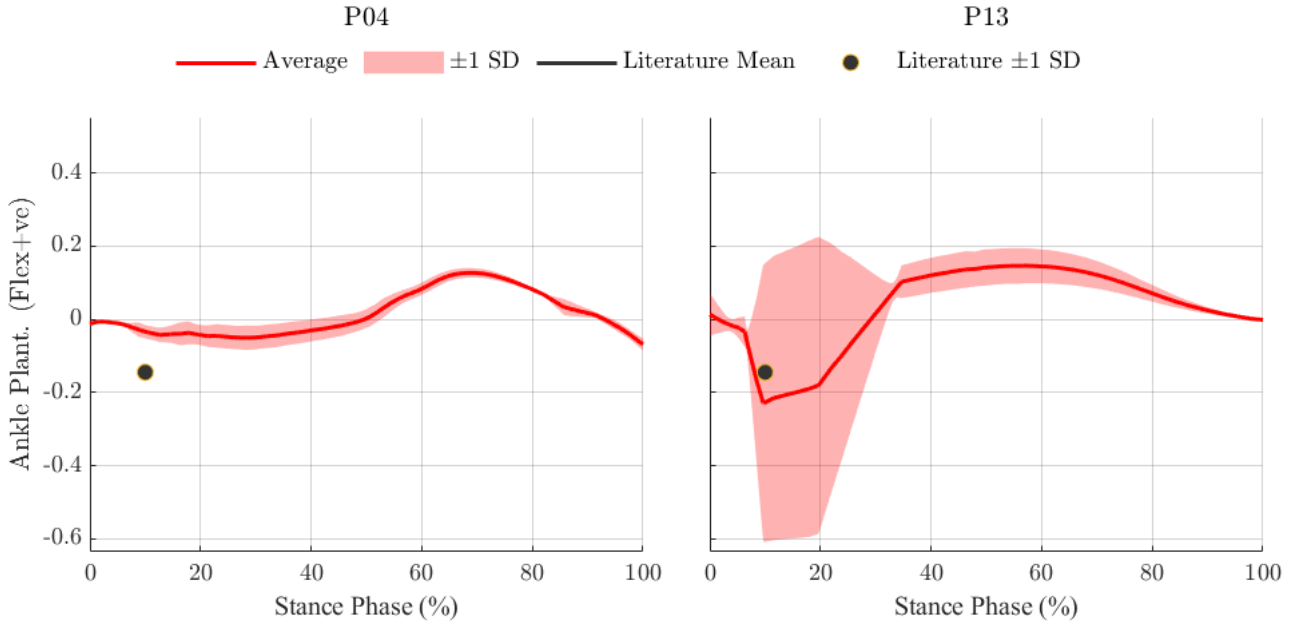


Figure 24: Subplot comparison of ankle plantarflexion moments across the stance phase for running trials, broken down by participant. *Moments normalised by participant body weight and height ( $BW \times Height$ ); time normalised as percentage (%) of stance phase.*

## 7.5 Summary of Biomechanical Analysis

In summary, biomechanical moment analysis across walking and running conditions revealed several key trends. Walking simulations showed relatively stable and literature-consistent moment profiles, particularly regarding hip DOFs, though ankle moments deviated substantially in magnitude. Running simulations, by contrast, exhibited markedly higher variability and noise across all joints, with the ankle and knee showing the largest deviations from expected patterns. Notably, variability tended to increase with the distance of the joint from the hip, reflecting the greater simulation challenges associated with modeling distal limb segments. Variability was also unevenly distributed throughout the stance phase across different exercise conditions: walking trials showed the most fluctuation at heel-strike and toe-off, while running trials displayed peak variability during mid-stance.

Interestingly, within the walking condition, the combination of elevated knee flexion and altered hip abduction moment profiles displayed similarities to patterns typically observed in crouch gait, despite no participants exhibiting clinical crouch gait during data collection. This suggests that some of the observed deviations from literature may reflect underlying methodological or modelling factors rather than true pathological gait behaviour.

Despite these challenges, the overall moment patterns captured key features of typical gait, suggesting that whilst absolute magnitudes may be impacted by model assumptions and filtering, the relative variability of simulation methodology was broadly reliable. To summarise key numerical findings, peak and RMS moment values across walking and running conditions are provided in Tables 10 and 11. These findings provide important context for interpreting the subsequent variability analysis in the following section.

Table 10: Summary of average RMS and peak positive and negative joint moments (Nm) for walking trials during stance phase, including SD.

Walking Joint DOF	RMS (Nm)		Peak(Nm)	
	Mean	SD	Mean	SD
Hip Flex./Ext.	39.4	1.76	85.8/65.1	10.7/11.7
Hip Abd./Add.	40.9	3.08	68.0/20.0	4.60/10.7
Hip Rot. Ex./In.	6.06	2.66	4.25/12.3	4.03/2.14
Knee Flex./Ext.	53.5	8.80	100.7/-8.41	32.0/13.4
Ankle Plant. Flex./Ext.	109.8	32.8	31.3/154.6	35.7/39.6

Table 11: Summary of average RMS and peak positive and negative joint moments (Nm) for running trials during stance phase, including SD.

Running Joint DOF	RMS (Nm)		Peak (Nm)	
	Mean	SD	Mean	SD
Hip Flex./Ext.	152.4	213.0	191.2/129.6	109.8/222.4
Hip Abd./Add.	81.4	29.6	128.1/33.0	63.7/32.5
Hip Rot. Ex./In.	30.9	11.8	11.8/55.8	15.5/21.3
Knee Flex./Ext.	227.4	184.9	408.3/57.2	341.6/62.4
Ankle Plant. Flex./Ext.	233.4	198.5	153.1/405.8	77.3/446.7

## 8 Results and Analysis III: Statistical Variability Analysis

### 8.1 Statistical Approach and Rationale

The aim of this analysis was to provide a quantitative assessment of the variability observed in the simulations of this study. Although several guidelines exist for evaluating the validity and accuracy of biomechanical simulations, such as those presented by [41], [50], [55], reporting of simulation variability in particular is often limited or informal, and rarely addressed as a distinct outcome. In an attempt to address this gap, the present analysis aims to explicitly quantify the variability observed in the simulation results of this study, with an intention of supporting more transparent and consistent reporting in future work.

Variability assessment was approached using a hierachal statistical analysis, outlined in Figure 12 as a means of overcoming the limitation of small sample sizes (six stance phases per participant, per exercise), hereafter referred to as “clusters”. First, within-cluster variability was calculated, measured using Mean-Normalised Standard Deviation (NSD) and Median-Normalised Median Absolute Deviation (NMAD). These metrics were then used to compare variability across exercises, joints, and participants, enabling an evaluation of overall simulation consistency using different frames of reference. The objective was to identify points in simulation methodology that may introduce increased variance, thereby informing on future methodological improvements.

Two primary statistical measures were employed: NSD (i.e. coefficient of variation, Equation 5) and NMAD. SD is a widely accepted measure of variability, but is sensitive to outliers, particularly when data points are several magnitudes larger than the sample mean [190]. Given the small samples involved in this analysis (up to six stances per sample), this sensitivity posed a risk of over-representing outliers. To address this, Median Absolute Deviation (MAD) was included as a complementary metric, a measure of the median deviation of data from the center (median) value of

a dataset (Shown in Equation 6.) Compared to traditional SD, MAD offers a more robust estimate of spread in small-sample contexts [190].

$$\text{SD}_{\text{norm}(\text{mean})} = \frac{\text{SD}}{\bar{x}} = \frac{\sqrt{\frac{1}{n} \sum_{i=1}^n (x_i - \bar{x})^2}}{\bar{x}} \quad (5)$$

$$\text{MAD}_{\text{norm}(\text{mean})} = \frac{\text{MAD}}{\bar{x}} = \frac{\text{median}(|x_i - \text{median}(x)|)}{\bar{x}} \quad (6)$$

In order to allow variability comparison across different metrics, sample SD and MADs were normalised by sample means and medians respectively to produce unit-less metrics. This was done for three variables per data cluster: moment RMS across the stance phase, peak moment, and peak negative moment. The resulting metrics were subsequently aggregated to allow for variability comparison across exercise conditions, joints, and participants, with results visualised using violin plots, i.e. a distribution of distributions. Violin plots are documented in this section, whereas a full table of statistical values can be found in Appendix K.

Table 12: Summary of data aggregation levels and statistical analysis approach

Analysis Level	Calculation Performed	Analysis Performed	Data Points
Per stance	RMS, Peak, Negative Peak moments calculated	—	1
Per trial	Two stance phases aggregated	—	2
Per participant	Three trials aggregated	NSD, NMAD	6
Per exercise	Aggregated across participants	NSD, NMAD violin plot, Figure 25	24
Across exercises	Aggregated across joints	Violin plot, Figure 25	24
Across joints	Aggregated across exercises	NSD, NMAD violin plot, Figure 26 and 27	24
Across participants	Aggregated across joints	Violin plots, Figures 28 and 29	24

*Notes:* All analyses conducted post-denoising; filter details in Appendix I

## 8.2 Variability Across Exercise Conditions

Figure 25 shows violin plots illustrating the variability of moment RMS (blue), peaks (red), and negative peaks (yellow) across the stance phase, aggregated over all exercise trials and participants. A summary of the variability statistics used to generate these plots is provided in Table 13, with a full breakdown available in Appendix K.

Overall, walking simulations exhibited less variability than running, with NSD values roughly half those observed in running (Refer to Table 13). Walking NSDs displayed multimodal distributions, visualised in the multiple concentration points throughout the violin plots. This was particularly noticeable in the peak positive walking moment plot, which showed a bimodal NSD distribution around 0.2 and 2.1. In contrast, running peak moment SDs were more normally distributed, although RMS variability followed a similarly multimodal pattern to walking. Multimodal distributions indicate several concentrations of variability throughout the study, implying that simulation consistency changes with the metric being examined.

Across both walking and running conditions, moment peaks consistently showed higher NSD and NMAD variability than RMS, suggesting that variability was greatest during early stance, particularly around the heel-strike phase where most peak moments occurred across most degrees of

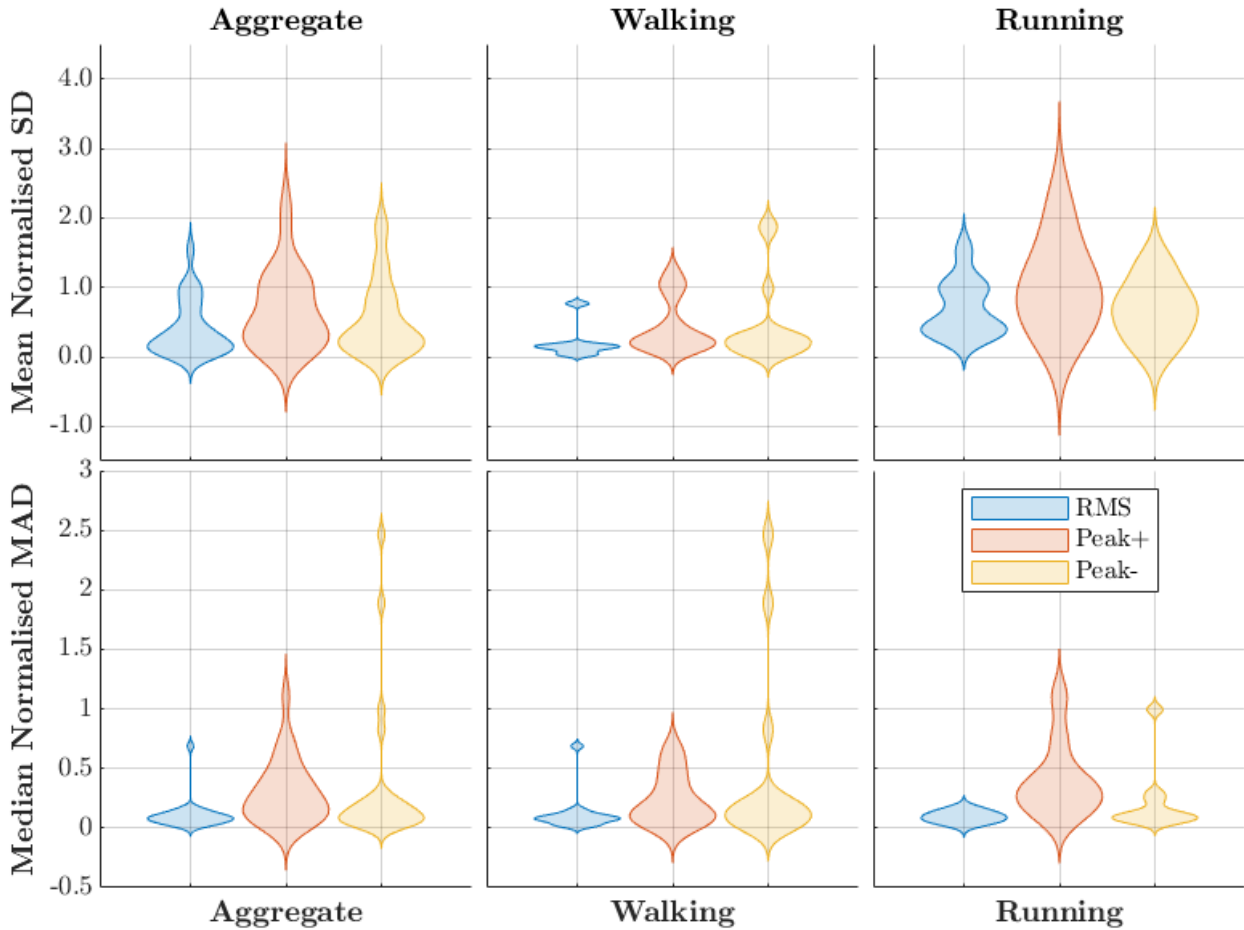


Figure 25: Exercise-wise violin plot NSD and NMAD comparison across joint moment metrics (RMS, Peak+, Peak-) for walking, running, and aggregated trials. Rows indicate the statistical measure; columns separate aggregate, walking-only, and running-only conditions.

freedom. In contrast, RMS values displayed narrower and more concentrated distributions, indicating that when aggregated across the entire stance phase, the simulations were more consistent.

NMAD distributions further reinforced these patterns, showing similar trends in variability between walking and running, with one notable exception: the walking peak moment NMAD, which exhibited multiple clusters of outlier values. These clusters correspond to variability metrics at the ankle joint, which are discussed later in Section 8.3.

Taken together, these findings highlight that the variability in biomechanical simulations is strongly influenced by the exercise condition, with running showing significantly higher variability across most measured metrics.

### 8.3 Variability Across Joints

In aggregate, variability metrics across all joints were comparable, as shown in yellow in Table 14. NSD values for all joints ranged modestly, with the least variability of 0.12 NSDs associated with the hip during walking, and the largest being 1.05 NSDs in the knee, during running. Across NMAD values, the most consistently performing joint was the knee (0.25 NMADs), and the least consistent was the hip (0.73 NMADs), both of which were during walking.

Table 13: Aggregated Statistical Summary of joint moment data (normalised SD and MAD), broken down for exercise condition comparison, rounded to two decimal places. See Appendix K for detailed results.

Exercise Condition	Participant	Standard Deviation			MAD		
		Norm. by Mean			Norm. by Median		
		RMS	Peak+	Peak-	RMS	Peak+	Peak-
Walking	<b>Participant 04</b>	0.10	0.34	0.32	0.07	0.21	0.26
	<b>Participant 10</b>	0.12	0.40	0.19	0.08	0.14	0.10
	<b>Participant 13</b>	0.38	0.61	0.88	0.21	0.37	0.94
	<b>Overall</b>	0.20	0.46	0.45	0.12	0.44	0.24
Running	<b>Participant 04</b>	0.86	1.33	0.72	0.07	0.50	0.29
	<b>Participant 13</b>	0.55	0.74	0.66	0.12	0.30	0.14
	<b>Overall</b>	0.70	1.03	0.69	0.09	0.40	0.21

However, viewing violin plots of these variability metrics reveals nuance to these trends. For NSD (shown in Figure 26), hip and knee joints exhibited clear multimodal distributions, particularly under walking conditions. Running trials consistently contributed the largest share of variability when data was aggregated across exercises, highlighting the greater variability associated with the movement. Compared to the hip, knee and ankle moments showed more irregular NSD distributions, suggesting a less consistent simulation performance for these joints. This was most striking in the ankle peak-negative moment for walking, which displayed a near-perfect bimodal distribution corresponding to the MAD threshold used during data filtering. This suggests that while averaging results across trials helped stabilise hip and knee moment estimates, the ankle remained highly sensitive to methodological noise, indicating potential weaknesses in how ankle dynamics were modelled.

In the NMAD plots (Shown in Figure 27), knee moments showed the most even and compact variability distribution across conditions. The ankle again showed a bimodal NMAD distributions near the noises-filtering cutoff, further suggesting that ankle moments were disproportionately affected by methodological error. Interestingly, the hip joint's walking peak-negative moment exhibited a long, narrow NMAD distribution, suggesting that while most trials were consistent, a small number of outliers remained. This pattern raises the possibility that filtering may have masked some underlying variability, giving the impression of more stable simulation performance than was truly present.

Together, these observations suggest that variability patterns differ meaningfully across joints, with the ankle requiring particular methodological attention in future work.

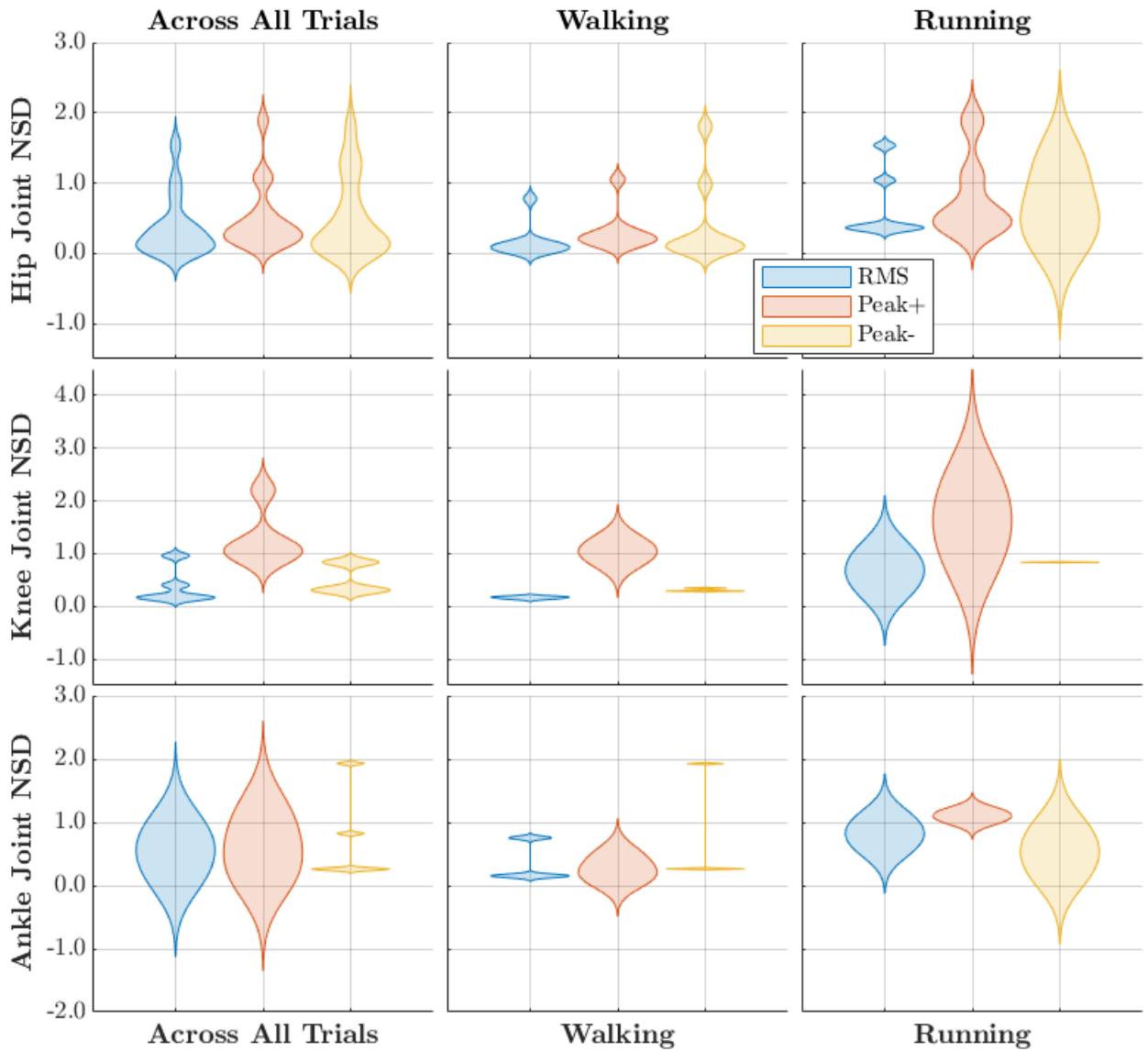


Figure 26: Joint-wise violin plot NSD comparison across joint moment metrics (RMS, Peak+, Peak-) for walking, running, and aggregated trials. Rows show joint of interest; columns separate aggregated, walking-only, and running-only conditions.

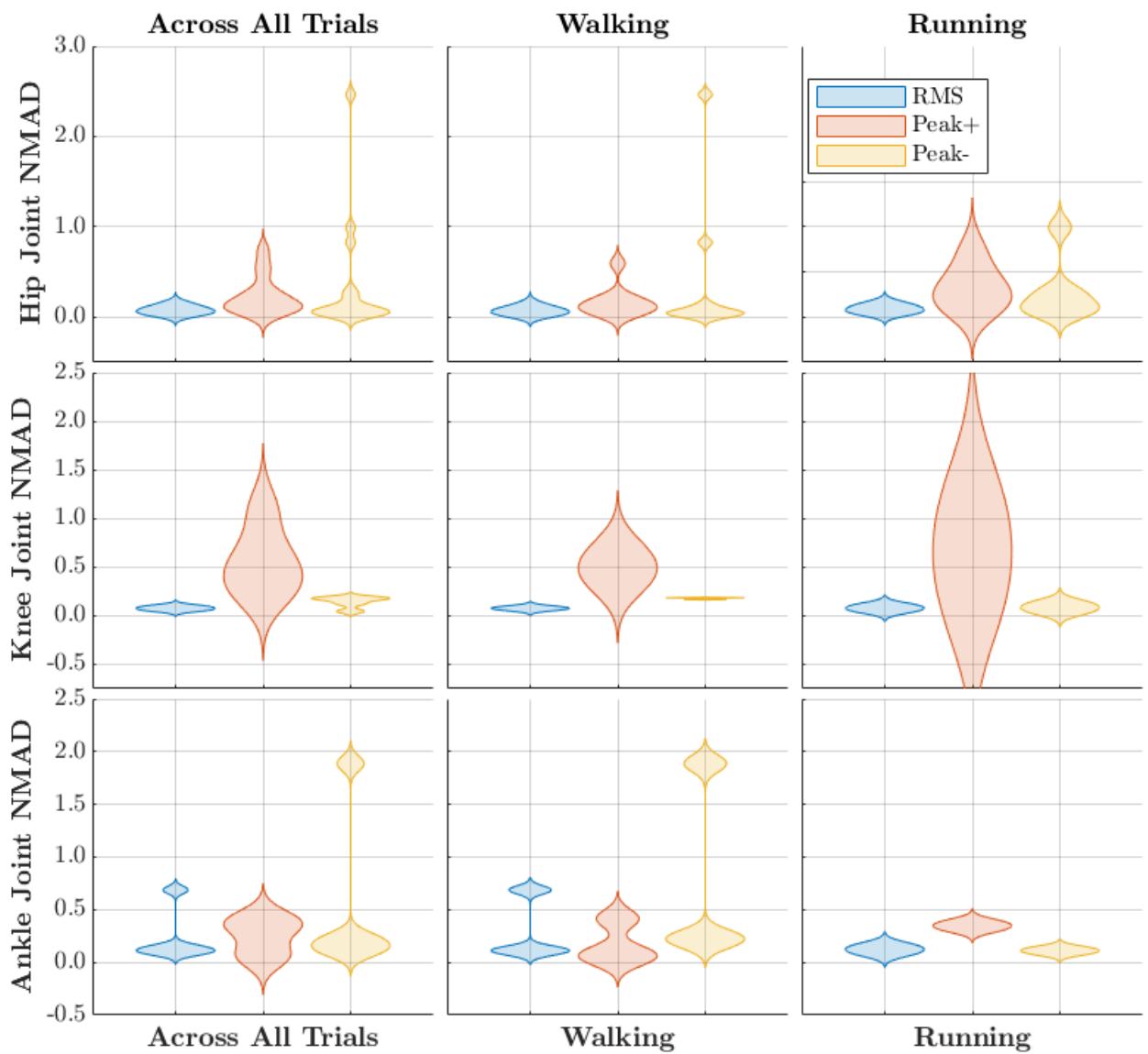


Figure 27: Joint-wise violin plot MAD comparison across joint moment metrics (RMS, Peak+, Peak-) for walking, running, and aggregated trials. Rows show joint of interest; columns separate aggregated, walking-only, and running-only conditions.

Table 14: Statistical summary of joint moment data (NSD and NMAD), broken down for joint-wise comparison across hip, knee, and ankle joints. See Appendix K for detailed statistical breakdown.

Joint	Condition	SD				MAD						
		Norm. by Mean		Norm. by Median		RMS	Peak+	Peak-	All Metrics	RMS	Peak+	Peak-
<b>Hip</b>	<b>Overall</b>	0.67	0.66	0.37	0.57	0.08	0.17	0.14	0.39			
	<b>Walk</b>	0.05	0.15	0.16	0.12	0.03	0.07	0.12	0.73			
	<b>Run</b>	1.29	1.18	0.58	1.01	0.12	0.28	0.16	0.19			
<b>Knee</b>	<b>Overall</b>	0.42	0.97	0.94	0.78	0.08	0.42	0.29	0.26			
	<b>Walk</b>	0.17	0.31	1.05	0.51	0.08	0.18	0.50	0.25			
	<b>Run</b>	0.68	1.63	0.84	1.05	0.08	0.66	0.08	0.27			
<b>Ankle</b>	<b>Overall</b>	0.59	0.96	0.40	0.65	0.21	0.56	0.15	0.31			
	<b>Walk</b>	0.35	0.82	0.27	0.48	0.30	0.78	0.18	0.42			
	<b>Run</b>	0.82	1.10	0.54	0.82	0.12	0.35	0.11	0.58			
<b>All Joints</b>		0.56	0.87	0.57	0.67	0.12	0.38	0.19	0.23			

## 8.4 Variability Across Participants

Finally, participant-wise variability was assessed to evaluate whether individual participant data disproportionately influenced aggregate results. Violin plots for NSD and NMAD are shown in Figures 28 and 29, respectively, with detailed statistics provided in Appendix K. Notably, running data for Participant 10 was excluded due to particularly poor noise quality.

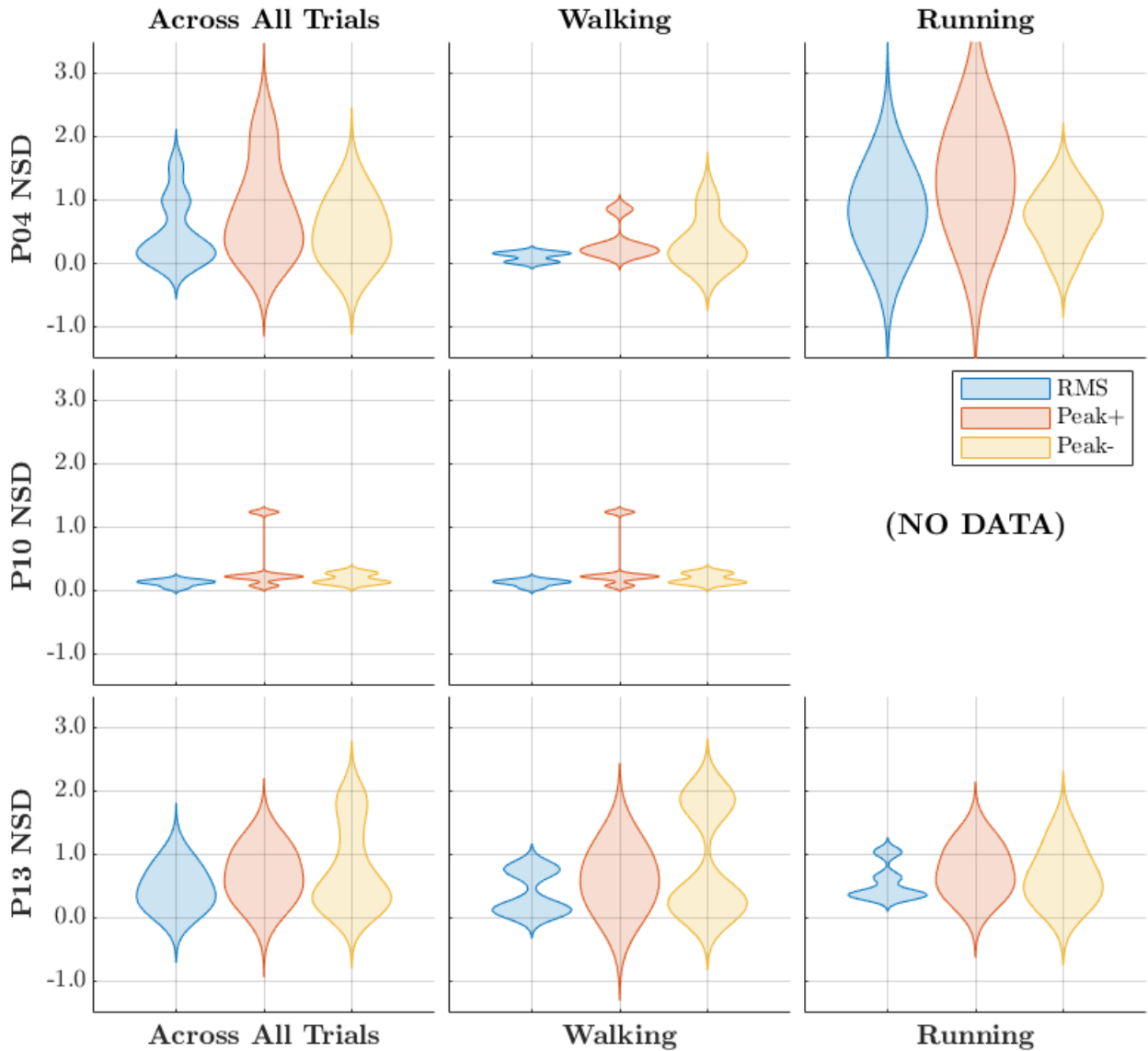


Figure 28: Participant-wise violin plot NSD comparison across lower-limb joint moment metrics: RMS, Peak positive (Peak+) and negative (Peak-) moments for walking, running, and aggregated trials. Rows show individual participants; columns separate aggregated, walking-only, and running-only conditions. **Note that no running NSD data was available for P10.**

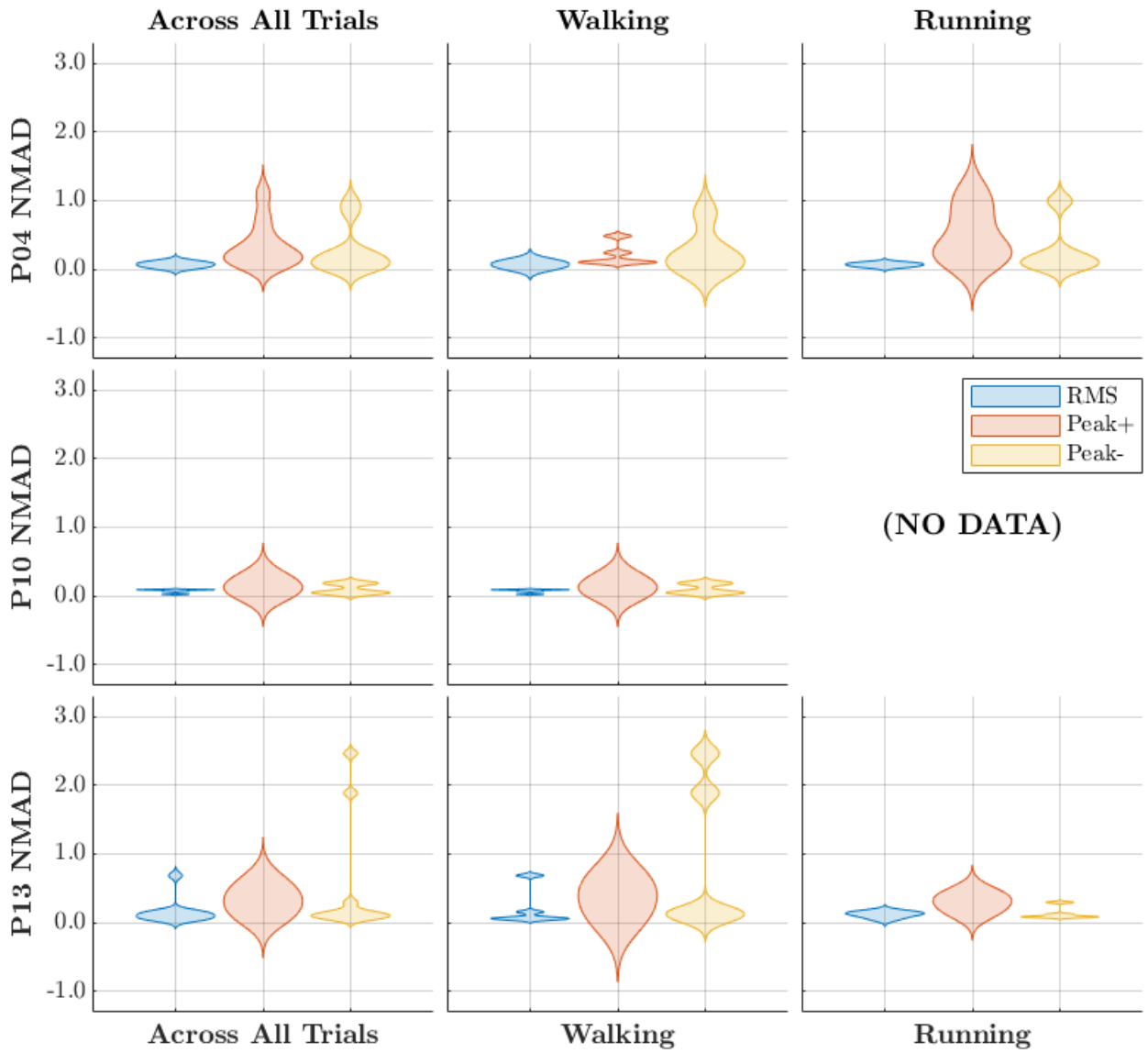


Figure 29: Participant-wise violin plot NMAD comparison across lower-limb joint moment metrics: RMS, Peak positive (Peak+) and negative (Peak-) moments for walking, running, and aggregated trials. Rows show individual participants; columns separate aggregated, walking-only, and running-only conditions. ***Note that no running MAD data was available for P10.***

Examining NSD, Participant 04 demonstrated better consistency during walking compared to running, whereas Participant 13 showed relatively consistent variability across both conditions; more consistent than Participant 04 in running, but less so in walking. Notably, all participants exhibited evidence of bimodal or multimodal variability distributions, particularly in peak negative moments. This pattern was mirrored in NMAD plots, where all participants displayed variability clustering around two or more main concentrations, and possibly indicates underlying methodological issues during simulation setup.

A possible cause of the observed bimodal distribution could be asymmetric gait, whereby left and right-side stance profiles differ meaningfully from one another. A potential example of this asymmetry is illustrated in Figure 30, which shows left-right differences in peak hip extension moments for Participant 04. However, since the study's primary aim was to generate aggregate joint moment

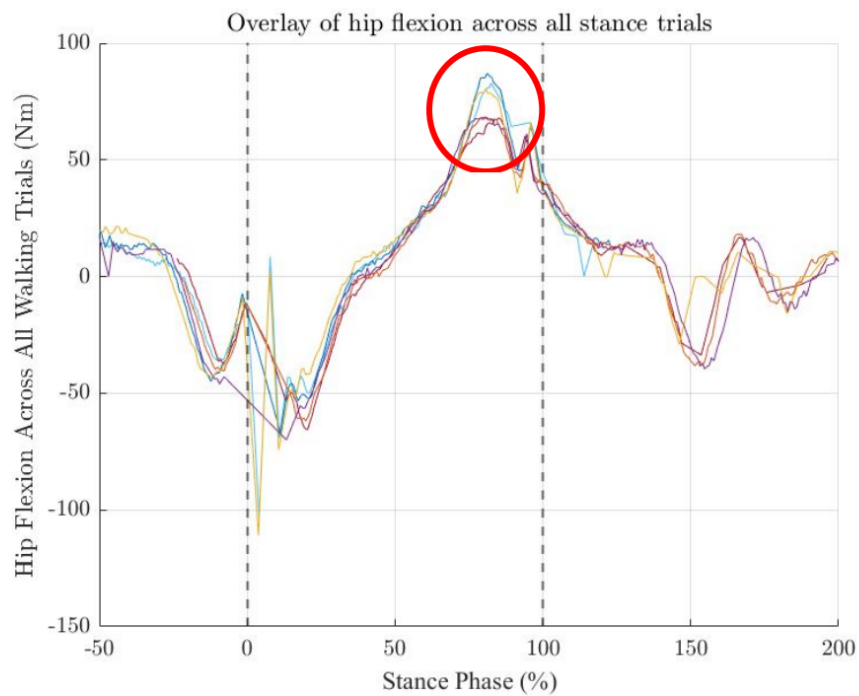
datasets rather than to investigate asymmetry specifically, this phenomenon was not explored in detail. Nonetheless, these findings highlight the importance of participant-specific model setup and provide potential points to explore in future work.

## 8.5 Variability Analysis Summary and Limitations

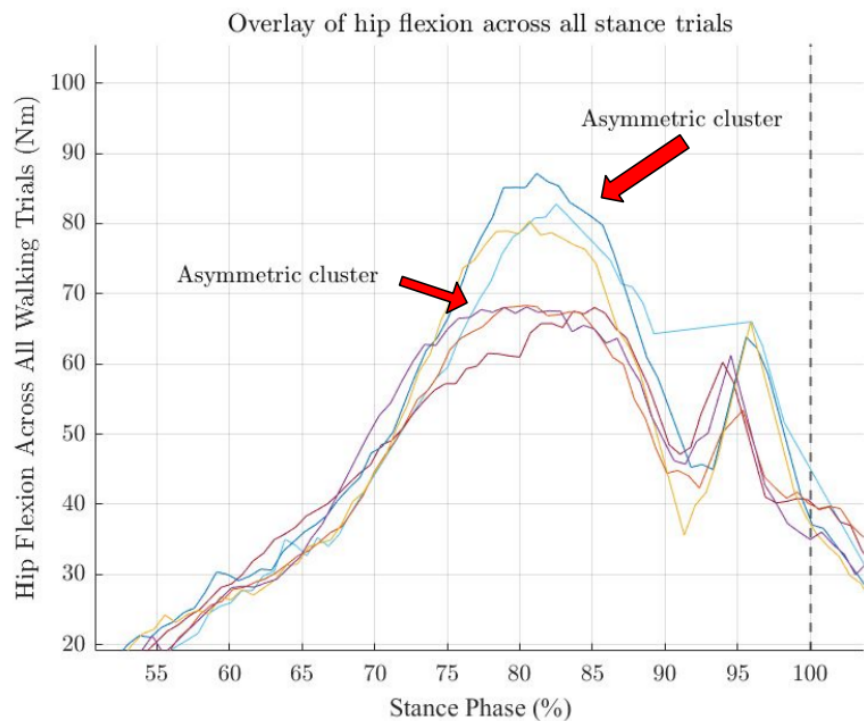
This statistical variability analysis provided a detailed examination of simulation consistency across exercises, joints, and participants. Overall, walking trials exhibited substantially lower variability than running, particularly in moment RMS values, while peak moments, especially during heel-strike, consistently showed the greatest variability spread across all conditions. Joint-level analysis revealed that the knee and ankle were more variable than the hip, with the ankle standing out for its irregular, often bimodal distributions, particularly under walking conditions. Participant-level trends further highlighted individual differences, with evidence of bimodal variability patterns across all participants and some indications of asymmetric gait. While these asymmetries were noted qualitatively, they were not systematically analysed, as the study's primary aim was to generate aggregate joint moment datasets rather than investigate inter-limb differences.

Despite the insights, several limitations should be acknowledged. First, the small sample size (six stance samples, per participant, per exercise condition) limits the generalisability of these findings, with the exclusion of running data from Participant 10 further reducing statistical confidence. Second, while normalising SD and MAD by mean or median enabled unitless comparisons across variables and conditions, this approach is sensitive to small or near-zero denominators. This potentially risks inflating variability estimates, especially in directions where mean and median values approach zero or change sign. Additionally, averaging variability metrics across degrees of freedom may have masked high variability in specific planes of motion, such as sagittal-plane knee flexion, under the smoother appearance of joint-level summary values. Finally, while the denoising filters improved overall data stability, they may have inadvertently suppressed meaningful variability or masked underlying errors, such as in the ankle, where methodological limitations appeared the most evident.

Overall, this analysis provides a quantitative characterisation of the variability patterns within this study's dataset, and highlights potential areas for methodological improvement in the future, such as improvements in ankle modelling, participant scaling, and filtering approaches.



(a) Scatter plot hip flexion moment across all walking trials for Participant 4, with detail b. circled in red.



(b) Zoomed in detail showing asymmetric effects in peak left and right hip extension moments

Figure 30: Scatter plot showing asymmetry in peak hip extension moment at left and right joints for Participant 4 during walking trials.

## 9 Discussion

### 9.1 Project Summary

This study investigated the biomechanical loading of the musculoskeletal system during exercise, with a particular focus on joint moments at the hip, knee, and ankle during the stance phase of walking and running. Mo-Cap and force-plate data from four healthy participants were used to initialise simulations in OpenSim and create individualised MSK models. Two muscle force estimation approaches, static optimisation and CMC, were explored to estimate joint moments; however, due to methodological constraints with CMC, final analysis relied exclusively on static optimisation.

Analysis was divided into three major sections, with the first section documenting the results of individual MSK scaling and inverse kinematics pertaining to initial simulation setup. The second section, forming the majority of analysis, reported joint moment profiles during walking and running for all participants, comparing observed trends against existing literature. Finally, the third stage of analysis involved conducting a statistical variability analysis across exercises, joints, and participants.

### 9.2 Interpretation

Generally, simulation results showed good agreement with the literature regarding overall moment patterns during stance, with the most agreement at the hip joint during walking. However, systematic differences in specific moment magnitudes were also observed, with notable deviations at the knee and ankle. This was especially noticeable during heel-strike and toe-off, associated with the highest-acceleration phases of stance. Statistical analysis quantitatively demonstrated that walking trials produced more consistent results than running, exhibiting roughly half the variability across NSD and NMAD metrics, and also highlighted the ankle joint as being particularly susceptible to simulation error. It is important to note, however, that factors such as small sample size and methodological data exclusions represent key limitations that provide important context before interpreting these results.

A particularly notable finding was the crouch gait moment profiles observed in one participant (Participant 10) during analysis. Upon inspection, this participant had the largest marker scaling error at the pelvis (iliac crest), unlike other participants who showed their largest errors in the upper limbs. This suggests that this inaccurate crouch gait pattern likely resulted from pelvic scaling error, and that future simulations should prioritise pelvic over upper-limb markers during scaling. Furthermore, it also indicates that the assumption made in this study that leg markers should be prioritised over torso markers during the scaling was invalid, as pelvic accuracy proved critical to downstream simulation accuracy.

This interpretation was further supported by the cross-joint variability analysis, which showed the least variability at the hip, moderate variability at the knee, and the greatest at the ankle. Whilst this may initially suggest that the hip joint is the least susceptible to error, it is more likely that variability originating at the hip propagates distally to the knee and ankle, due to the hierarchical way these segments are defined within the OpenSim musculoskeletal model. That is, scaling at the hip should be *prioritised over* more distal segments.

Together, these findings point towards scaling errors, especially at the pelvis, as a key driver of the observed variability within this research. However, it is also worth noting that idealisations within the MSK model itself, such as simplified knee and ankle joints, likely also contributed to

these inconsistencies, and should also be considered during methodological planning.

Given the body of evidence surrounding scaling error, it is likely that this was the cause of failure within the dynamic CMC algorithm, which is more sensitive to noise than static optimisation [55], [120], [121]. That is, due to CMC’s higher sensitivity, the downstream effects of scaling errors likely prevented it from generating plausible solutions within the physiological constraints of the musculoskeletal model.

In summary, whilst the aggregate moment profiles generated in this study indicated broadly reasonable simulation performance, the subsequent variability analysis highlighted methodological weaknesses in scaling quality. This was identified as the critical limiting factor in achieving more reliable and consistent results, aligning with the well-documented importance of accurate scaling in musculoskeletal modelling pipelines [55], [87].

## 9.3 Limitations

### 9.3.1 Scope

This study focused on estimating MSK joint moments during walking and running, providing insight into lower-limb loading patterns during gait. However, a key limitation is that it did not estimate direct MSK or joint-reaction forces, and instead focused exclusively on moments. Whilst moments offer useful mechanical proxies in biomechanical research, future work incorporating muscle force and skeletal-load estimation would improve the clinical and biomechanical relevance of this work to its applications in FEM bone modelling and osteoporotic care.

Moments analysis was also limited to examining joint loading conditions in just the stance phase, which do not fully capture the biomechanical demands of gait, especially regarding running, where swing-phase muscle contributions and higher accelerations play important roles [175], [182]. Furthermore, this study focused exclusively on musculoskeletal load demands, and did not directly consider neurological activation factors that also play an important role during exercise.

Regarding sample representation, the dataset used in this study was small, with only three participants (two males, one female) used in the final analysis. This limits the generalisability of the findings in this work, especially noting that the base Rajagopal model used was male-based, and may not have captured important sex-specific differences. Asymmetry within participants was also briefly observed but not systematically explored, leaving another potential source of variability unexamined.

### 9.3.2 Methodological Factors

This study relied on marker-based motion capture data, which introduces inherent limitations. Markers can shift relative to the underlying bone, introducing STA errors, particularly during high-acceleration movements. Consequently, while such systems can provide highly accurate estimates for overall kinematic patterns, they are less reliable for detailed joint-level analyses [61].

In terms of modelling, the scaling process in this study required manual adjustments to match the provided dataset. Scaling was only performed once per participant using a static trial before using the produced model for all remaining simulations, which may have allowed small errors to propagate across conditions. This decision to scale using a single trial for all conditions was necessary given scope-limitations, but may have affected accuracy.

Finally, while the statistical variability framework developed in this study offers a promising approach to quantifying consistency across biomechanical simulations in the future, it carries several important limitations. First, the small sample size used within this study reduces statistical power, and heightens the risk of over-emphasising participant-specific effects. Second, the variability metrics involved in the framework, NSD and NMAD, are sensitive to sample means or medians near zero and to distributions extending into the negative domain. This makes the method particularly vulnerable to the influence of noisy or poor-quality samples, or to contexts where variability has already been substantially reduced. Without a reference standard or ground-truth dataset, it also remains difficult to assess how well these metrics reflect true biomechanical variability. Nonetheless, these limitations present an opportunity for further development, validation, and testing of the statistical framework in future studies with larger and more diverse datasets.

## 9.4 Implications

The findings of this study highlight several important implications for biomechanical modelling practices. First and foremost, scaling inaccuracies were found to consistently propagate downstream from the pelvis, compromising knee and ankle kinematics. This underscores the importance of precise and robust scaling procedures, particularly when physiological accuracy is a priority. While participant-specific findings such as the crouch gait patterns observed in Participant 10 may initially appear to be isolated cases, the recurrence of similar variability patterns across joints and exercises within this study suggest a more systematic challenge within the simulation methods used.

Notably, the variability analysis framework developed in this study offers a promising tool to help address these challenges. While aggregate moment profiles broadly matched published literature, this framework uncovered subtle but systematic instabilities that may otherwise have gone undetected. Integrating such statistical approaches into routine simulation analysis could provide real-time feedback, helping to identify data quality or modelling issues before they compromise downstream results. As the field moves toward larger datasets and increasingly automated pipelines, the ability to monitor quality at scale will become increasingly critical.

An intriguing trade-off also emerged from the findings of this study: Although poor scaling clearly affected individual trial reliability, aggregated results across participants and trials still aligned reasonably well with literature benchmarks. This raises a valuable question for future database development: whether relaxing individual scaling criteria, in favour of processing larger datasets, could be a viable strategy when the primary goal is to generate robust, population-level insights.

## 9.5 Future work and Recommendations

Based on the findings of this work, several directions for future research can be identified. First, improving scaling accuracy, particularly at the pelvis, presents the most immediate opportunity for enhancing simulation quality. Trial-specific scaling approaches or the integration of automated scaling tools may assist in this, helping to improve simulation consistency and MSK model quality.

Second, the analysis of this study interestingly suggest that some of the variability introduced by imperfect scaling can be partially mitigated when simulations are aggregated across sufficiently large and diverse participant groups. This raises an opportunity to explore the feasibility and limits of such aggregation, as well as to investigate how factors like gender, age, and gait asymmetry influence biomechanical outcomes across populations. If aggregation proves to be an effective tool for improving dataset reliability, it presents a potential opportunity to relax current scaling requirements, significantly broadening the scope and efficiency of large-scale biomechanical research.

Third, the statistical variability framework developed in this study presents a potential tool for monitoring simulation quality, identifying subtle instabilities, and guiding dataset curation. However, given the small scale of this study, its broader applicability and usefulness across larger and more diverse datasets remains uncertain. This presents a potential opportunity for future research, which may help establish the framework's utility as a diagnostic tool and potentially contribute to improving the reliability and scalability of biomechanical simulation pipelines.

## 10 Conclusion

This dissertation explored the biomechanical moment loading patterns of the musculoskeletal system during the stance phase of walking and running, focusing on estimating hip, knee, and ankle joint moments using the OpenSim software. Based on motion capture and force plate data sourced from previous research, simulations generally reproduced literature-reported moment patterns, particularly at the hip joint whilst walking. However, systematic discrepancies in moment magnitudes were noted at the knee and ankle, especially during high-acceleration phases. This revealed methodological inadequacies, and statistical analysis showed that walking trials were approximately twice as consistent as running trials, and that the ankle exhibited the highest variability of the studied joints.

A key observation throughout this work was the role of scaling error, especially at the pelvis, in driving simulation quality. This was exemplified by one participant who displayed a crouch gait patterns in simulation despite being having definitively healthy gait during Mo-Cap. This participant had to be excluded from running trials due to simulation quality, underscoring how poor MSK scaling can severely compromise downstream kinematics.

While the results of this study offered valuable insights, several limitations are acknowledged. The small sample size limits generalisability, and this work focused only on joint moments without estimating muscle or joint contact forces. Additionally, the statistical variability framework developed for analysis was tested on a limited dataset, and its broader utility remains to be determined.

This dissertation identifies several promising avenues for future research. Enhancing scaling accuracy, particularly at the pelvis, appears to offer the greatest potential for improving simulation quality, with trial-specific or automated approaches presenting a promising solution. Notably, the findings of this research also suggest that aggregating simulations across larger and more diverse participant groups may partially mitigate individual scaling errors; presenting an opportunity to examine the feasibility of relaxing strict scaling requirements provided a large enough participant sample size. Finally, the statistical variability framework developed in this study demonstrates potential as a tool for monitoring simulation quality and informing dataset curation. However, its broader applicability remains to be established through validation on larger and more heterogeneous datasets, presenting another opportunity for future work.

## References

- [1] OpenAI, *ChatGPT-4*, 2024. [Online]. Available: <https://openai.com/>.
- [2] V. M. Porter JL, *Osteoporosis*, 2023. [Online]. Available: <https://www.ncbi.nlm.nih.gov/books/NBK441901/>.
- [3] A. Minkley, *Osteoporosis and Bone Health*. [Online]. Available: <https://www.desertspineandsports.com>.
- [4] I. O. F and I. O. Foundation, “Epidemiology, Burden, and Treatment of Osteoporosis in the United Kingdom,” Online, Tech. Rep., 2021.
- [5] M. A. Clynes, N. C. Harvey, E. M. Curtis, N. R. Fuggle, E. M. Dennison, and C. Cooper, “The epidemiology of osteoporosis,” eng, *Br Med Bull*, vol. 133, no. 1, pp. 105–117, 2020, ISSN: 0007-1420 (Print) 0007-1420. DOI: 10.1093/bmb/ldaa005.
- [6] C. G. Moran, R. T. Wenn, M. Sikand, and A. M. Taylor, “Early mortality after hip fracture: is delay before surgery important?” eng, *J Bone Joint Surg Am*, vol. 87, no. 3, pp. 483–489, 2005, ISSN: 0021-9355 (Print) 0021-9355. DOI: 10.2106/jbjs.D.01796.
- [7] M. Rizkallah, F. Bachour, M. E. Khoury, et al., “Comparison of morbidity and mortality of hip and vertebral fragility fractures: Which one has the highest burden?” eng, *Osteoporos Sarcopenia*, vol. 6, no. 3, pp. 146–150, 2020, ISSN: 2405-5255 (Print) 2405-5255. DOI: 10.1016/j.afos.2020.07.002.
- [8] Y. K. Lee, S. Jang, S. Jang, et al., “Mortality after vertebral fracture in Korea: analysis of the National Claim Registry,” eng, *Osteoporos Int*, vol. 23, no. 7, pp. 1859–1865, 2012, ISSN: 0937-941X. DOI: 10.1007/s00198-011-1833-5.
- [9] C. Downey, M. Kelly, and J. F. Quinlan, “Changing trends in the mortality rate at 1-year post hip fracture - a systematic review,” eng, *World J Orthop*, vol. 10, no. 3, pp. 166–175, 2019, ISSN: 2218-5836 (Print) 2218-5836. DOI: 10.5312/wjo.v10.i3.166. [Online]. Available: <https://www.wjgnet.com/2218-5836/full/v10/i3/166.htm>.
- [10] O. Johnell, J. A. Kanis, A. Odén, et al., “Mortality after osteoporotic fractures,” eng, *Osteoporos Int*, vol. 15, no. 1, pp. 38–42, 2004, ISSN: 0937-941X (Print) 0937-941X. DOI: 10.1007/s00198-003-1490-4.
- [11] O. Johnell, J. A. Kanis, A. Odén, et al., “Fracture risk following an osteoporotic fracture,” *Osteoporosis international : a journal established as result of cooperation between the European Foundation for Osteoporosis and the National Osteoporosis Foundation of the USA*, vol. 15, no. 3, pp. 175–179, 2004, ISSN: 0937-941X. DOI: 10.1007/S00198-003-1514-0. [Online]. Available: <https://pubmed.ncbi.nlm.nih.gov/14691617/>.
- [12] I. Hallberg, M. Bachrach-Lindström, S. Hammerby, G. Toss, and A. C. Ek, “Health-related quality of life after vertebral or hip fracture: a seven-year follow-up study,” *BMC musculoskeletal disorders*, vol. 10, no. 1, 2009, ISSN: 1471-2474. DOI: 10.1186/1471-2474-10-135. [Online]. Available: <https://pubmed.ncbi.nlm.nih.gov/19886998/>.
- [13] L. Johansson, H. K. Svensson, J. Karlsson, et al., “Decreased physical health-related quality of life-a persisting state for older women with clinical vertebral fracture,” *Osteoporosis international : a journal established as result of cooperation between the European Foundation for Osteoporosis and the National Osteoporosis Foundation of the USA*, vol. 30, no. 10, pp. 1961–1971, Oct. 2019, ISSN: 1433-2965. DOI: 10.1007/S00198-019-05044-0. [Online]. Available: <https://pubmed.ncbi.nlm.nih.gov/31227884/>.
- [14] F. Salaffi, M. Cimmino, N. Malavolta, et al., “The burden of prevalent fractures on health-related quality of life in postmenopausal women with osteoporosis: the IMOF study.,” *Journal of Rheumatology*, 2007.
- [15] J. Catherine Bree and D. Meenakshi, “Osteoporosis in Older Adults,” *Medical Clinics of North America*, vol. 104, no. 5, pp. 873–884, 2020, ISSN: 0025-7125. DOI: <https://doi.org/>

- 10.1016/j.mcna.2020.06.004. [Online]. Available: <https://www.sciencedirect.com/science/article/pii/S0025712520300560>.
- [16] National Health Service, *Osteoporosis*, 2022. [Online]. Available: <https://www.nhs.uk/conditions/osteoporosis/>.
- [17] J. A. Kanis, O. Johnell, A. Oden, *et al.*, “Long-term risk of osteoporotic fracture in Malmö,” eng, *Osteoporos Int*, vol. 11, no. 8, pp. 669–674, 2000, ISSN: 0937-941X (Print) 0937-941x. DOI: 10.1007/s001980070064.
- [18] B. Kirk, J. Zanker, and G. Duque, “Osteosarcopenia: epidemiology, diagnosis, and treatment-facts and numbers,” eng, *J Cachexia Sarcopenia Muscle*, vol. 11, no. 3, pp. 609–618, 2020, ISSN: 2190-5991 (Print) 2190-5991. DOI: 10.1002/jcsm.12567.
- [19] L. J. Melton 3rd, E. J. Atkinson, M. K. O’Connor, W. M. O’Fallon, and B. L. Riggs, “Bone density and fracture risk in men,” eng, *J Bone Miner Res*, vol. 13, no. 12, pp. 1915–1923, 1998, ISSN: 0884-0431 (Print) 0884-0431. DOI: 10.1359/jbmr.1998.13.12.1915.
- [20] “The World Population Prospects: 2015 Revision,” United Nations Department of Economic and Social Affairs, New York, Tech. Rep., Jul. 2015. [Online]. Available: <https://www.un.org/en/development/desa/publications/world-population-prospects-2015-revision.html#:~:text=The%20current%20world%20population%20of,2015%20Revision%E2%80%9D%2C%20launched%20today..>
- [21] C. Cooper, G. Campion, and L. J. Melton 3rd, “Hip fractures in the elderly: a world-wide projection,” eng, *Osteoporos Int*, vol. 2, no. 6, pp. 285–289, 1992, ISSN: 0937-941X (Print) 0937-941x. DOI: 10.1007/bf01623184.
- [22] C. Cooper, Z. A. Cole, C. R. Holroyd, *et al.*, “Secular trends in the incidence of hip and other osteoporotic fractures,” eng, *Osteoporos Int*, vol. 22, no. 5, pp. 1277–1288, 2011, ISSN: 0937-941X (Print) 0937-941x. DOI: 10.1007/s00198-011-1601-6.
- [23] International Osteoporosis Foundation, *Osteoporosis Prevention*, 2024. [Online]. Available: <https://www.osteoporosis.foundation/patients/prevention>.
- [24] EUR to GBP – Euros to Pound Sterlings Source: <https://eur.currencyrate.today/convert/amount-5500000-to-gbp.html>, Apr. 2025.
- [25] L. Warming, C. Hassager, and C. Christiansen, “Changes in bone mineral density with age in men and women: a longitudinal study,” eng, *Osteoporos Int*, vol. 13, no. 2, pp. 105–112, 2002, ISSN: 0937-941X (Print) 0937-941x. DOI: 10.1007/s001980200001.
- [26] J. S. Kenkre and J. Bassett, “The bone remodelling cycle,” eng, *Ann Clin Biochem*, vol. 55, no. 3, pp. 308–327, 2018, ISSN: 0004-5632. DOI: 10.1177/0004563218759371.
- [27] J. K. Hodges, S. Cao, D. P. Cladis, and C. M. Weaver, “Lactose Intolerance and Bone Health: The Challenge of Ensuring Adequate Calcium Intake,” eng, *Nutrients*, vol. 11, no. 4, 2019, ISSN: 2072-6643. DOI: 10.3390/nu11040718.
- [28] S. R. Cummings, M. C. Nevitt, W. S. Browner, *et al.*, “Risk Factors for Hip Fracture in White Women,” ISSN: 12.
- [29] OrthoInfo, *Osteoporosis Prevention and Treatment*, 2024. [Online]. Available: <https://orthoinfo.aaos.org/en/staying-healthy/osteoporosis-prevention/>.
- [30] D. W. Barry and W. M. Kohrt, “Exercise and the preservation of bone health,” eng, *J Cardiopulm Rehabil Prev*, vol. 28, no. 3, pp. 153–162, 2008, ISSN: 1932-7501 (Print) 1932-7501. DOI: 10.1097/01.HCR.0000320065.50976.7c.
- [31] M. Izquierdo, P. de Souto Barreto, H. Arai, *et al.*, “Global consensus on optimal exercise recommendations for enhancing healthy longevity in older adults (ICFSR),” *The journal of nutrition, health & aging*, vol. 29, no. 1, Jan. 2025, ISSN: 1760-4788. DOI: 10.1016/J.JNHA.2024.100401. [Online]. Available: <https://pubmed.ncbi.nlm.nih.gov/39743381/>.

- [32] M. G. Benedetti, G. Furlini, A. Zati, and G. Letizia Mauro, “The Effectiveness of Physical Exercise on Bone Density in Osteoporotic Patients,” eng, *Biomed Res Int*, vol. 2018, p. 4840531, 2018, ISSN: 2314-6133 (Print). DOI: 10.1155/2018/4840531.
- [33] D. B. Jepsen, J. Ryg, S. Hansen, N. R. Jørgensen, J. Gram, and T. Masud, “The combined effect of Parathyroid hormone (1-34) and whole-body Vibration exercise in the treatment of postmenopausal OSteoporosis (PaVOS study): a randomized controlled trial,” eng, *Osteoporos Int*, vol. 30, no. 9, pp. 1827–1836, 2019, ISSN: 0937-941X (Print) 0937-941x. DOI: 10.1007/s00198-019-05029-z.
- [34] L. D. Moreira, M. L. Oliveira, A. P. Lirani-Galvão, R. V. Marin-Mio, R. N. Santos, and M. Lazaretti-Castro, “Physical exercise and osteoporosis: effects of different types of exercises on bone and physical function of postmenopausal women,” eng, *Arq Bras Endocrinol Metabol*, vol. 58, no. 5, pp. 514–522, 2014, ISSN: 0004-2730. DOI: 10.1590/0004-2730000003374.
- [35] S. E. Linke, L. C. Gallo, and G. J. Norman, “Attrition and Adherence Rates of Sustained vs. Intermittent Exercise Interventions,” *Annals of behavioral medicine : a publication of the Society of Behavioral Medicine*, vol. 42, no. 2, p. 197, Oct. 2011, ISSN: 08836612. DOI: 10.1007/S12160-011-9279-8. [Online]. Available: <https://pmc.ncbi.nlm.nih.gov/articles/PMC3181282/>.
- [36] M. L. Pollock, G. A. Gaesser, J. D. Butcher, *et al.*, “The recommended quantity and quality of exercise for developing and maintaining cardiorespiratory and muscular fitness, and flexibility in healthy adults,” *Medicine and Science in Sports and Exercise*, vol. 30, no. 6, pp. 975–991, 1998, ISSN: 01959131. DOI: 10.1097/00005768-199806000-00032.
- [37] *Attrition and Adherence Rates of Sustained vs. Intermittent Exercise Interventions - PMC*. [Online]. Available: <https://pmc.ncbi.nlm.nih.gov/articles/PMC3181282/>.
- [38] J. P. Regnaux, M. M. Lefevre-Colau, L. Trinquart, *et al.*, “High-intensity versus low-intensity physical activity or exercise in people with hip or knee osteoarthritis,” *The Cochrane Database of Systematic Reviews*, vol. 2015, no. 10, p. CD010203, Oct. 2015, ISSN: 1469493X. DOI: 10.1002/14651858.CD010203.PUB2. [Online]. Available: <https://pmc.ncbi.nlm.nih.gov/articles/PMC9270723/>.
- [39] S. Kast, M. Shojaa, M. Kohl, *et al.*, “Effects of different exercise intensity on bone mineral density in adults: a comparative systematic review and meta-analysis,” *Osteoporosis International*, vol. 33, no. 8, p. 1643, Aug. 2022, ISSN: 14332965. DOI: 10.1007/S00198-022-06329-7. [Online]. Available: <https://pmc.ncbi.nlm.nih.gov/articles/PMC9499891/>.
- [40] M. Abdullah, A. A. Hulleck, R. Katmah, K. Khalaf, and M. El-Rich, “Multibody dynamics-based musculoskeletal modeling for gait analysis: a systematic review,” *Journal of NeuroEngineering and Rehabilitation*, vol. 21, no. 1, p. 178, Oct. 2024, ISSN: 1743-0003. DOI: 10.1186/s12984-024-01458-y. [Online]. Available: <https://jneuroengrehab.biomedcentral.com/articles/10.1186/s12984-024-01458-y>.
- [41] M. S. Andersen, “Introduction to musculoskeletal modelling,” *Computational Modelling of Biomechanics and Biotribology in the Musculoskeletal System: Biomaterials and Tissues*, pp. 41–80, Jan. 2021. DOI: 10.1016/B978-0-12-819531-4.00004-3.
- [42] *Orthoload: Loading of Orthopaedic Implants*, 2025. [Online]. Available: <https://orthoload.com>.
- [43] B. J. Fregly, T. F. Besier, D. G. Lloyd, *et al.*, “Grand challenge competition to predict in vivo knee loads,” *Journal of Orthopaedic Research*, vol. 30, no. 4, pp. 503–513, Apr. 2012, ISSN: 1554-527X. DOI: 10.1002/JOR.22023. [Online]. Available: <https://onlinelibrary.wiley.com/doi/full/10.1002/jor.22023%20https://onlinelibrary.wiley.com/doi/abs/10.1002/jor.22023%20https://onlinelibrary.wiley.com/doi/10.1002/jor.22023>.

- [44] D. J. Hadjidakis and I. I. Androulakis, "Bone remodeling," *Annals of the New York Academy of Sciences*, vol. 1092, pp. 385–396, 2006, ISSN: 0077-8923. DOI: 10.1196/ANNALS.1365.035. [Online]. Available: <https://pubmed.ncbi.nlm.nih.gov/17308163/>.
- [45] H. M. Frost, "Skeletal structural adaptations to mechanical usage (SATMU): 1. Redefining Wolff's Law: The bone modeling problem," *The Anatomical Record*, vol. 226, no. 4, pp. 403–413, 1990, ISSN: 10970185. DOI: 10.1002/AR.1092260402.
- [46] A. Bouguecha, N. Weigel, B. A. Behrens, C. Stukenborg-Colsman, and H. Waizy, "Numerical simulation of strain-adaptive bone remodelling in the ankle joint," *BioMedical Engineering Online*, vol. 10, Jul. 2011, ISSN: 1475925X. DOI: 10.1186/1475-925X-10-58.
- [47] A. Pant, E. Paul, G. L. Niebur, and A. Vahdati, "Integration of mechanics and biology in computer simulation of bone remodeling," eng, *Prog Biophys Mol Biol*, vol. 164, pp. 33–45, 2021, ISSN: 0079-6107. DOI: 10.1016/j.pbiomolbio.2021.05.001.
- [48] D. H. Pahr and A. G. Reisinger, "A Review on Recent Advances in the Constitutive Modeling of Bone Tissue," *Current osteoporosis reports*, vol. 18, no. 6, pp. 696–704, Dec. 2020, ISSN: 1544-2241. DOI: 10.1007/S11914-020-00631-1. [Online]. Available: <https://pubmed.ncbi.nlm.nih.gov/33068252/>.
- [49] D. M. Geraldes, L. Modenese, and A. T. Phillips, "Consideration of multiple load cases is critical in modelling orthotropic bone adaptation in the femur," eng, *Biomech Model Mechanobiol*, vol. 15, no. 5, pp. 1029–1042, 2016, ISSN: 1617-7959 (Print) 1617-7940. DOI: 10.1007/s10237-015-0740-7.
- [50] S. L. Delp, F. C. Anderson, A. S. Arnold, *et al.*, "OpenSim: Open-source software to create and analyze dynamic simulations of movement," *IEEE Transactions on Biomedical Engineering*, vol. 54, no. 11, pp. 1940–1950, Nov. 2007, ISSN: 00189294. DOI: 10.1109/TBME.2007.901024.
- [51] *AnyBody Technology. The AnyBody Modeling System.*
- [52] "Motek. Human Body Model," [Online]. Available: <https://www.motekmedical.com/software/hbm/>.
- [53] L. H. Sloot and M. M. Van der Krog, "Interpreting joint moments and powers in gait," *Handbook of Human Motion*, vol. 1-3, pp. 625–643, Apr. 2018. DOI: 10.1007/978-3-319-14418-4\\_\\_32/FIGURES/2. [Online]. Available: [https://link.springer.com/referenceworkentry/10.1007/978-3-319-14418-4\\_32](https://link.springer.com/referenceworkentry/10.1007/978-3-319-14418-4_32).
- [54] L. E. Diamond, K. Allison, F. Dobson, and M. Hall, "Hip joint moments during walking in people with hip osteoarthritis: a systematic review and meta-analysis," *Osteoarthritis and cartilage*, vol. 26, no. 11, pp. 1415–1424, Nov. 2018, ISSN: 1522-9653. DOI: 10.1016/J.JOCA.2018.03.011. [Online]. Available: <https://pubmed.ncbi.nlm.nih.gov/29621605/>.
- [55] J. L. Hicks, T. K. Uchida, A. Seth, A. Rajagopal, and S. L. Delp, "Is my model good enough? Best practices for verification and validation of musculoskeletal models and simulations of movement," *Journal of biomechanical engineering*, vol. 137, no. 2, Feb. 2015, ISSN: 1528-8951. DOI: 10.1115/1.4029304. [Online]. Available: <https://pubmed.ncbi.nlm.nih.gov/25474098/>.
- [56] *BioCV Motion Capture Dataset - University of Bath Research Data Archive*. [Online]. Available: <https://researchdata.bath.ac.uk/1258/>.
- [57] A. A. Hulleck, D. Menoth Mohan, N. Abdallah, M. El Rich, and K. Khalaf, "Present and future of gait assessment in clinical practice: Towards the application of novel trends and technologies," *Frontiers in Medical Technology*, vol. 4, 2022, ISSN: 26733129. DOI: 10.3389/FMEDT.2022.901331.
- [58] Sheng Kai Wong, "Project Scoping Report: Biomechanical Loading During Exercise for Maintaining Musculoskeletal System," University of Bath, Tech. Rep., Nov. 2024.
- [59] SimTK, *Home Page*, 2024. [Online]. Available: <https://simtk.org/>.

- [60] R. Parent, "Motion Capture," *Computer Animation*, pp. 187–198, 2012. DOI: 10.1016/B978-0-12-415842-9.00006-X. [Online]. Available: <https://linkinghub.elsevier.com/retrieve/pii/B978012415842900006X>.
- [61] G. Lamberto, S. Martelli, A. Cappozzo, and C. Mazzà, "To what extent is joint and muscle mechanics predicted by musculoskeletal models sensitive to soft tissue artefacts?" *Journal of Biomechanics*, vol. 62, pp. 68–76, Sep. 2017, ISSN: 18732380. DOI: 10.1016/J.JBIOMECH.2016.07.042.
- [62] N. A. Glover, R. S. Kakar, and A. M. Chaudhari, "Effects of spinal coupling and marker set on tracking of spine models during running," *Journal of Biomechanics*, vol. 116, Feb. 2021, ISSN: 18732380. DOI: 10.1016/j.jbiomech.2020.110217.
- [63] B. M. Potvin, M. S. Shourijeh, K. B. Smale, and D. L. Benoit, "A practical solution to reduce soft tissue artifact error at the knee using adaptive kinematic constraints," *Journal of Biomechanics*, vol. 62, pp. 124–131, Sep. 2017, ISSN: 18732380. DOI: 10.1016/J.JBIOMECH.2017.02.006.
- [64] S. Skals, K. P. Rasmussen, K. M. Bendtsen, J. Yang, and M. S. Andersen, "A musculoskeletal model driven by dual Microsoft Kinect Sensor data," *Multibody System Dynamics*, vol. 41, no. 4, pp. 297–316, Dec. 2017, ISSN: 1573272X. DOI: 10.1007/S11044-017-9573-8.
- [65] J. Rasmussen, M. Damsgaard, and M. Voigt, "Muscle recruitment by the min/max criterion - A comparative numerical study," *Journal of Biomechanics*, vol. 34, no. 3, pp. 409–415, 2001, ISSN: 00219290. DOI: 10.1016/S0021-9290(00)00191-3.
- [66] M. Eltoukhy, C. Kuenze, M. S. Andersen, J. Oh, and J. Signorile, "Prediction of ground reaction forces for Parkinson's disease patients using a kinect-driven musculoskeletal gait analysis model," *Medical Engineering and Physics*, vol. 50, pp. 75–82, Dec. 2017, ISSN: 18734030. DOI: 10.1016/J.MEDENGPHY.2017.10.004.
- [67] L. Needham, M. Evans, L. Wade, *et al.*, "The development and evaluation of a fully automated markerless motion capture workflow," *Journal of Biomechanics*, vol. 144, Nov. 2022, ISSN: 18732380. DOI: 10.1016/j.jbiomech.2022.111338.
- [68] M. Evans, L. Needham, L. Wade, *et al.*, "Synchronised Video, Motion Capture and Force Plate Dataset for Validating Markerless Human Movement Analysis," *Scientific Data*, vol. 11, no. 1, p. 1300, Nov. 2024, ISSN: 2052-4463. DOI: 10.1038/S41597-024-04077-3. [Online]. Available: <https://researchportal.bath.ac.uk/en/publications/synchronised-video-motion-capture-and-force-plate-dataset-for-val>.
- [69] I. Coll, M. P. Mavor, T. Karakolis, R. B. Graham, and A. L. Clouthier, "Validation of Markerless Motion Capture for Soldier Movement Patterns Assessment Under Varying Body-Borne Loads," *Annals of Biomedical Engineering*, vol. 53, no. 2, pp. 358–370, Feb. 2025, ISSN: 0090-6964. DOI: 10.1007/S10439-024-03622-W. [Online]. Available: <https://link.springer.com/10.1007/s10439-024-03622-w>.
- [70] T. T. Brunyé, J. McIntyre, G. I. Hughes, and E. L. Miller, "Movement Sensing Opportunities for Monitoring Dynamic Cognitive States.,," *Sensors (Basel, Switzerland)*, vol. 24, no. 23, Nov. 2024, ISSN: 1424-8220. DOI: 10.3390/s24237530. [Online]. Available: <http://www.ncbi.nlm.nih.gov/pubmed/39686067%20http://www.ncbi.nlm.nih.gov/pmc/articles/PMC11644645>.
- [71] W. van den Hoorn, A. Fabre, G. Nardese, *et al.*, "The Future of Clinical Active Shoulder Range of Motion Assessment, Best Practice, and Its Challenges: Narrative Review.,," *Sensors (Basel, Switzerland)*, vol. 25, no. 3, Jan. 2025, ISSN: 1424-8220. DOI: 10.3390/s25030667. [Online]. Available: <http://www.ncbi.nlm.nih.gov/pubmed/39943306%20http://www.ncbi.nlm.nih.gov/pmc/articles/PMC11820973>.
- [72] P. Bonato, V. Feipel, G. Corniani, G. Arin-Bal, and A. Leardini, "Position paper on how technology for human motion analysis and relevant clinical applications have evolved over

- the past decades: Striking a balance between accuracy and convenience,” *Gait and Posture*, vol. 113, pp. 191–203, Sep. 2024, ISSN: 18792219. DOI: 10.1016/j.gaitpost.2024.06.007.
- [73] C. A. Bailey, T. K. Uchida, J. Nantel, and R. B. Graham, “Validity and sensitivity of an inertial measurement unit-driven biomechanical model of motor variability for gait,” *Sensors*, vol. 21, no. 22, Nov. 2021, ISSN: 14248220. DOI: 10.3390/S21227690.
- [74] A. Karatsidis, M. Jung, H. M. Schepers, *et al.*, “Musculoskeletal model-based inverse dynamic analysis under ambulatory conditions using inertial motion capture,” *Medical Engineering & Physics*, vol. 65, pp. 68–77, Mar. 2019, ISSN: 1350-4533. DOI: 10.1016/J.MEDENGPHY.2018.12.021.
- [75] J. F. Hafer, J. A. Mihy, A. Hunt, R. F. Zernicke, and R. T. Johnson, “Lower Extremity Inverse Kinematics Results Differ Between Inertial Measurement Unit- and Marker-Derived Gait Data,” *Journal of Applied Biomechanics*, vol. 39, no. 3, pp. 133–142, Jun. 2023, ISSN: 15432688. DOI: 10.1123/JAB.2022-0194.
- [76] L. Pacher, L. Carcreff, S. Armand, C. Chatellier, R. Vauzelle, and L. Fradet, “Gait kinematics based on inertial measurement units with the sensor-to-segment calibration and multibody optimization adapted to the patient’s motor capacities, a pilot study,” *Gait and Posture*, vol. 108, pp. 275–281, Feb. 2024, ISSN: 18792219. DOI: 10.1016/J.GAITPOST.2023.12.015.
- [77] M. Couvertier, L. Pacher, and L. Fradet, “Does IMU redundancy improve multi-body optimization results to obtain lower-body kinematics? A preliminary study says no,” *Journal of Biomechanics*, vol. 168, May 2024, ISSN: 18732380. DOI: 10.1016/j.jbiomech.2024.112091.
- [78] K. Ahmed, S. Taheri, I. Weygers, and M. Ortiz-Catalan, “Validation of IMU against optical reference and development of open-source pipeline: proof of concept case report in a participant with transfemoral amputation fitted with a Percutaneous Osseointegrated Implant,” *Journal of NeuroEngineering and Rehabilitation*, vol. 21, no. 1, Dec. 2024, ISSN: 17430003. DOI: 10.1186/S12984-024-01426-6.
- [79] M. Gutierrez, B. Gomez, G. Retamal, *et al.*, “Comparing Optical and Custom IoT Inertial Motion Capture Systems for Manual Material Handling Risk Assessment Using the NIOSH Lifting Index,” *Technologies 2024, Vol. 12, Page 180*, vol. 12, no. 10, p. 180, Sep. 2024, ISSN: 2227-7080. DOI: 10.3390/TECHNOLOGIES12100180. [Online]. Available: <https://www.mdpi.com/2227-7080/12/10/180>
- [80] N. K. Mangal and A. K. Tiwari, “A review of the evolution of scientific literature on technology-assisted approaches using RGB-D sensors for musculoskeletal health monitoring,” *Computers in Biology and Medicine*, vol. 132, May 2021, ISSN: 18790534. DOI: 10.1016/J.COMPBIOMED.2021.104316.
- [81] N. Dur, M. Wesseling, E. Macri, and J. Runhaar, “Fluoroscopy: Taking a closer look at joint motion in osteoarthritis,” *Osteoarthritis Imaging*, vol. 4, no. 3, p. 100240, Sep. 2024, ISSN: 27726541. DOI: 10.1016/J.OSTIMA.2024.100240.
- [82] M. S. Zihlmann, H. Gerber, A. Stacoff, K. Burckhardt, G. Székely, and E. Stüssi, “Three-dimensional kinematics and kinetics of total knee arthroplasty during level walking using single plane video-fluoroscopy and force plates: A pilot study,” *Gait and Posture*, vol. 24, no. 4, pp. 475–481, Dec. 2006, ISSN: 09666362. DOI: 10.1016/J.GAITPOST.2005.12.012.
- [83] K. Matsuki, K. O. Matsuki, T. Kenmoku, S. Yamaguchi, T. Sasho, and S. A. Banks, “In vivo kinematics of early-stage osteoarthritic knees during pivot and squat activities,” *Gait and Posture*, vol. 58, pp. 214–219, Oct. 2017, ISSN: 18792219. DOI: 10.1016/J.GAITPOST.2017.07.116.
- [84] S. Hodel, B. Postolka, A. Flury, *et al.*, “Influence of Bone Morphology on In Vivo Tibio-Femoral Kinematics in Healthy Knees during Gait Activities,” *Journal of Clinical Medicine*, vol. 11, no. 17, Sep. 2022, ISSN: 20770383. DOI: 10.3390/JCM11175082.

- [85] A. Karatsidis, G. Bellusci, H. M. Schepers, M. de Zee, M. S. Andersen, and P. H. Veltink, “Estimation of ground reaction forces and moments during gait using only inertial motion capture,” *Sensors (Switzerland)*, vol. 17, no. 1, Jan. 2017, ISSN: 14248220. DOI: 10.3390/S17010075.
- [86] E. D. Syrett, C. L. Peterson, and B. J. Darter, “Assessing the effects of gait asymmetry: Using a split-belt treadmill walking protocol to change step length and peak knee joint contact force symmetry,” *Journal of Biomechanics*, vol. 125, Aug. 2021, ISSN: 18732380. DOI: 10.1016/J.JBIOMECH.2021.110583.
- [87] M. S. Andersen, “How sensitive are predicted muscle and knee contact forces to normalization factors and polynomial order in the muscle recruitment criterion formulation?” *International Biomechanics*, vol. 5, no. 1, pp. 88–103, Jan. 2018, ISSN: 23335432. DOI: 10.1080/23335432.2018.1514278. [Online]. Available: <https://www.tandfonline.com/doi/abs/10.1080/23335432.2018.1514278>.
- [88] C. Pizzolato, D. G. Lloyd, M. Sartori, *et al.*, “CEINMS: A toolbox to investigate the influence of different neural control solutions on the prediction of muscle excitation and joint moments during dynamic motor tasks,” *Journal of Biomechanics*, vol. 48, no. 14, pp. 3929–3936, Nov. 2015, ISSN: 0021-9290. DOI: 10.1016/J.JBIOMECH.2015.09.021.
- [89] M. Sartori, D. Farina, and D. G. Lloyd, “Hybrid neuromusculoskeletal modeling to best track joint moments using a balance between muscle excitations derived from electromyograms and optimization,” *Journal of Biomechanics*, vol. 47, no. 15, pp. 3613–3621, Nov. 2014, ISSN: 0021-9290. DOI: 10.1016/J.JBIOMECH.2014.10.009.
- [90] J. J. Banks, B. R. Umberger, and G. E. Caldwell, “EMG optimization in OpenSim: A model for estimating lower back kinetics in gait,” *Medical Engineering and Physics*, vol. 103, May 2022, ISSN: 18734030. DOI: 10.1016/J.MEDENGPHY.2022.103790.
- [91] H. X. Hoang, L. E. Diamond, D. G. Lloyd, and C. Pizzolato, “A calibrated EMG-informed neuromusculoskeletal model can appropriately account for muscle co-contraction in the estimation of hip joint contact forces in people with hip osteoarthritis,” *Journal of Biomechanics*, vol. 83, pp. 134–142, Jan. 2019, ISSN: 18732380. DOI: 10.1016/J.JBIOMECH.2018.11.042.
- [92] A. Bu, M. K. MacLean, and D. P. Ferris, “EMG-informed neuromuscular model assesses the effects of varied bodyweight support on muscles during overground walking,” *Journal of Biomechanics*, vol. 151, Apr. 2023, ISSN: 18732380. DOI: 10.1016/J.JBIOMECH.2023.111532.
- [93] K. Veerkamp, W. Schallig, J. Harlaar, *et al.*, “The effects of electromyography-assisted modelling in estimating musculotendon forces during gait in children with cerebral palsy,” *Journal of Biomechanics*, vol. 92, pp. 45–53, Jul. 2019, ISSN: 18732380. DOI: 10.1016/J.JBIOMECH.2019.05.026.
- [94] M. Romanato, D. Volpe, A. Guiotto, F. Spolaor, M. Sartori, and Z. Sawacha, “Electromyography-informed modeling for estimating muscle activation and force alterations in Parkinson’s disease,” *Computer Methods in Biomechanics and Biomedical Engineering*, vol. 25, no. 1, pp. 14–26, 2022, ISSN: 14768259. DOI: 10.1080/10255842.2021.1925887.
- [95] C. M. Butowicz, P. R. Golyski, J. C. Acasio, and B. D. Hendershot, “Comparing spinal loads in individuals with unilateral transtibial amputation with and without chronic low back pain: An EMG-informed approach,” *Journal of Biomechanics*, vol. 166, Mar. 2024, ISSN: 18732380. DOI: 10.1016/J.JBIOMECH.2024.111966.
- [96] S. L. Delp, J. P. Loan, M. G. Hoy, F. E. Zajac, E. L. Topp, and J. M. Rosen, “An Interactive Graphics-Based Model of the Lower Extremity to Study Orthopaedic Surgical Procedures,” *IEEE Transactions on Biomedical Engineering*, vol. 37, no. 8, pp. 757–767, 1990, ISSN: 15582531. DOI: 10.1109/10.102791.

- [97] G. T. Yamaguchi and F. E. Zajac, “A planar model of the knee joint to characterize the knee extensor mechanism,” *Journal of Biomechanics*, vol. 22, no. 1, pp. 1–10, 1989, ISSN: 00219290. DOI: 10.1016/0021-9290(89)90179-6.
- [98] F. C. Anderson and M. G. Pandy, “A dynamic optimization solution for vertical jumping in three dimensions,” *Computer Methods in Biomechanics and Biomedical Engineering*, vol. 2, no. 3, pp. 201–231, 1999, ISSN: 10255842. DOI: 10.1080/10255849908907988.
- [99] L. Modenese, A. T. Phillips, and A. M. Bull, “An open source lower limb model: Hip joint validation,” *Journal of Biomechanics*, vol. 44, no. 12, pp. 2185–2193, Aug. 2011, ISSN: 00219290. DOI: 10.1016/j.jbiomech.2011.06.019.
- [100] A. Rajagopal, C. L. Dembia, M. S. DeMers, D. D. Delp, J. L. Hicks, and S. L. Delp, “Full-Body Musculoskeletal Model for Muscle-Driven Simulation of Human Gait,” *IEEE Transactions on Biomedical Engineering*, vol. 63, no. 10, pp. 2068–2079, Oct. 2016, ISSN: 15582531. DOI: 10.1109/TBME.2016.2586891.
- [101] A. M. Willson, *A Quasi-Passive Biarticular Prosthesis and Novel Musculoskeletal Model for Transtibial Amputees*, 2017. [Online]. Available: <http://hdl.handle.net/1773/40644>.
- [102] R. Carloni, R. Luinge, and V. Raveendranathan, “The gait1415+2 OpenSim musculoskeletal model of transfemoral amputees with a generic bone-anchored prosthesis,” *Medical Engineering and Physics*, vol. 123, Jan. 2024, ISSN: 18734030. DOI: 10.1016/J.MEDENGPHY.2023.104091.
- [103] Y. Lin, J. W. Rankin, L. P. Lamas, M. Moazen, and J. R. Hutchinson, “Hindlimb kinematics, kinetics and muscle dynamics during sit-to-stand and sit-to-walk transitions in emus (<i>Dromaius novaehollandiae</i>),” *Journal of Experimental Biology*, vol. 227, no. 24, Dec. 2024, ISSN: 0022-0949. DOI: 10.1242/JEB.247519. [Online]. Available: <https://journals.biologists.com/jeb/article/227/24/jeb247519/363280/Hindlimb-kinematics-kinetics-and-muscle-dynamics>.
- [104] J. N. Maharaj, M. J. Rainbow, A. G. Cresswell, et al., “Modelling the complexity of the foot and ankle during human locomotion: the development and validation of a multi-segment foot model using biplanar videoradiography,” *Computer Methods in Biomechanics and Biomedical Engineering*, vol. 25, no. 5, pp. 554–565, 2022, ISSN: 14768259. DOI: 10.1080/10255842.2021.1968844.
- [105] M. A. Zandbergen, W. Schallig, J. A. Stebbins, J. Harlaar, and M. M. van der Krog, “The effect of mono- versus multi-segment musculoskeletal models of the foot on simulated triceps surae lengths in pathological and healthy gait,” *Gait and Posture*, vol. 77, pp. 14–19, Mar. 2020, ISSN: 18792219. DOI: 10.1016/J.GAITPOST.2020.01.010.
- [106] M. S. Harrington and T. A. Burkhardt, “Validation of a musculoskeletal model to investigate hip joint mechanics in response to dynamic multiplanar tasks,” *Journal of Biomechanics*, vol. 158, Sep. 2023, ISSN: 18732380. DOI: 10.1016/J.JBIOMECH.2023.111767.
- [107] S. R. Hamner and S. L. Delp, “Muscle contributions to fore-aft and vertical body mass center accelerations over a range of running speeds,” *Journal of Biomechanics*, vol. 46, no. 4, pp. 780–787, Feb. 2013, ISSN: 00219290. DOI: 10.1016/j.jbiomech.2012.11.024.
- [108] A. K. Lai, A. S. Arnold, and J. M. Wakeling, “Why are Antagonist Muscles Co-activated in My Simulation? A Musculoskeletal Model for Analysing Human Locomotor Tasks,” *Annals of Biomedical Engineering*, vol. 45, no. 12, pp. 2762–2774, Dec. 2017, ISSN: 15739686. DOI: 10.1007/s10439-017-1920-7.
- [109] E. J. Caruthers, J. A. Thompson, A. M. Chaudhari, et al., “Muscle Forces and Their Contributions to Vertical and Horizontal Acceleration of the Center of Mass During Sit-to-Stand Transfer in Young, Healthy Adults,” *Journal of Applied Biomechanics*, vol. 32, no. 5, pp. 487–503, Oct. 2016, ISSN: 1065-8483. DOI: 10.1123/JAB.2015-0291. [Online]. Available: <https://journals.human kinetics.com/view/journals/jab/32/5/article-p487.xml>.

- [110] S. A. Roelker, E. J. Caruthers, R. K. Baker, N. C. Pelz, A. M. Chaudhari, and R. A. Siston, “Interpreting Musculoskeletal Models and Dynamic Simulations: Causes and Effects of Differences Between Models,” *Annals of Biomedical Engineering*, vol. 45, no. 11, pp. 2635–2647, Nov. 2017, ISSN: 15739686. DOI: 10.1007/S10439-017-1894-5.
- [111] C. Curreli, F. Di Puccio, G. Davico, L. Modenese, and M. Viceconti, “Using Musculoskeletal Models to Estimate in vivo Total Knee Replacement Kinematics and Loads: Effect of Differences Between Models,” *Frontiers in Bioengineering and Biotechnology*, vol. 9, Jul. 2021, ISSN: 22964185. DOI: 10.3389/FBIOE.2021.703508.
- [112] B. Mathai and S. Gupta, “Numerical predictions of hip joint and muscle forces during daily activities: A comparison of musculoskeletal models,” *Proceedings of the Institution of Mechanical Engineers, Part H: Journal of Engineering in Medicine*, vol. 233, no. 6, pp. 636–647, Jun. 2019, ISSN: 20413033. DOI: 10.1177/0954411919840524.
- [113] A. Di Pietro, A. Bersani, C. Curreli, and F. Di Puccio, “AST: An OpenSim-based tool for the automatic scaling of generic musculoskeletal models,” *Computers in Biology and Medicine*, vol. 175, Jun. 2024, ISSN: 18790534. DOI: 10.1016/J.COMPBIMED.2024.108524.
- [114] H. Kainz, H. X. Hoang, C. Stockton, R. R. Boyd, D. G. Lloyd, and C. P. Carty, “Accuracy and reliability of marker-based approaches to scale the pelvis, thigh, and shank segments in musculoskeletal models,” *Journal of Applied Biomechanics*, vol. 33, no. 5, pp. 354–360, Oct. 2017, ISSN: 15432688. DOI: 10.1123/JAB.2016-0282.
- [115] B. A. Killen, M. Willems, and I. Jonkers, “An open-source framework for the generation of OpenSim models with personalised knee joint geometries for the estimation of articular contact mechanics,” *Journal of Biomechanics*, vol. 177, p. 112387, Dec. 2024, ISSN: 00219290. DOI: 10.1016/J.JBIOMECH.2024.112387. [Online]. Available: <https://linkinghub.elsevier.com/retrieve/pii/S0021929024004652>.
- [116] Y. Z. Arslan, D. Karabulut, F. Ortes, and M. B. Popovic, “Exoskeletons, Exomusculatures, Exosuits: Dynamic Modeling and Simulation,” *Biomechatronics*, pp. 305–331, Jan. 2019. DOI: 10.1016/B978-0-12-812939-5.00011-2.
- [117] U. Trinler, K. Hollands, R. Jones, and R. Baker, “A systematic review of approaches to modelling lower limb muscle forces during gait: Applicability to clinical gait analyses,” *Gait & posture*, vol. 61, pp. 353–361, Mar. 2018, ISSN: 1879-2219. DOI: 10.1016/J.GAITPOST.2018.02.005. [Online]. Available: <https://pubmed.ncbi.nlm.nih.gov/29433090/>.
- [118] U. Trinler, H. Schwameder, R. Baker, and N. Alexander, “Muscle force estimation in clinical gait analysis using AnyBody and OpenSim,” *Journal of Biomechanics*, vol. 86, pp. 55–63, Mar. 2019, ISSN: 18732380. DOI: 10.1016/J.JBIOMECH.2019.01.045.
- [119] M. T. Karimi, F. Hemmati, M. A. Mardani, *et al.*, “Determination of the correlation between muscle forces obtained from OpenSim and muscle activities obtained from electromyography in the elderly,” *Physical and Engineering Sciences in Medicine*, vol. 44, no. 1, pp. 243–251, Mar. 2021, ISSN: 26624737. DOI: 10.1007/S13246-021-00973-9.
- [120] S. Wang, Y. Wang, Y. C. Pai, E. Wang, and T. Bhatt, “Effects of Optimization Technique on Simulated Muscle Activations and Forces,” *Journal of applied biomechanics*, vol. 36, no. 4, pp. 217–227, 2020, ISSN: 1543-2688. DOI: 10.1123/JAB.2018-0332. [Online]. Available: <https://pubmed.ncbi.nlm.nih.gov/32663800/>.
- [121] D. G. Thelen and F. C. Anderson, “Using computed muscle control to generate forward dynamic simulations of human walking from experimental data,” *Journal of Biomechanics*, vol. 39, no. 6, pp. 1107–1115, 2006, ISSN: 00219290. DOI: 10.1016/J.JBIOMECH.2005.02.010.
- [122] F. E. Zajac, “Muscle and tendon: properties, models, scaling, and application to biomechanics and motor control,” *Critical reviews in biomedical engineering*, vol. 17, no. 4, pp. 359–411, 1989, ISSN: 0278940X.

- [123] “The heat of shortening and the dynamic constants of muscle,” *Proceedings of The Royal Society B: Biological Sciences*, vol. 126, no. 843, pp. 136–195, Oct. 1938, ISSN: 0962-8452. DOI: 10.1098/RSPB.1938.0050. [Online]. Available: <https://scispace.com/papers/the-heat-of-shortening-and-the-dynamic-constants-of-muscle-27oirhcos9>.
- [124] J. M. Wakeling, M. Febrer-Nafria, and F. De Groote, “A review of the efforts to develop muscle and musculoskeletal models for biomechanics in the last 50 years,” *Journal of Biomechanics*, vol. 155, p. 111657, Jun. 2023, ISSN: 0021-9290. DOI: 10.1016/J.JBIOMECH.2023.111657.
- [125] L. H. Ting and J. M. Macpherson, “A limited set of muscle synergies for force control during a postural task,” *Journal of Neurophysiology*, vol. 93, no. 1, pp. 609–613, Jan. 2005, ISSN: 00223077. DOI: 10.1152/JN.00681.2004/ASSET/IMAGES/LARGE/Z9K0010543461003.jpeg. [Online]. Available: <https://journals.physiology.org/doi/10.1152/jn.00681.2004>.
- [126] A. D’Avella, P. Saltiel, and E. Bizzi, “Combinations of muscle synergies in the construction of a natural motor behavior,” *Nature Neuroscience* 2003 6:3, vol. 6, no. 3, pp. 300–308, Feb. 2003, ISSN: 1546-1726. DOI: 10.1038/nn1010. [Online]. Available: <https://www.nature.com/articles/nn1010>.
- [127] F. Heinen, M. E. Lund, J. Rasmussen, and M. De Zee, “Muscle-tendon unit scaling methods of Hill-type musculoskeletal models: An overview,” *Proceedings of the Institution of Mechanical Engineers, Part H: Journal of Engineering in Medicine*, vol. 230, no. 10, pp. 976–984, Oct. 2016, ISSN: 20413033. DOI: 10.1177/0954411916659894.
- [128] B. Xiong, N. Zeng, Y. Li, et al., “Determining the online measurable input variables in human joint moment intelligent prediction based on the hill muscle model,” *Sensors (Switzerland)*, vol. 20, no. 4, Feb. 2020, ISSN: 14248220. DOI: 10.3390/S20041185.
- [129] *OpenSense - Kinematics with IMU Data - OpenSim Documentation - OpenSim*. [Online]. Available: <https://opensimconfluence.atlassian.net/wiki/spaces/OpenSim/pages/53084203/OpenSense+-+Kinematics+with+IMU+Data>.
- [130] *SimTK: OpenSim Moco: Project Home*. [Online]. Available: <https://simtk.org/projects/opensim-moco>.
- [131] J. Lavikainen, P. Vartiainen, L. Stenroth, and P. A. Karjalainen, “Open-source software library for real-time inertial measurement unit data-based inverse kinematics using OpenSim,” *PeerJ*, vol. 11, 2023, ISSN: 21678359. DOI: 10.7717/PEERJ.15097.
- [132] H. Dinovitzer, M. Shushtari, and A. Arami, “Accurate Real-Time Joint Torque Estimation for Dynamic Prediction of Human Locomotion,” *IEEE Transactions on Biomedical Engineering*, vol. 70, no. 8, pp. 2289–2297, Aug. 2023, ISSN: 15582531. DOI: 10.1109/TBME.2023.3240879.
- [133] D. Ao, G. Li, M. S. Shourijeh, C. Patten, and B. J. Fregly, “EMG-Driven Musculoskeletal Model Calibration With Wrapping Surface Personalization,” *IEEE Transactions on Neural Systems and Rehabilitation Engineering*, vol. 31, pp. 4235–4244, 2023, ISSN: 15580210. DOI: 10.1109/TNSRE.2023.3323516.
- [134] K. S. Halonen, C. M. Dziale, M. Mannisi, M. S. Venäläinen, M. De Zee, and M. S. Andersen, “Workflow assessing the effect of gait alterations on stresses in the medial tibial cartilage - combined musculoskeletal modelling and finite element analysis,” *Scientific Reports 2017 7:1*, vol. 7, no. 1, pp. 1–14, Dec. 2017, ISSN: 2045-2322. DOI: 10.1038/s41598-017-17228-x. [Online]. Available: <https://www.nature.com/articles/s41598-017-17228-x>.
- [135] S. Wang, K. Hase, and S. Ota, “A Computationally Efficient Lower Limb Finite Element Musculoskeletal Framework Directly Driven Solely by Inertial Measurement Unit Sensors,” *Journal of biomechanical engineering*, vol. 144, no. 5, May 2022, ISSN: 15288951. DOI: 10.1115/1.4053211/1129236. [Online]. Available: <https://dx.doi.org/10.1115/1.4053211>.
- [136] S. Wang, K. Hase, S. Kita, and S. Ogaya, “Biomechanical effects of medial meniscus radial tears on the knee joint during gait: A concurrent finite element musculoskeletal framework

- investigation,” *Frontiers in Bioengineering and Biotechnology*, vol. 10, p. 957435, Oct. 2022, ISSN: 22964185. DOI: 10.3389/FBIOE.2022.957435/BIBTEX.
- [137] J. W. Seo, D. W. Kang, J. Y. Kim, *et al.*, “Finite element analysis of the femur during stance phase of gait based on musculoskeletal model simulation,” *Bio-Medical Materials and Engineering*, vol. 24, no. 6, pp. 2485–2493, 2014, ISSN: 18783619. DOI: 10.3233/BME-141062.
- [138] E. P. Ravera, M. J. Crespo, and P. A. Catalfamo Formento, “A subject-specific integrative biomechanical framework of the pelvis for gait analysis,” *Proceedings of the Institution of Mechanical Engineers, Part H: Journal of Engineering in Medicine*, vol. 232, no. 11, pp. 1083–1097, Nov. 2018, ISSN: 20413033. DOI: 10.1177/0954411918803125.
- [139] B. M. Gaffney, S. T. Williams, J. N. Todd, J. A. Weiss, and M. D. Harris, “A Musculoskeletal Model for Estimating Hip Contact Pressure During Walking,” *Annals of Biomedical Engineering*, vol. 50, no. 12, pp. 1954–1963, Dec. 2022, ISSN: 15739686. DOI: 10.1007/S10439-022-03016-W.
- [140] M. Akrami, Z. Qian, Z. Zou, D. Howard, C. J. Nester, and L. Ren, “Subject-specific finite element modelling of the human foot complex during walking: sensitivity analysis of material properties, boundary and loading conditions,” *Biomechanics and Modeling in Mechanobiology*, vol. 17, no. 2, pp. 559–576, Apr. 2018, ISSN: 16177940. DOI: 10.1007/S10237-017-0978-3.
- [141] Z. Kamal, E. E. Hekman, and G. J. Verkerke, “A combined musculoskeletal and finite element model of a foot to predict plantar pressure distribution,” *Biomedical Physics and Engineering Express*, vol. 10, no. 3, May 2024, ISSN: 20571976. DOI: 10.1088/2057-1976/AD233D.
- [142] R. H. Miller, E. M. Bell, and E. R. Esposito, “Transfemoral limb loss modestly increases the metabolic cost of optimal control simulations of walking,” *PeerJ*, vol. 12, 2024, ISSN: 21678359. DOI: 10.7717/PEERJ.16756.
- [143] A. Falisse, G. Serrancolí, C. L. Dembia, J. Gillis, and F. DeGroote, “Algorithmic differentiation improves the computational efficiency of OpenSim-based trajectory optimization of human movement,” *PLoS ONE*, vol. 14, no. 10, Oct. 2019, ISSN: 19326203. DOI: 10.1371/JOURNAL.PONE.0217730.
- [144] C. M. Buffinton, R. K. Blaho, and K. A. Bieryla, “Biomechanics of single stair climb with implications for inverted pendulum modeling,” *Journal of Biomechanical Engineering*, vol. 143, no. 8, Aug. 2021, ISSN: 15288951. DOI: 10.1115/1.4050639.
- [145] B. Ostrach and R. Riemer, “Rethinking Exoskeleton Simulation-Based Design: The Effect of Using Different Cost Functions,” *IEEE Transactions on Neural Systems and Rehabilitation Engineering*, vol. 32, pp. 2153–2164, 2024, ISSN: 15580210. DOI: 10.1109/TNSRE.2024.3409633.
- [146] K. Nowakowski, P. Carvalho, J. B. Six, *et al.*, “Human locomotion with reinforcement learning using bioinspired reward reshaping strategies,” *Medical and Biological Engineering and Computing*, vol. 59, no. 1, pp. 243–256, Jan. 2021, ISSN: 17410444. DOI: 10.1007/S11517-020-02309-3.
- [147] L. De Vree and R. Carloni, “Deep reinforcement learning for physics-based musculoskeletal simulations of healthy subjects and transfemoral prostheses’ users during normal walking,” *IEEE Transactions on Neural Systems and Rehabilitation Engineering*, vol. 29, pp. 607–618, 2021, ISSN: 15580210. DOI: 10.1109/TNSRE.2021.3063015.
- [148] W. S. Burton, C. A. Myers, and P. J. Rullkoetter, “Machine learning for rapid estimation of lower extremity muscle and joint loading during activities of daily living,” *Journal of Biomechanics*, vol. 123, Jun. 2021, ISSN: 18732380. DOI: 10.1016/J.JBIOMECH.2021.110439.
- [149] A. Dainis, *Original C3D Technical User Manual*, 1987.

- [150] “The C3D File Format A Technical User Guide By Motion Lab Systems The C3D File Format A Technical User Guide,” English, Motion Lab Systems, Tech. Rep., Oct. 2021. [Online]. Available: [www.motion-labs.com](http://www.motion-labs.com).
- [151] S. U. Yavuz, A. Şendemir-Ürkmez, and K. S. Türker, “Effect of gender, age, fatigue and contraction level on electromechanical delay,” *Clinical Neurophysiology*, vol. 121, no. 10, pp. 1700–1706, Oct. 2010, ISSN: 1388-2457. DOI: 10.1016/J.CLINPH.2009.10.039.
- [152] B. Fischer and P. Mitteroecker, “Allometry and Sexual Dimorphism in the Human Pelvis,” *The Anatomical Record*, vol. 300, no. 4, pp. 698–705, Apr. 2017, ISSN: 1932-8494. DOI: 10.1002/AR.23549. [Online]. Available: <https://onlinelibrary.wiley.com/doi/full/10.1002/ar.23549> <https://onlinelibrary.wiley.com/doi/abs/10.1002/ar.23549> <https://anatomypubs.onlinelibrary.wiley.com/doi/10.1002/ar.23549>.
- [153] F. Yazdani, M. Razeghi, M. T. Karimi, H. Raeisi Shahraki, and M. Salimi Bani, “The influence of foot hyperpronation on pelvic biomechanics during stance phase of the gait: A biomechanical simulation study,” *Proceedings of the Institution of Mechanical Engineers, Part H: Journal of Engineering in Medicine*, vol. 232, no. 7, pp. 708–717, Jul. 2018, ISSN: 20413033. DOI: 10.1177/0954411918778077.
- [154] K. K. Ismail and C. L. Lewis, “Effect of simulated changes in pelvic tilt on hip joint forces,” *Journal of Biomechanics*, vol. 135, Apr. 2022, ISSN: 18732380. DOI: 10.1016/J.JBIOMECH.2022.111048.
- [155] M. Vlutters, E. H. van Asseldonk, and H. van der Kooij, “Lower extremity joint-level responses to pelvis perturbation during human walking,” *Scientific Reports*, vol. 8, no. 1, Dec. 2018, ISSN: 20452322. DOI: 10.1038/S41598-018-32839-8.
- [156] *Physiology, Body Mass Index - PubMed*. [Online]. Available: <https://pubmed.ncbi.nlm.nih.gov/30571077/>.
- [157] Z. F. Lerner, D. J. Haight, M. S. DeMers, W. J. Board, and R. C. Browning, “The effects of walking speed on tibiofemoral loading estimated via musculoskeletal modeling,” *Journal of Applied Biomechanics*, vol. 30, no. 2, pp. 197–205, 2014, ISSN: 15432688. DOI: 10.1123/jab.2012-0206.
- [158] B. Horsak, B. Pobatschnig, C. Schwab, A. Baca, A. Kranzl, and H. Kainz, “Reliability of joint kinematic calculations based on direct kinematic and inverse kinematic models in obese children,” *Gait and Posture*, vol. 66, pp. 201–207, Oct. 2018, ISSN: 18792219. DOI: 10.1016/J.GAITPOST.2018.08.027.
- [159] Z. F. Lerner, W. J. Board, and R. C. Browning, “Effects of Obesity on Lower Extremity Muscle Function During Walking at Two Speeds,” *Gait & posture*, vol. 39, no. 3, p. 978, 2013, ISSN: 18792219. DOI: 10.1016/J.GAITPOST.2013.12.020. [Online]. Available: <https://pmc.ncbi.nlm.nih.gov/articles/PMC3960344/>.
- [160] H. Toda, A. Nagano, and Z. Luo, “Age-related differences in muscle control of the lower extremity for support and propulsion during walking,” *Journal of Physical Therapy Science*, vol. 28, no. 3, pp. 794–801, Mar. 2016, ISSN: 0915-5287. DOI: 10.1589/JPTS.28.794.
- [161] Z. Chegini, B. Yasrebi, S. Haghipour, F. T. Ghomsheh, A. Pahlievanian, and M. Mohammadi, “Impact of age-related characteristics in females on neuromuscular and motor control: Musculoskeletal modeling using OpenSim software,” *Gait & Posture*, vol. 113, pp. 146–147, Sep. 2024, ISSN: 0966-6362. DOI: 10.1016/J.GAITPOST.2024.07.162.
- [162] G. G. Handsfield, C. H. Meyer, J. M. Hart, M. F. Abel, and S. S. Blemker, “Relationships of 35 lower limb muscles to height and body mass quantified using MRI,” *Journal of Biomechanics*, vol. 47, no. 3, pp. 631–638, Feb. 2014, ISSN: 00219290. DOI: 10.1016/J.JBIOMECH.2013.12.002.

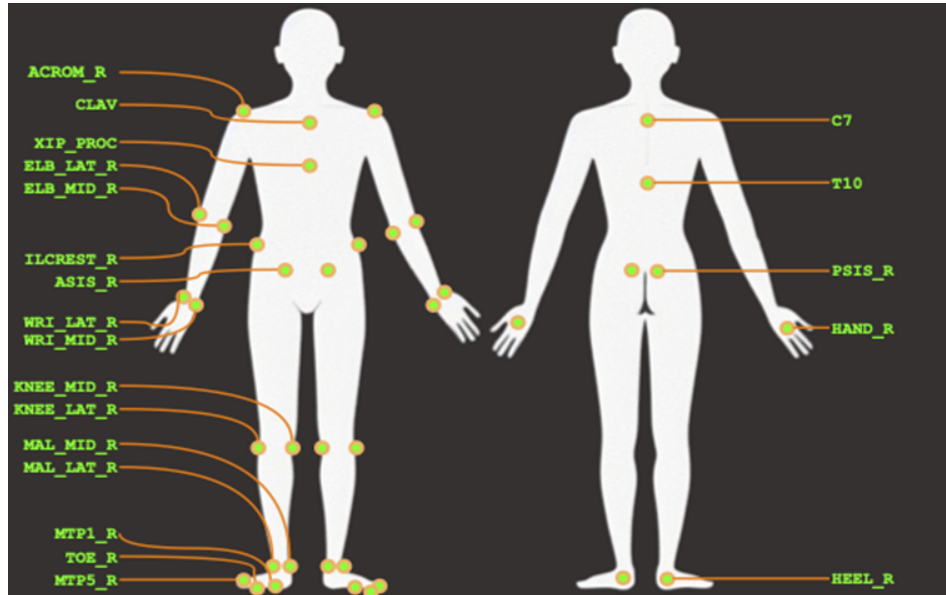
- [163] A. Nandy, S. Chakraborty, J. Chakraborty, and G. Venture, "Introduction," *Modern Methods for Affordable Clinical Gait Analysis*, pp. 1–15, Jan. 2021. DOI: 10.1016/B978-0-323-85245-6.00012-6.
- [164] M. Millard, T. Uchida, A. Seth, and S. L. Delp, "Flexing computational muscle: Modeling and simulation of musculotendon dynamics," *Journal of Biomechanical Engineering*, vol. 135, no. 2, Feb. 2013, ISSN: 01480731. DOI: 10.1115/1.4023390/371394. [Online]. Available: <https://dx.doi.org/10.1115/1.4023390>.
- [165] J. Hicks, *How to Use the Scale Tool - OpenSim Documentation - OpenSim*, Jul. 2022. [Online]. Available: <https://opensimconfluence.atlassian.net/wiki/spaces/OpenSim/pages/53087627/How+to+Use+the+Scale+Tool>.
- [166] J. Hicks, *Working with Static Optimization - OpenSim Documentation - OpenSim*, Mar. 2024. [Online]. Available: <https://opensimconfluence.atlassian.net/wiki/spaces/OpenSim/pages/53085189/Working+with+Static+Optimization>.
- [167] A. Leal-Junior and A. Frizera-Neto, "Gait analysis: overview, trends, and challenges," *Optical Fiber Sensors for the Next Generation of Rehabilitation Robotics*, pp. 53–64, Jan. 2022. DOI: 10.1016/B978-0-32-385952-3.00011-1.
- [168] A. A. Al-Munajjed, J. E. Bischoff, M. A. Dharia, S. Telfer, J. Woodburn, and S. Carbes, "Metatarsal Loading During Gait-A Musculoskeletal Analysis," *Journal of biomechanical engineering*, vol. 138, no. 3, Mar. 2016, ISSN: 1528-8951. DOI: 10.1115/1.4032413. [Online]. Available: <https://pubmed.ncbi.nlm.nih.gov/26719905/>.
- [169] J. S. Park and C. H. Kim, "Ground-Reaction-Force-Based Gait Analysis and Its Application to Gait Disorder Assessment: New Indices for Quantifying Walking Behavior," *Sensors 2022, Vol. 22, Page 7558*, vol. 22, no. 19, p. 7558, Oct. 2022, ISSN: 1424-8220. DOI: 10.3390/S22197558. [Online]. Available: <https://www.mdpi.com/1424-8220/22/19/7558/htm%20https://www.mdpi.com/1424-8220/22/19/7558>.
- [170] B. Horsak, D. Slijepcevic, A. M. Raberger, C. Schwab, M. Worisch, and M. Zeppelzauer, "GaitRec, a large-scale ground reaction force dataset of healthy and impaired gait," *Scientific Data*, vol. 7, no. 1, Dec. 2020, ISSN: 20524463. DOI: 10.1038/S41597-020-0481-Z.
- [171] D. Martínez-Pascual, J. M. Catalán, A. Blanco-Ivorra, M. Sanchís, F. Arán-Ais, and N. García-Aracil, "Estimating vertical ground reaction forces during gait from lower limb kinematics and vertical acceleration using wearable inertial sensors," *Frontiers in Bioengineering and Biotechnology*, vol. 11, 2023, ISSN: 22964185. DOI: 10.3389/FBIOE.2023.1199459. [Online]. Available: [https://click.endnote.com/viewer?doi=10.3389%2Ffbioe.2023.1199459&token=WzMwNjU4NzQsIjEwLjMzODkvZmJpb2UuMjAyMy4xMTk5NDU5I10.zzqz\\_krwgBtOs8X\\_xyDg55Kmj18](https://click.endnote.com/viewer?doi=10.3389%2Ffbioe.2023.1199459&token=WzMwNjU4NzQsIjEwLjMzODkvZmJpb2UuMjAyMy4xMTk5NDU5I10.zzqz_krwgBtOs8X_xyDg55Kmj18).
- [172] M. Sangeux, "Biomechanics of the Hip During Gait," *The Pediatric and Adolescent Hip: Essentials and Evidence*, pp. 53–71, Jan. 2019. DOI: 10.1007/978-3-030-12003-0\\_\\_3.
- [173] A. Thomas, *The Four Planes of the Body*, English, Apr. 2024. [Online]. Available: <https://simpelnursing.com/how-to-remember-4-planes-body/>.
- [174] J. Hicks, *Getting Started with CMC - OpenSim Documentation - OpenSim*, Mar. 2024. [Online]. Available: <https://opensimconfluence.atlassian.net/wiki/spaces/OpenSim/pages/53089712/Getting+Started+with+CMC>.
- [175] M. Constantinou, A. Loureiro, C. Carty, P. Mills, and R. Barrett, "Hip joint mechanics during walking in individuals with mild-to-moderate hip osteoarthritis," *Gait & Posture*, vol. 53, pp. 162–167, Mar. 2017, ISSN: 0966-6362. DOI: 10.1016/J.GAITPOST.2017.01.017.
- [176] J. Skubich and S. Piszcztowski, "Model of loadings acting on the femoral bone during gait," *Journal of Biomechanics*, vol. 87, pp. 54–63, Apr. 2019, ISSN: 0021-9290. DOI: 10.1016/J.JBIOMECH.2019.02.018.

- [177] M. A. Hunt, T. B. Birmingham, J. R. Giffin, and T. R. Jenkyn, “Associations among knee adduction moment, frontal plane ground reaction force, and lever arm during walking in patients with knee osteoarthritis,” *Journal of Biomechanics*, vol. 39, no. 12, pp. 2213–2220, Jan. 2006, ISSN: 0021-9290. DOI: 10.1016/J.JBIOMECH.2005.07.002.
- [178] B. W. Stansfield and A. C. Nicol, “Hip joint contact forces in normal subjects and subjects with total hip prostheses: walking and stair and ramp negotiation,” *Clinical Biomechanics*, vol. 17, no. 2, pp. 130–139, Feb. 2002, ISSN: 0268-0033. DOI: 10.1016/S0268-0033(01)00119-X.
- [179] F. Molina-Rueda, A. Cuesta-Gómez, M. Carratalá-Tejada, P. Fernández-González, J. C. Miangolarra-Page, and I. M. Alguacil-Diego, “Joint internal moments in subjects with unilateral transtibial amputation during walking,” *Journal of Orthopedics and Orthopedic Surgery*, vol. 2, no. 1, pp. 1–6, Apr. 2021. DOI: 10.29245/2767-5130/2021/1.1118.
- [180] E. Montefiori, C. Fiifi Hayford, and C. Mazzà, “Variations of lower-limb joint kinematics associated with the use of different ankle joint models,” *Journal of Biomechanics*, vol. 136, May 2022, ISSN: 18732380. DOI: 10.1016/J.JBIOMECH.2022.111072.
- [181] C. A. Fukuchi, R. K. Fukuchi, and M. Duarte, “A public dataset of overground and treadmill walking kinematics and kinetics in healthy individuals,” *PeerJ*, vol. 2018, no. 4, 2018, ISSN: 21678359. DOI: 10.7717/PEERJ.4640/FIG-4.
- [182] B. C. Heiderscheit, E. S. Chumanov, M. P. Michalski, C. M. Wille, and M. B. Ryan, “Effects of Step Rate Manipulation on Joint Mechanics during Running,” *Medicine and science in sports and exercise*, vol. 43, no. 2, p. 296, Feb. 2011, ISSN: 01959131. DOI: 10.1249/MSS.0B013E3181EBEDF4. [Online]. Available: <https://pmc.ncbi.nlm.nih.gov/articles/PMC3022995/>.
- [183] R. J. Schmitz, D. Harrison, H. M. Wang, and S. J. Shultz, “Sagittal-Plane Knee Moment During Gait and Knee Cartilage Thickness,” *Journal of Athletic Training*, vol. 52, no. 6, p. 560, Jun. 2017, ISSN: 1938162X. DOI: 10.4085/1062-2050-52.4.05. [Online]. Available: <https://pmc.ncbi.nlm.nih.gov/articles/PMC5488846/>.
- [184] H. Y. Hsiao, B. A. Knarr, J. S. Higginson, and S. A. Binder-Macleod, “The Relative Contribution of Ankle Moment and Trailing Limb Angle to Propulsive Force during Gait,” *Human movement science*, vol. 0, p. 212, Feb. 2014, ISSN: 18727646. DOI: 10.1016/J.HUMOV.2014.11.008. [Online]. Available: <https://pmc.ncbi.nlm.nih.gov/articles/PMC4272868/>.
- [185] H. L. Teng, T. D. MacLeod, T. M. Link, S. Majumdar, and R. B. Souza, “Higher Knee Flexion Moment During the Second Half of the Stance Phase of Gait Is Associated With the Progression of Osteoarthritis of the Patellofemoral Joint on Magnetic Resonance Imaging,” *The Journal of orthopaedic and sports physical therapy*, vol. 45, no. 9, p. 656, Sep. 2015, ISSN: 01906011. DOI: 10.2519/JOSPT.2015.5859. [Online]. Available: <https://pmc.ncbi.nlm.nih.gov/articles/PMC4718079/>.
- [186] P. R. G. Lucareli, M. D. O. Lima, J. G. D. A. Lucarelli, and F. P. S. Lima, “CHANGES IN JOINT KINEMATICS IN CHILDREN WITH CEREBRAL PALSY WHILE WALKING WITH AND WITHOUT A FLOOR REACTION ANKLE-FOOT ORTHOSIS,” *Clinics*, vol. 62, no. 1, pp. 63–68, Jan. 2007, ISSN: 1807-5932. DOI: 10.1590/S1807-59322007000100010.
- [187] P. Kedem and D. M. Scher, “Evaluation and management of crouch gait,” *Current Opinion in Pediatrics*, vol. 28, no. 1, pp. 55–59, Feb. 2016, ISSN: 1531698X. DOI: 10.1097/MOP.000000000000316. [Online]. Available: [https://journals.lww.com/co-pediatrics/fulltext/2016/02000/evaluation\\_and\\_management\\_of\\_crouch\\_gait.10.aspx](https://journals.lww.com/co-pediatrics/fulltext/2016/02000/evaluation_and_management_of_crouch_gait.10.aspx).
- [188] J. Petersen, R. O. Nielsen, S. Rasmussen, and H. Sørensen, “Comparisons of increases in knee and ankle joint moments following an increase in running speed from 8 to 12 to 16km·h(-1),” *Clinical biomechanics (Bristol, Avon)*, vol. 29, no. 9, pp. 959–964, Nov. 2014, ISSN: 1879-1271.

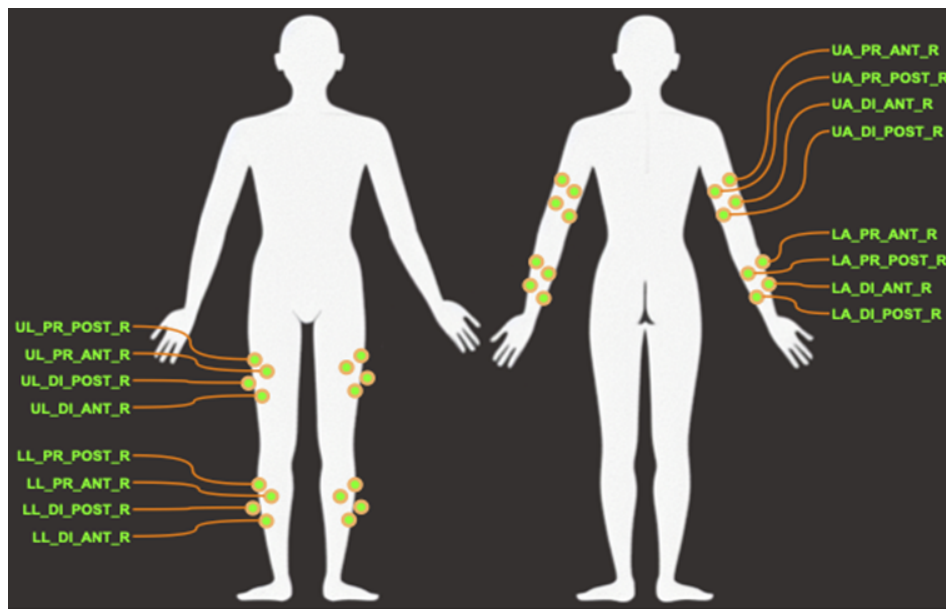
- DOI: 10.1016/J.CLINBIOMECH.2014.09.003. [Online]. Available: <https://pubmed.ncbi.nlm.nih.gov/25242200/>.
- [189] B. J. Stetter, F. C. Krafft, S. Ringhof, T. Stein, and S. Sell, “A Machine Learning and Wearable Sensor Based Approach to Estimate External Knee Flexion and Adduction Moments During Various Locomotion Tasks,” *Frontiers in Bioengineering and Biotechnology*, vol. 8, Jan. 2020, ISSN: 22964185. DOI: 10.3389/FBIOE.2020.00009.
- [190] C. Leys, C. Ley, O. Klein, P. Bernard, and L. Licata, “Detecting outliers: Do not use standard deviation around the mean, use absolute deviation around the median,” *Journal of Experimental Social Psychology*, vol. 49, no. 4, pp. 764–766, Jul. 2013, ISSN: 0022-1031. DOI: 10.1016/J.JESP.2013.03.013. [Online]. Available: <https://www.sciencedirect.com/science/article/abs/pii/S0022103113000668>.

# Appendices

## Appendix A Marker Locations



(a) Marker Locations for joint clusters



(b) Marker Locations for arm and leg clusters

Figure 31: Marker Locations for Motion-Capture, Courtesy of [56]

## Appendix B Markerset parent frames

Table 15: Markerset parent frames

Sagittal Plane Symmetry	Parent Frame (/bodyset/NAME)	Marker Name	Weighting
Symmetric	torso	ACROM_R	1.0
	pelvis	ASIS_R	1.0
	pelvis	ILCREST_R	1.0
	pelvis	PSIS_R	1.0
	humerus_r	UA_PR_ANT_R	1.0
	humerus_r	UA_DI_POST_R	1.0
	humerus_r	UA_DI_ANT_R	1.0
	humerus_r	UA_PR_POST_R	1.0
	humerus_r	ELB_LAT_R	1.0
	humerus_r	ELB_MED_R	1.0
	ulna_r	LA_PR_ANT_R	1.0
	ulna_r	LA_PR_POST_R	1.0
	ulna_r	LA_DI_POST_R	1.0
	ulna_r	LA_DI_ANT_R	1.0
	radius_r	WRI_LAT_R	1.0
	radius_r	WRI_MED_R	1.0
	hand_r	HAND_R	1.0
	femur_r	UL_PR_POST_R	1.0
	femur_r	UL_PR_ANT_R	1.0
	femur_r	UL_DI_POST_R	1.0
	femur_r	UL_DI_ANT_R	1.0
	femur_r	KNEE_LAT_R	1.0
	femur_r	KNEE_MED_R	1.0
	tibia_r	LL_PR_POST_R	1.0
	tibia_r	LL_PR_ANT_R	1.0
	tibia_r	LL_DI_POST_R	1.0
	tibia_r	LL_DI_ANT_R	1.0
	tibia_r	MAL_LAT_R	1.0
	tibia_r	MAL_MED_R	1.0
	caln_r	HEEL_R	1.0
	caln_r	MTP1_R	1.0
	caln_r	MTP5_R	1.0
	caln_r	TOE_R	1.0
Non-Symmetric	torso	C7	1.0
	torso	T10	1.0
	torso	CLAV	1.0
	torso	XIP_PROC	1.0

# Appendix C Scaling Tool

## C.1 Screenshot of Scaling Tool Setup

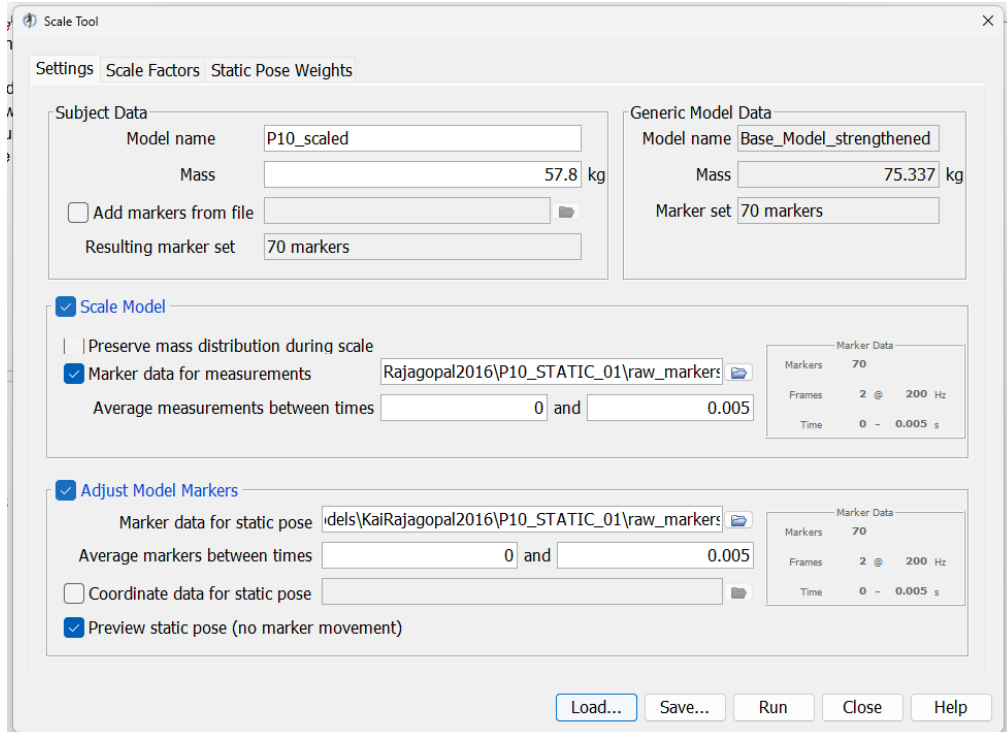


Figure 32: Scale Tool Setup: Main settings

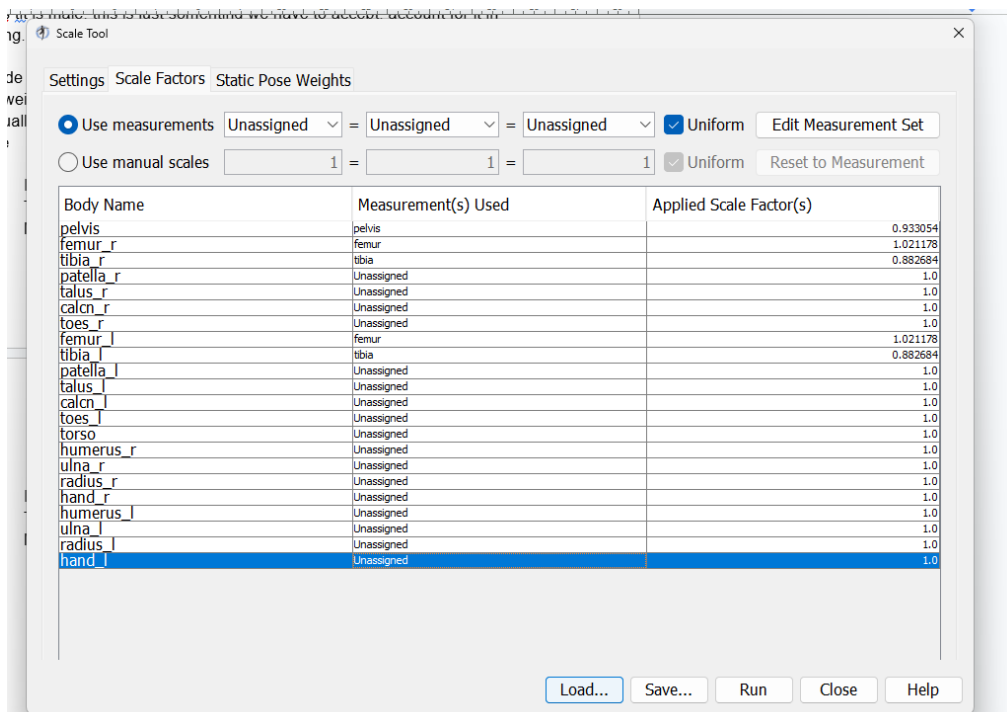


Figure 33: Scale Tool Setup: For factors refer to Figure C.2

## C.2 Screenshot of Scaling Factor Setup

Table 16: Scaling Marker Weightings

Symmetry	Marker	Weighting
Non-Symmetric	C7	3.0
	T10	3.0
	CLAV	3.0
	XIP_PROC	3.0
Symmetric	ACROM_R	3.0
	UA_PR_ANT_R	1.0
	UA_DI_POST_R	1.0
	UA_DI_ANT_R	1.0
	UA_PR_POST_R	1.0
	ELB_LAT_R	1.0
	ELB_MED_R	1.0
	LA_PR_ANT_R	1.0
	LA_PR_POST_R	1.0
	LA_DI_POST_R	1.0
	LA_DI_ANT_R	1.0
	WRI_LAT_R	1.0
	WRI_MED_R	1.0
	HAND_R	1.0
	ILCREST_R	3.0
	PSIS_R	3.0
	UL_PR_POST_R	5.0
	UL_PR_ANT_R	5.0
	UL_DI_POST_R	5.0
	UL_DI_ANT_R	5.0
	KNEE_LAT_R	5.0
	KNEE_MED_R	5.0
	LL_PR_POST_R	5.0
	LL_PR_ANT_R	5.0
	LL_DI_POST_R	5.0
	LL_DI_ANT_R	5.0
	MAL_LAT_R	5.0
	MAL_MED_R	5.0
	HEEL_R	5.0
	MTP1_R	5.0
	MTP5_R	5.0
	TOE_R	5.0
	ASIS_R	3.0

## Appendix D Proposed Amendment to Automated Scaling Tool

During MSK scaling, one attempted method at automating the process was the use of the AST developed by Di Pietro et al. in MATLAB [113]. However, what was found that while some markers would converge to minimise total scaling error as intended, other markers consistently led to an exponential blow-up in scaling error as a result of the incremental 'step' over-shooting the desired marker position and doubling for the next loop (Refer to line 6 in 1.

```

1 %% control to sign and step size: if err rises, go back of 2 step
2 if k~=1
3   if err(k) >= err(k-1) && strcmp(Merr(k),Merr(k-1)) && direction(k) ==
4     direction(k-1) %&& if the Max error arises at next cycle to the same
5     marker and to the same direction it means that the right sign is the
6     opposite one
7     s=-s;
8     disp('sign changed');
9     step(k)=2*step(k-1);% doubling this step because the step at
10    iteration k-1 was wrong
11  end
12 end

```

Listing 1: Code to be amended, lines 168-175 AST\_core\_v1.m file documented in [113]

To overcome this issue, a proposed amendment would be to introduce a 'damping' parameter in the nested for-loop as illustrated in lines 3-6 in 2. This would theoretically allow for an overshoot to be detected before blow-out, upon which the step-size, instead of being doubled in the original algorithm, is reduced by a given 'damper' ratio (with a value between zero and one) predefined earlier in the script. With this, the script returns back to the original algorithm as noted in the source documentation.

```

1 %% control to sign and step size: if err rises, go back of 2 step
2 if k~=1
3   if err(k) >= err(k-1) && strcmp(Merr(k),Merr(k-1)) && direction(k) ~=
4     direction(k-1) %If error increases but in the opposite direction,
5     shrink step by a predetermined damping value (parameter called 'damper')
6     s=-s;
7     disp('sign changed, potential blow-up detected');
8     step(k)=damper*step(k-1);% doubling this step because the step at
9     iteration k-1 was wrong
10
11 elseif err(k) >= err(k-1) && strcmp(Merr(k),Merr(k-1)) && direction(k) ==
12     direction(k-1) %&& if the Max error arises at next cycle to the
13     same marker and to the same direction it means that the right sign is
     the opposite one
     s=-s;
     disp('sign changed');
     step(k)=2*step(k-1);% doubling this step because the step at
     iteration k-1 was wrong
14   end
15 end

```

Listing 2: Proposed amendment, lines 168-175 AST\_core\_v1.m file documented in [113]

Unfortunately, this proposal could not be validated given the limited time-frame of this research project, and limited data to use as study. However, it presents a possible avenue for future work

looking to make use of the Opensim-MATLAB interface.

## Appendix E List of Trial files used

Participant ID	Walking Trial No.			Running Trial No.		
	1	2	3	1	2	3
P04	W01	W02	W03	R01	R02	R03
P06	W01	W02	W03	R01	R02	R03
P10	W01	W02	W03	R01	R02	R03
P13	W01	W02	W03	R01	R02	R03

Table 17: List of trial IDs used in producing this research from dataset [56]).

## Appendix F Example of Applied Ground Reaction Force

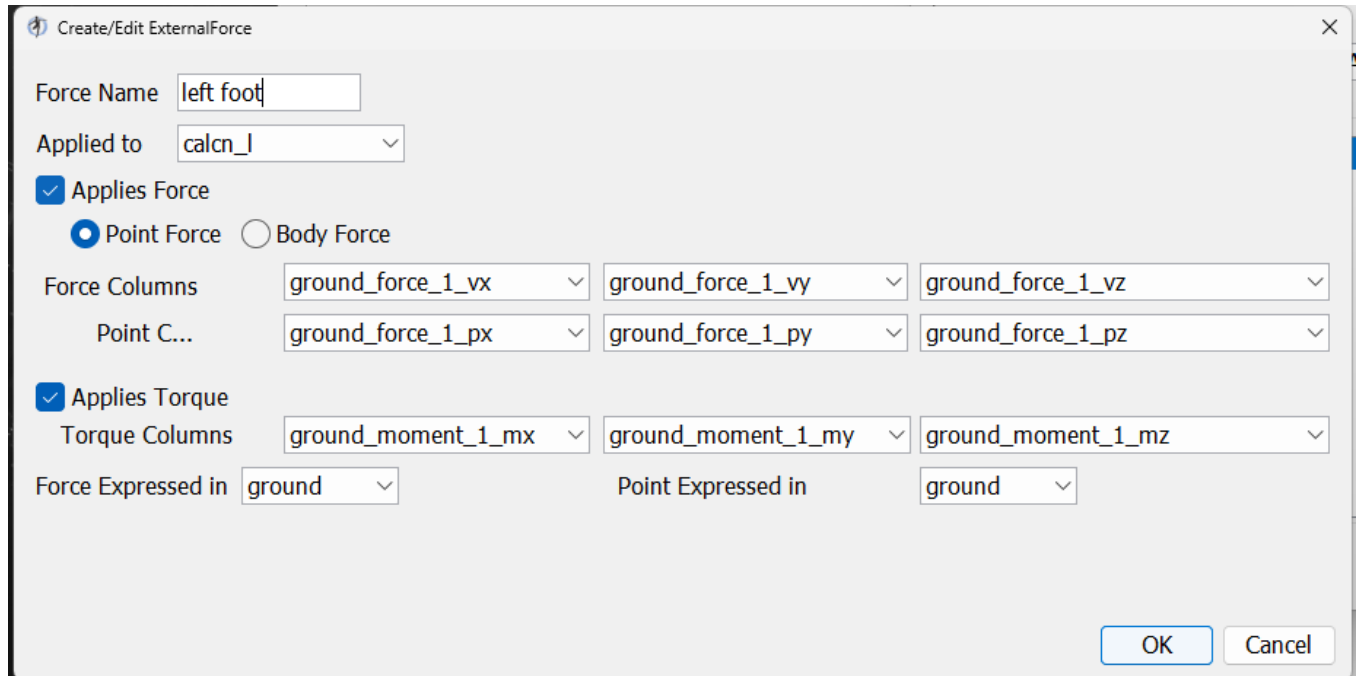


Figure 34: Example of how force-plate data was applied. Note that force and moments were applied to the calcanei

# Appendix G Initial setup of OpenSim Computed Muscle Control Tool

## G.1 CMC lookup table: main settings

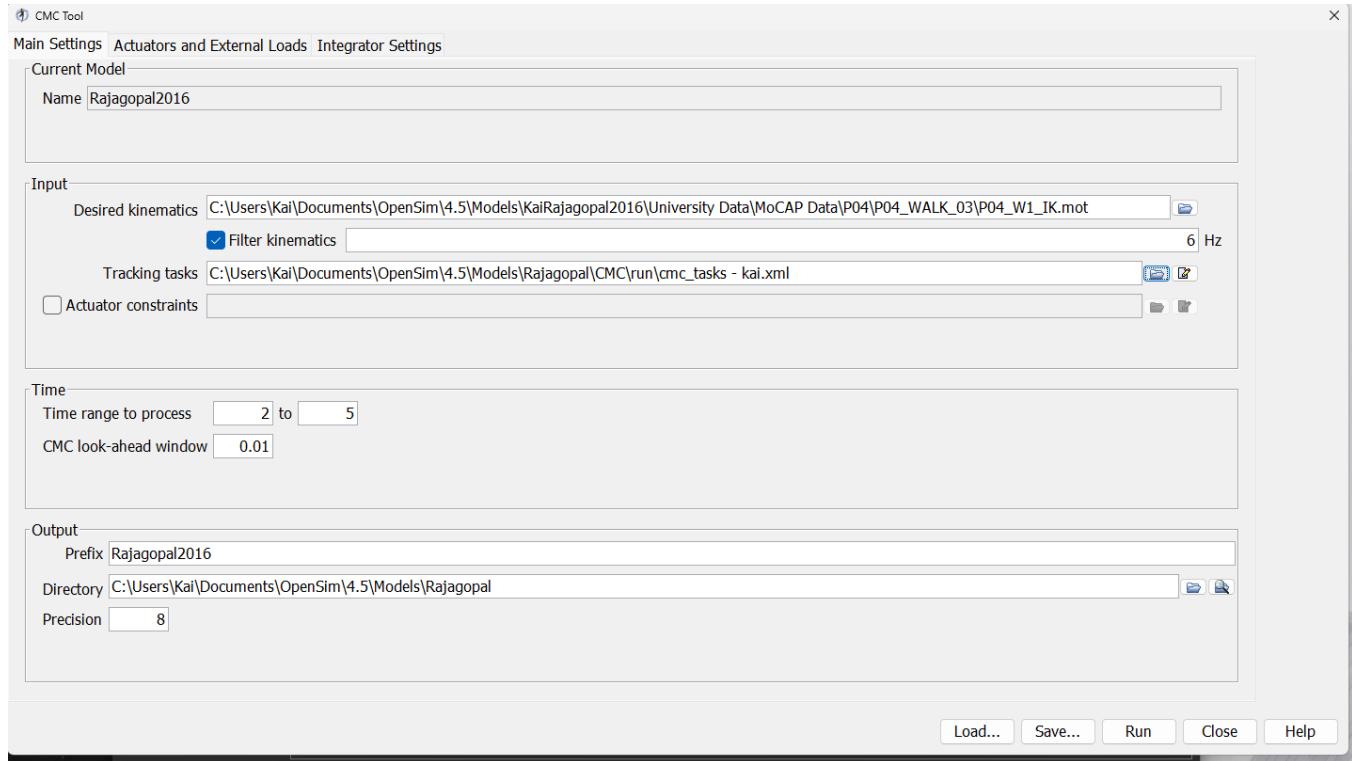


Figure 35: CMC settings lookup table main page. Note that the tracking tasks here have been edited from the original Rajagopal CMC tasks to weigh lower limbs more, and upper limbs less.

## G.2 CMC lookup table: Integrator settings

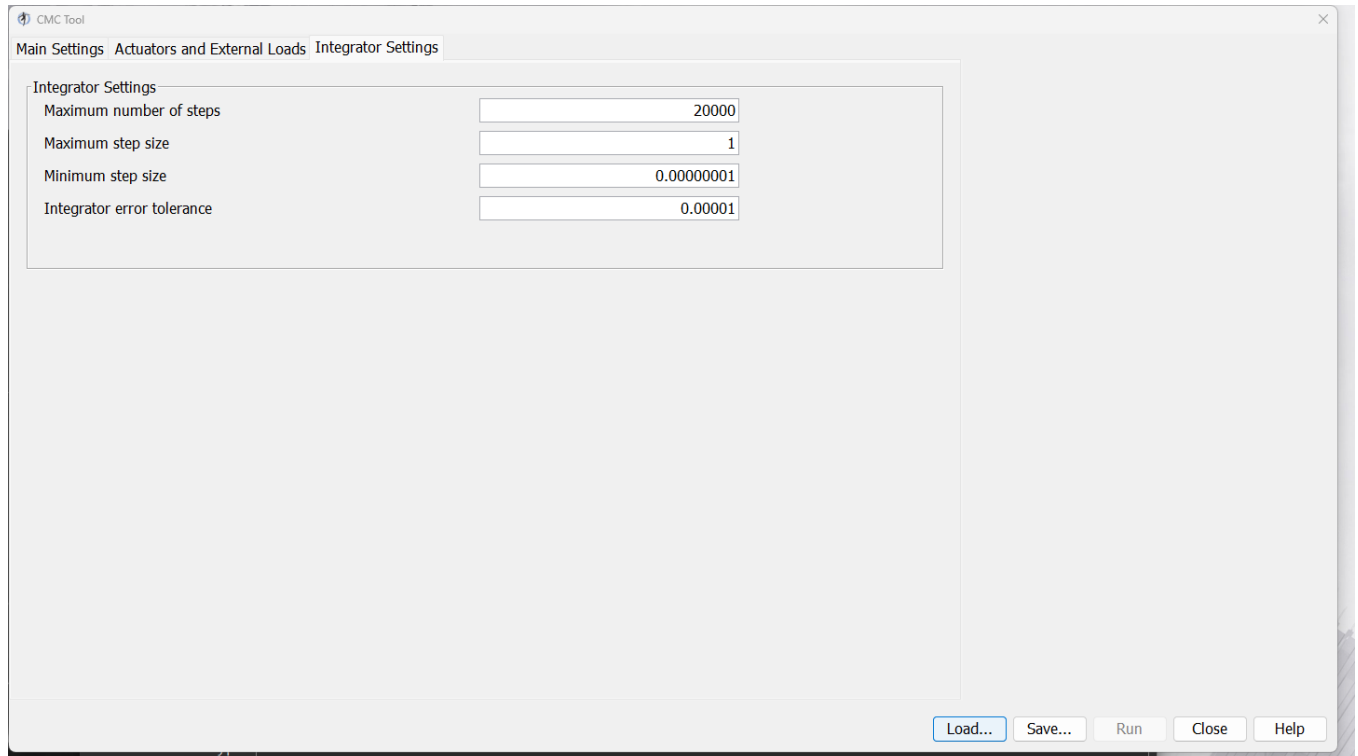


Figure 36: CMC settings lookup table

## G.3 CMC task setup: changes from base Rajagopal model file [100]

Table 18: Computed Muscle Control task file amendments

*Note: coordinate names ending in '\_r' denote 'right', implying that task weighting changes were symmetric (i.e. same changes applied to '\_l' coordinates)*

Exercise Condition	Coordinate	Original Weighting	New Weighting
Run	ankle_angle_r	100	30
	hip_flexion_r	1	2
	hip_adduction_r	1	2
	hip_rotation_r	1	2
	knee_angle_r	1	2
	ankle_angle_r	1	2

## Appendix H Uncleaned Aggregate Plot of Running Trials Across All Participants

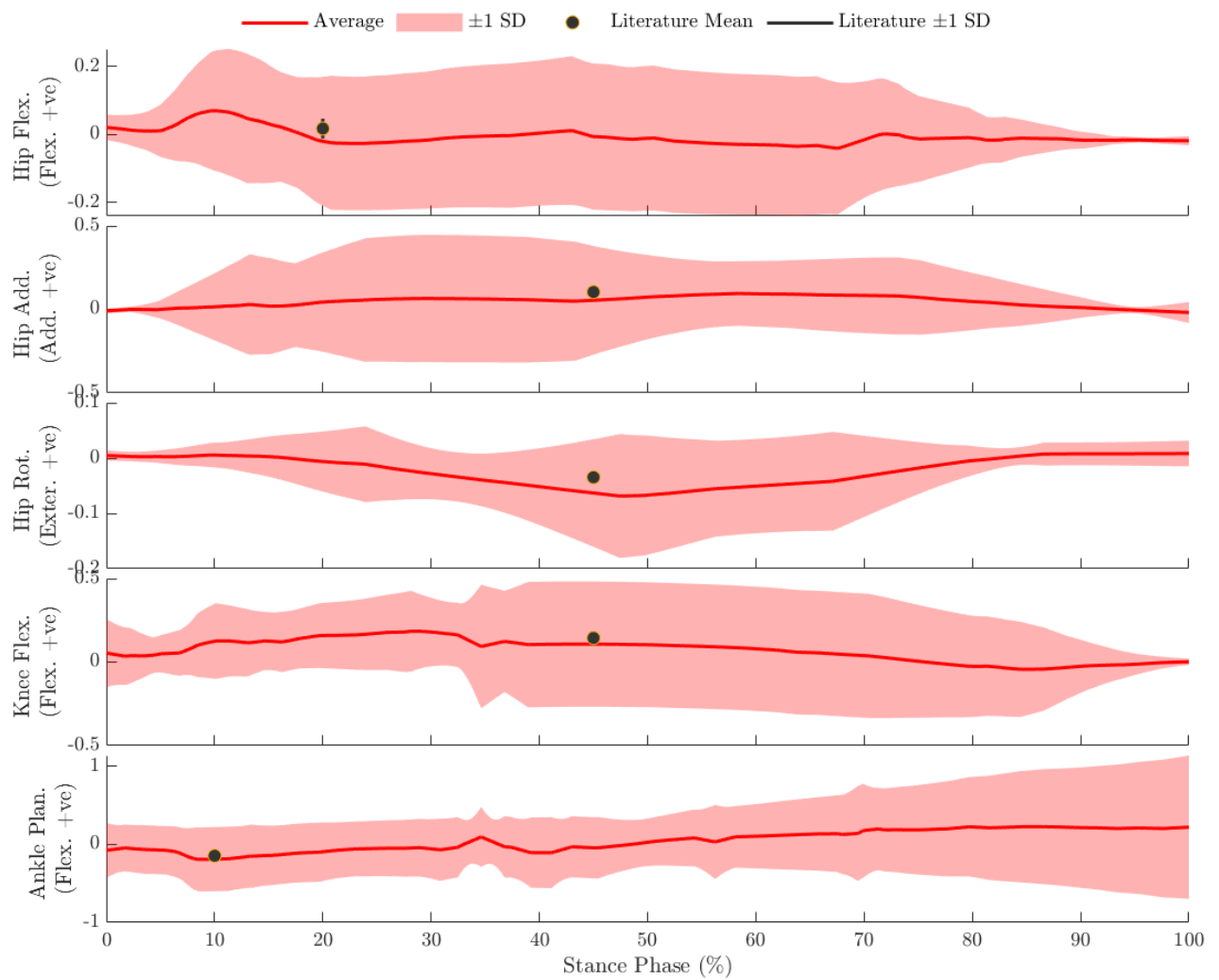


Figure 37: Uncleaned Aggregate Plot of Running Trials Across All Participants. Moments at various joints during stance period, normalised by  $BW \times height$

# Appendix I Denoising Filter Settings

Prior to analysis, each batch of raw simulation data (in .sto format) was denoised using a two-stage filtering process. First, the variable of interest (e.g., "hip\_flexion\_r") was processed through a gradient-based filter applied over the stance phase, defined as the period during which the corresponding force plate recorded forces exceeding 20N. This step removed high-magnitude transient spikes. Second, the data was further refined by calculating the sample's MAD and excluding any values that exceeded a specified MAD threshold.

The filter parameters applied for each movement during running and walking are summarised in Table 19. These settings were chosen by manually testing a range of combinations until the resulting trends appeared stable. *Note: Filters were applied to the raw moment data. That is, data measured in Nm, and not yet normalised by participant BW and height!!*

Table 19: Filtering Parameters Used for Denoising Data for Moments Analysis. (Note: all moment data was normalised by participant body weight and height ( $BW \times H$ ) prior to filtering.)

Movement	Running		Walking	
	Gradient	MAD Limit	Gradient	MAD Limit
Hip Flex./Ext.	$10^4$	10	$10^4$	5
Hip Abd./Add	$10^4$	10	$10^4$	5
Hip Rot. Ex./In	$10^3$	10	500	1.6
Knee Flex./Ext.	$10^7$	10	800	2.2
Ankle Plant. Flex./Ext	$10^6$	100	0	5

# Appendix J Uncleaned data plots (Unfiltered)

This section contains unfiltered MATLAB plots of various moment profiles over the stance phase for those interested in viewing just how rough of a time I was having with simulation quality. Whoever is reading this, please know that I tried my best!! I'm really happy with how the plots turned out - in truth, I made a MATLAB script for automating subplots and just really wanted to get good mileage out of it - so here we are!!! Anyways, for the filter settings I did eventually use, refer to Appendix I.

## J.0.1 Aggregate Plots for Walking and Running

### J.1 Ankle Joint

### J.2 Participant-wise Comparison of Moments, including Participant 10

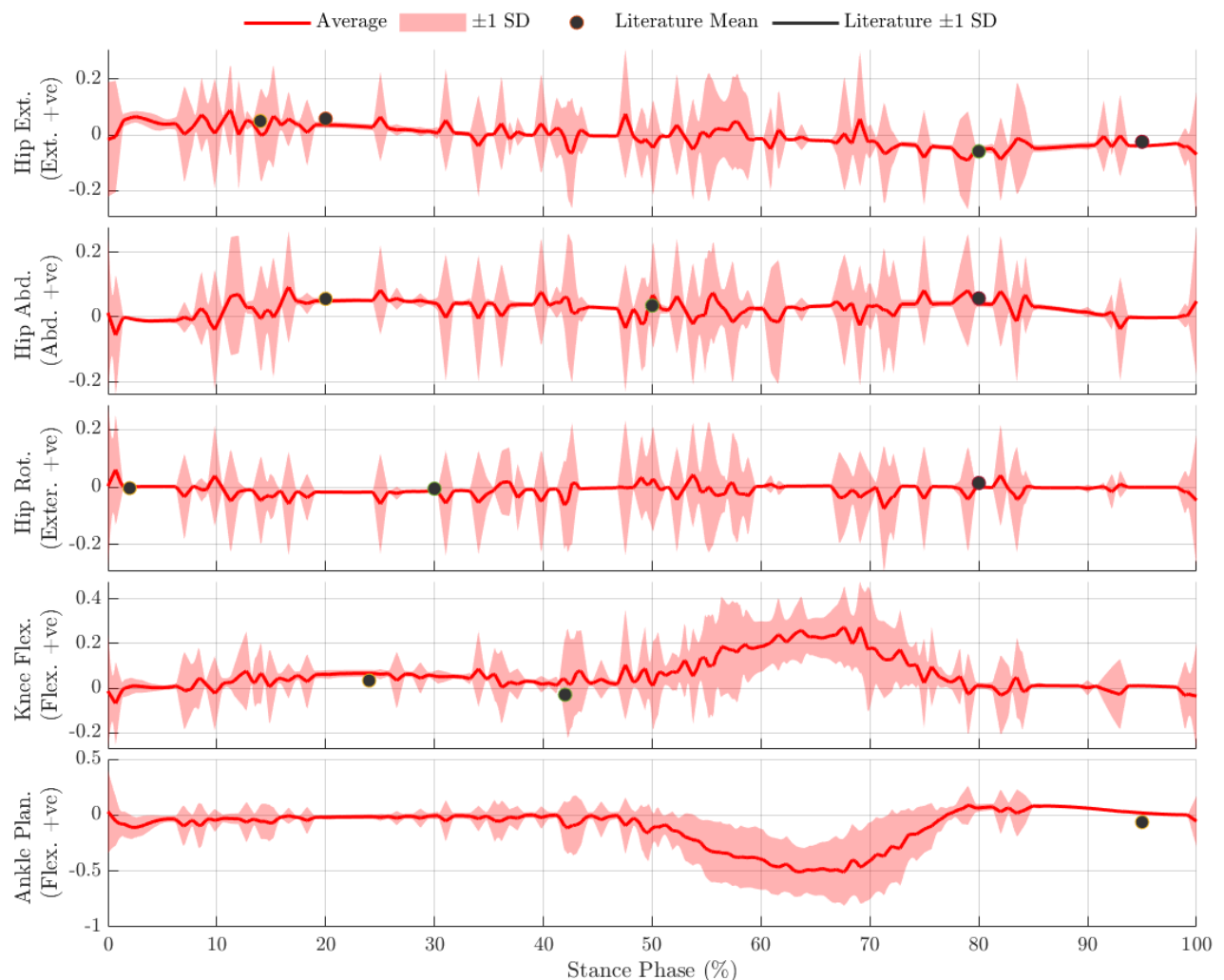


Figure 38: Unfiltered moment plots for walking trials

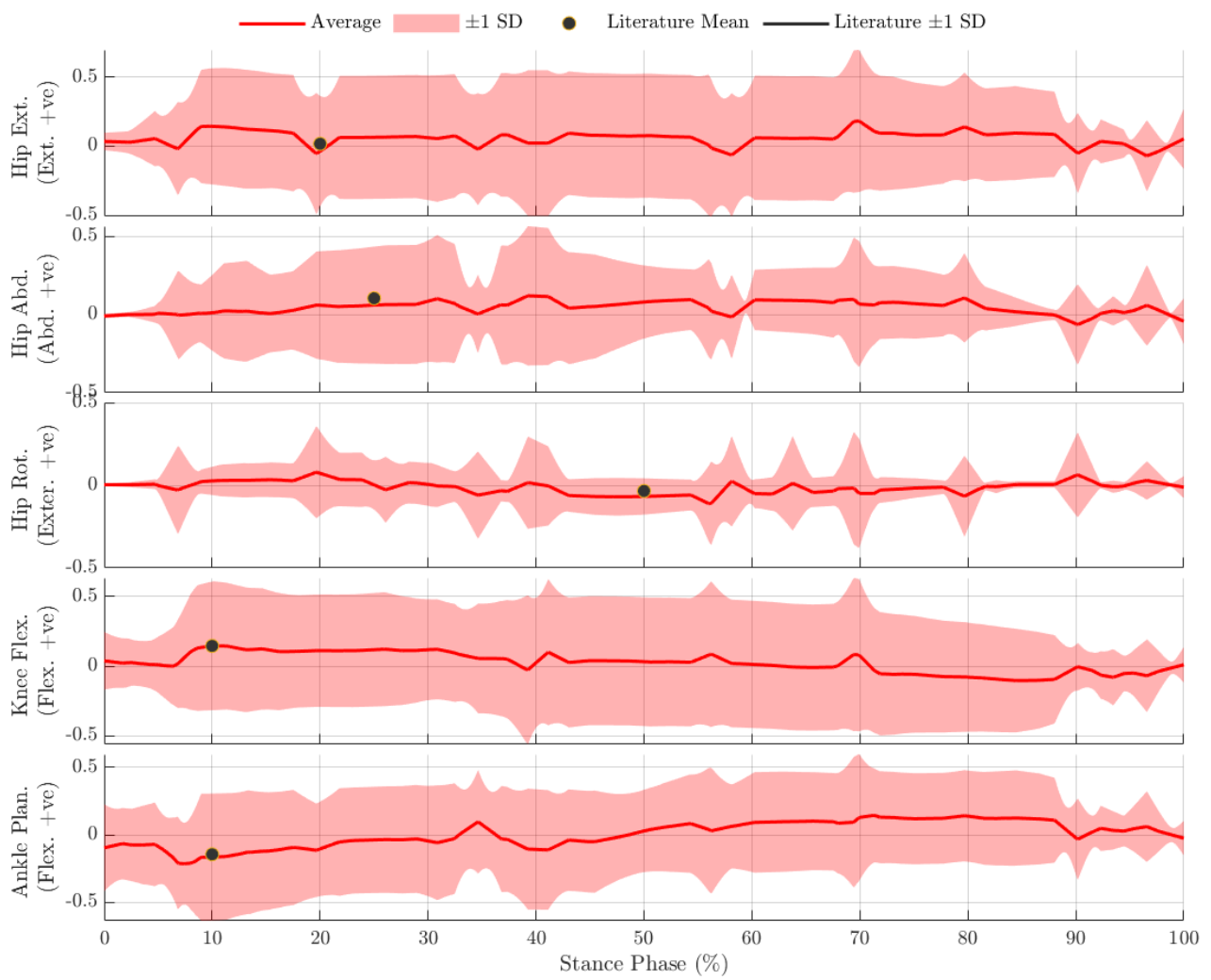


Figure 39: Unfiltered moment plots for running trials

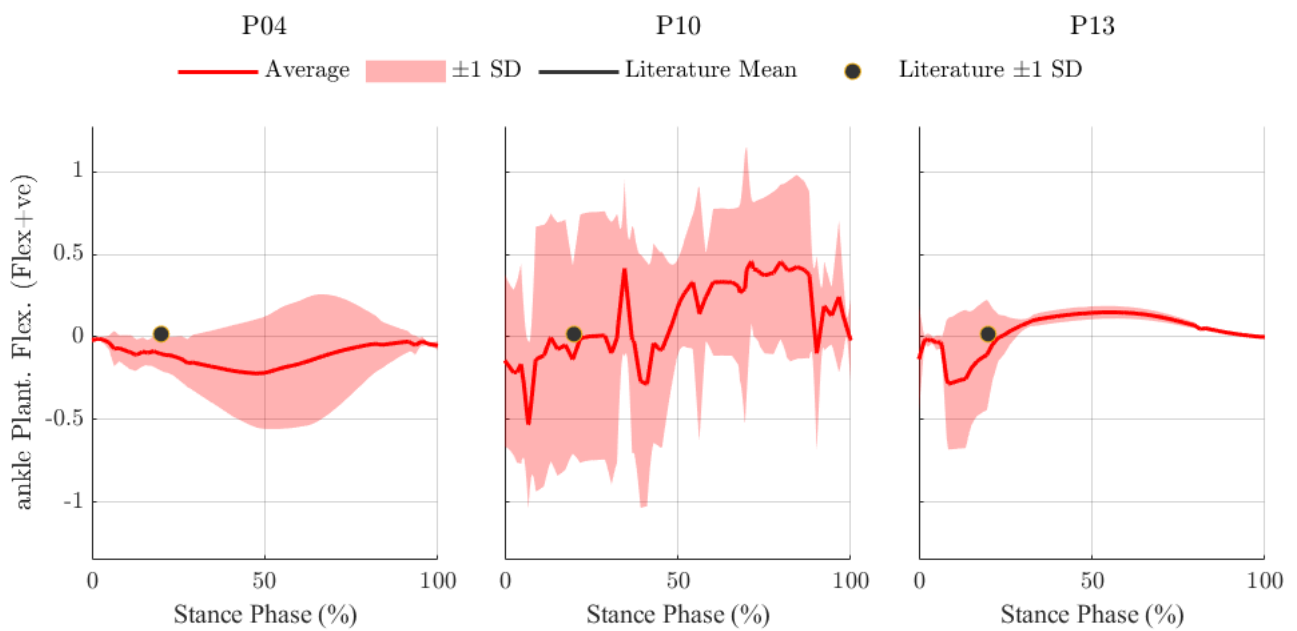


Figure 40: Unfiltered moment plots for walking trials

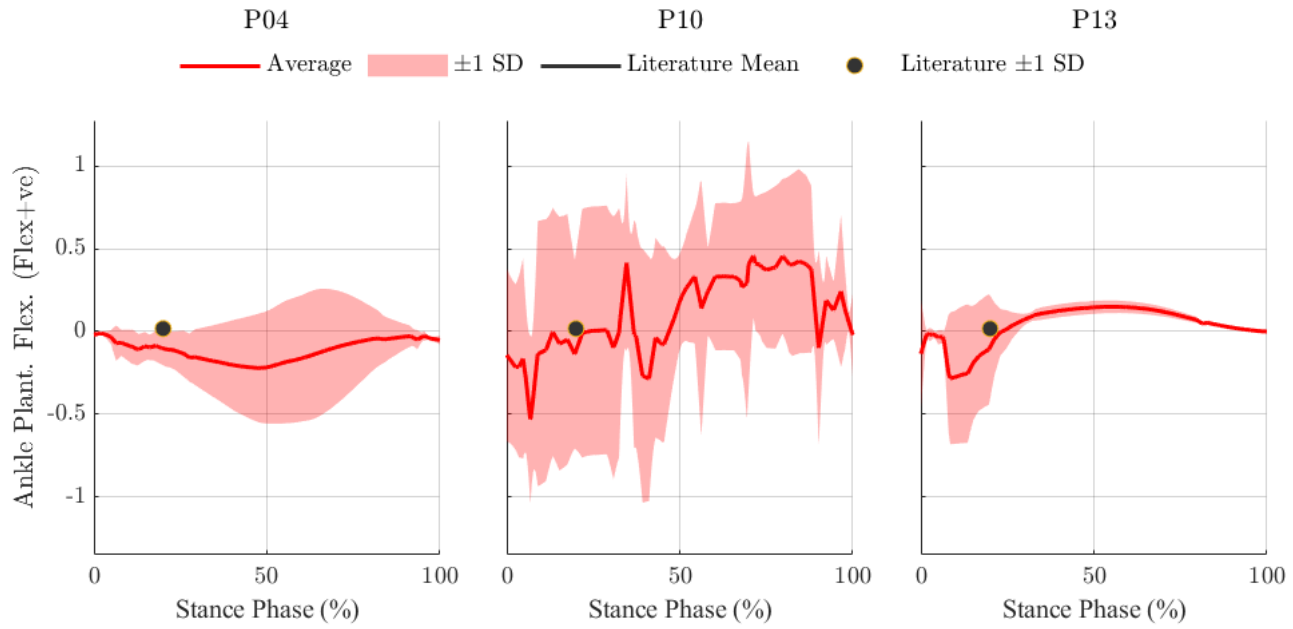


Figure 41: Unfiltered moment plots for running trials

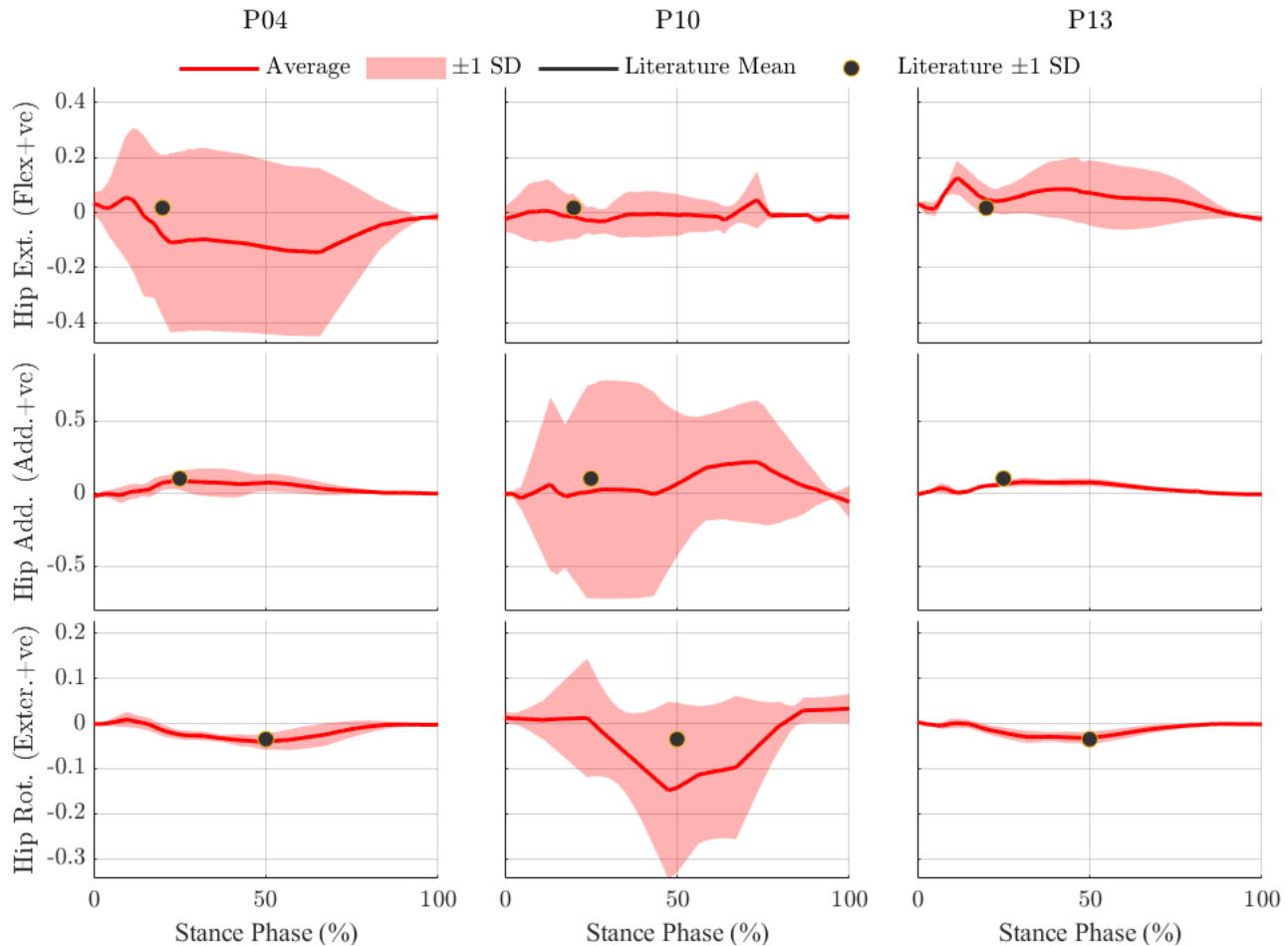


Figure 42: Subplot comparison of hip joint moments across the stance phase for running trials, broken down by participant and hip DOF. *Moments normalised by participant body weight and height ( $BW \times Height$ ); time normalised as percentage (%) of stance phase.*

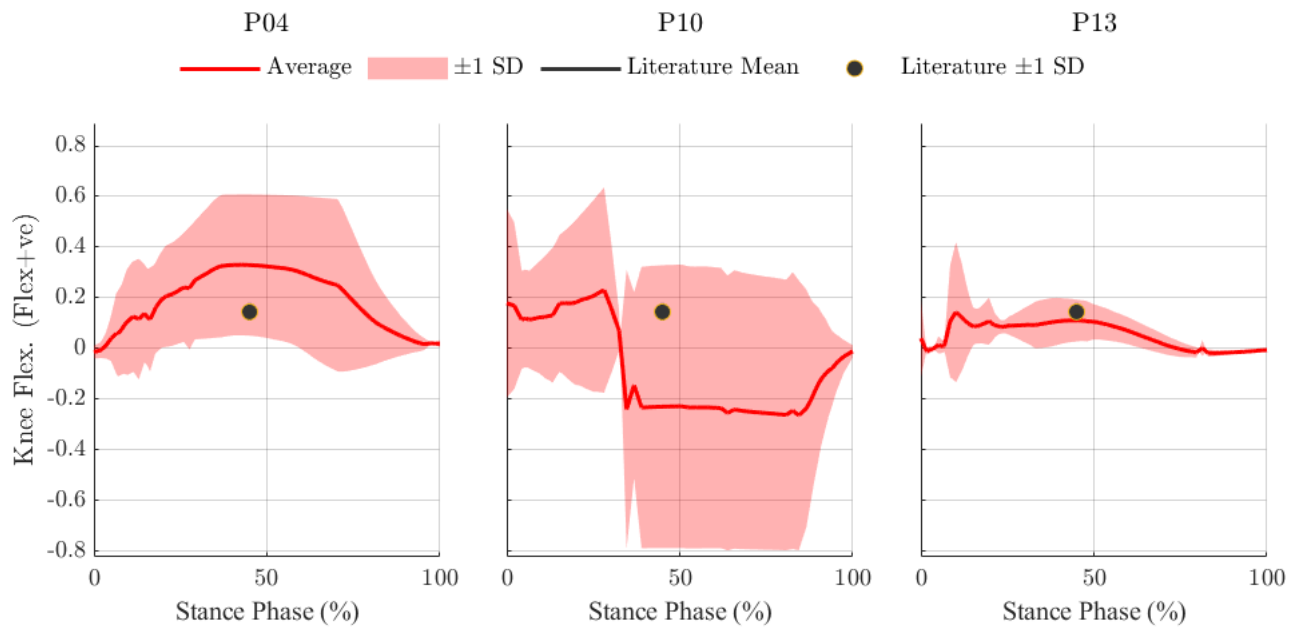


Figure 43: Subplot comparison of knee joint moments across the stance phase for running trials, broken down by participant. *Moments normalised by participant body weight and height ( $BW \times Height$ ); time normalised as percentage (%) of stance phase.*

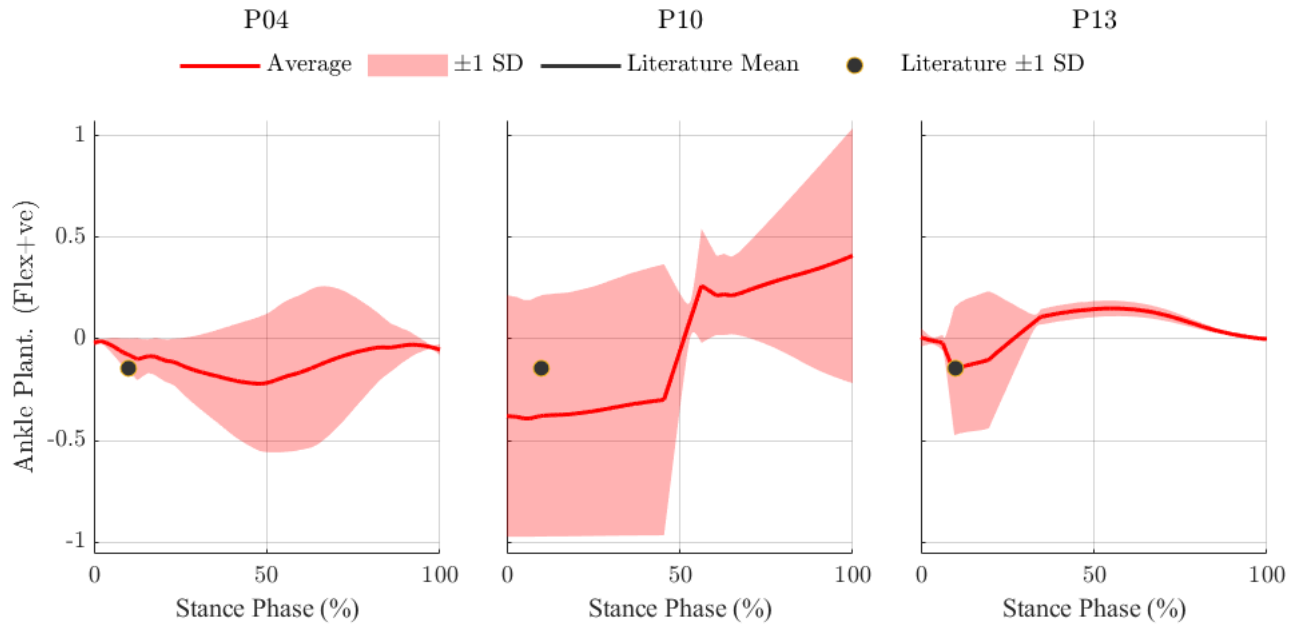


Figure 44: Subplot comparison of ankle joint moments across the stance phase for running trials, broken down by participant. *Moments normalised by participant body weight and height ( $BW \times Height$ ); time normalised as percentage (%) of stance phase.*



## Appendix K Detailed Results Statistical Analysis

Table 20: Statistical Breakdown of Simulation Moment Data: Normalised Standard Deviation and Median Absolute Deviations across stance-cycle moment RMS, positive peak, and negative peak values.

*Joint DoFs:* Flex./Ext. = Flexion/Extension, Abd./Add. = Abduction/Adduction, Rot. Ex./In. = External/Internal Rotation, Plant. Flex./Ext. = Plantarflexion/Dorsiflexion.

Subject	Exercise	Joint DOF	Standard Deviation (Norm. by Mean)			MAD (Norm. by Median)		
			RMS	Peak+	Peak-	RMS	Peak+	Peak-
<b>P04</b>	Walk	Hip Flex./Ext.	0.0224	0.1823	0.0396	0.0185	0.1199	0.0116
		Hip Abd./Add.	0.0242	0.2947	0.0288	0.0188	0.2439	0.0211
		Hip Rot. Ex./In.	0.1735	0.1214	0.9819	0.1143	0.0996	0.8258
		Knee Flex./Ext.	0.1410	0.8575	0.2892	0.0770	0.4864	0.1836
		Ankle Plant. Flex./Ext	0.1633	0.2272	0.2660	0.1280	0.0975	0.2543
<b>P10</b>	Walk	Hip Flex./Ext.	0.0422	0.2179	0.1437	0.0268	0.1871	0.0496
		Hip Abd./Add.	0.1111	0.2449	0.1075	0.0747	0.0024	0.0629
		Hip Rot. Ex./In.	0.1396	0.2066	0.1434	0.0916	0.1589	0.0355
		Knee Flex./Ext.	0.1719	1.2400	0.2943	0.0929	0.3264	0.1855
		Ankle Plant. Flex./Ext.	0.1423	0.0784	0.2622	0.0964	0.0282	0.1905
<b>P13</b>	Walk	Hip Flex./Ext.	0.0728	0.0892	0.2576	0.0539	0.0524	0.1394
		Hip Abd./Add.	0.1167	1.0492	0.0807	0.0725	0.5950	0.0670
		Hip Rot. Ex./In.	0.7775	0.3683	1.8015	0.1588	0.0818	2.4636
		Knee Flex./Ext.	0.1879	1.0418	0.3460	0.0594	0.6822	0.1673
		Ankle Plant. Flex./Ext.	0.7548	0.4958	1.9291	0.6873	0.4143	1.8870
<b>Mean</b>	<b>Walk</b>	Hip Flex./Ext.	0.0458	0.1470	0.1631	0.0331	0.0669	0.1198
		Hip Abd./Add.	0.0840	0.0723	0.5296	0.0553	0.0503	0.2804
		Hip Rot. Ex./In.	0.3635	0.9756	0.2321	0.1216	1.1083	0.1134
		Knee Flex./Ext.	0.1669	0.3098	1.0464	0.0764	0.1788	0.4983
		Ankle Plant. Flex./Ext	0.3535	0.8191	0.2671	0.3039	0.7773	0.1800
<b>Overall</b>			0.2027	0.4648	0.4477	0.1181	0.4363	0.2384
<b>P04</b>	Run	Hip Flex./Ext.	1.5370	1.8871	0.5548	0.0700	0.2460	0.2313
		Hip Abd./Add	0.3827	1.1049	0.0604	0.0308	0.7504	0.0604
		Hip Rot. Ex./In	0.3882	0.4067	1.3087	0.1020	0.1072	0.9942
		Knee Flex./Ext.	0.9607	2.2063	0.8384	0.0511	1.1052	0.0453
		Ankle Plant. Flex./Ext	1.0087	1.0299	0.8214	0.0899	0.3159	0.1340
<b>P13</b>	Run	Hip Flex./Ext.	1.0386	0.4744	0.5962	0.1640	0.3160	0.0904
		Hip Abd./Add	0.3347	0.6281	0.3061	0.1257	0.4787	0.0792
		Hip Rot. Ex./In	0.3534	0.3433	1.3256	0.0497	0.1068	0.2972
		Knee Flex./Ext.	0.4028	1.0624	0.8342	0.1054	0.2093	0.1242
		Ankle Plant. Flex./Ext	0.6384	1.1744	0.2489	0.1566	0.3795	0.0889
<b>Mean</b>	<b>Run</b>	Hip Flex./Ext.	1.2878	1.1808	0.5755	0.1170	0.2810	0.1609
		Hip Abd./Add	0.3587	0.8665	0.1833	0.0783	0.6146	0.0698
		Hip Rot. Ex./In	0.3708	0.3750	1.3172	0.0759	0.1070	0.6457
		Knee Flex./Ext.	0.6817	1.6344	0.8363	0.0783	0.6572	0.0848
		Ankle Plant. Flex./Ext	0.8236	1.1021	0.5351	0.1232	0.3477	0.1115
<b>Overall</b>			0.7045	1.0318	0.6895	0.0945	0.4015	0.2145

## K.1 Detailed reporting of moments

Table 21: Summary of Results: Peak and RMS Moments at the Hip, Knee, and Ankle Joints During Stance.

*Joint DoFs:* Flex./Ext. = Flexion/Extension, Abd./Add. = Abduction/Adduction, Rot. Ex./In. = External/Internal Rotation, Plant. Flex./Ext. = Plantarflexion/Dorsiflexion.

Participant	Condition	Joint DOF	RMS (Nm)		Peak (Nm)	
			Mean	SD	Mean	SD
<b>P04</b>	Walk	Hip Flex./Ext.	47.42	1.06	111.82/83.5	4.43/15.23
		Hip Abd./Add.	52.89	1.28	82.17/18.75	2.37/5.52
		Hip Rot. Ex./In.	5.81	0.90	3.31/13.73	3.25/1.67
		Knee Flex./Ext.	63.00	8.88	121.67/-20.23	35.19/17.35
		Ankle Plant. Flex./Ext	143.71	23.46	103.78/208.90	27.67/47.46
<b>P10</b>	Walk	Hip Flex./Ext.	38.91	1.91	85.97/60.38	12.35/13.16
		Hip Abd./Add.	33.43	3.71	59.76/20.82	6.42/5.10
		Hip Rot. Ex./In.	3.99	0.56	4.91/10.74	0.70/2.22
		Knee Flex./Ext.	48.68	8.37	70.75/-12.24	20.82/15.18
		Ankle Plant. Flex./Ext.	106.41	15.14	-79.7/131.76	20.90/10.32
<b>P13</b>	Walk	Hip Flex./Ext.	31.79	2.32	59.53/51.49	15.34/4.59
		Hip Abd./Add.	36.34	4.24	62.08/20.46	5.01/21.46
		Hip Rot. Ex./In.	8.39	6.52	4.52/12.29	8.14/4.53
		Knee Flex./Ext.	48.74	9.16	109.6/7.26	37.93/7.56
		Ankle Plant. Flex./Ext.	79.14	59.73	-29.22/123.21	56.37/61.08
<b>Average</b>	Walk	Hip Flex./Ext.	39.37	1.76	85.77/65.12	10.71/11.66
		Hip Abd./Add.	40.89	3.08	68.00/20.01	4.60/10.69
		Hip Rot. Ex./In.	6.06	2.66	4.25/12.25	4.03/2.14
		Knee Flex./Ext.	53.47	8.80	100.67/-8.41	31.98/13.36
		Ankle Plant. Flex./Ext.	109.75	32.78	31.29/154.62	35.65/39.62
<b>P04</b>	Run	Hip Flex./Ext.	219.57	337.47	202.5/229.50	112.35/430.8
		Hip Abd./Add	98.68	37.77	148.59/49.21	94.39/54.37
		Hip Rot. Ex./In	38.17	14.82	16.58/66.62	21.69/27.10
		Knee Flex./Ext.	334.34	321.21	480.24/77.32	402.66/85.54
		Ankle Plant. Flex./Ext	267.02	269.34	116.63/413.95	107.47/426.34
<b>P13</b>	Run	Hip Flex./Ext.	85.30	88.59	179.83/29.63	107.22/14.05
		Hip Abd./Add	64.10	21.46	107.62/16.79	32.95/10.54
		Hip Rot. Ex./In	23.52	8.67	7.09/44.96	9.39/15.43
		Knee Flex./Ext.	120.36	48.48	336.33/37.03	280.57/39.34
		Ankle Plant. Flex./Ext	199.85	127.59	189.49/397.72	47.17/467.09
<b>Average</b>	Run	Hip Flex./Ext.	152.44	213.03	191.17/129.57	109.79/222.43
		Hip Abd./Add	81.39	29.61	128.11/33.00	63.67/32.46
		Hip Rot. Ex./In	30.85	11.75	11.84/55.79	15.54/21.27
		Knee Flex./Ext.	227.35	184.85	408.29/57.18	341.62/62.44
		Ankle Plant. Flex./Ext	233.44	198.47	153.06/405.84	77.32/446.72